



CENTER FOR INFRASTRUCTURE ENGINEERING STUDIES

EVALUATION OF EXTERNALLY BONDED CFRP SYSTEMS FOR THE STRENGTHENING OF RC SLABS

By

KAH YONG TAN

University of Missouri-Rolla

**CIES
02-32**

Disclaimer

The contents of this report reflect the views of the author(s), who are responsible for the facts and the accuracy of information presented herein. This document is disseminated under the sponsorship of the Center for Infrastructure Engineering Studies (CIES), University of Missouri -Rolla, in the interest of information exchange. CIES assumes no liability for the contents or use thereof.

The mission of CIES is to provide leadership in research and education for solving society's problems affecting the nation's infrastructure systems. CIES is the primary conduit for communication among those on the UMR campus interested in infrastructure studies and provides coordination for collaborative efforts. CIES activities include interdisciplinary research and development with projects tailored to address needs of federal agencies, state agencies, and private industry as well as technology transfer and continuing/distance education to the engineering community and industry.

Center for Infrastructure Engineering Studies (CIES)
University of Missouri-Rolla
223 Engineering Research Lab
1870 Miner Circle
Rolla, MO 65409-0710
Tel: (573) 341-6223; fax -6215
E-mail: cies@umr.edu
www.cies.umr.edu

EVALUATION OF EXTERNALLY BONDED CFRP SYSTEMS FOR THE
STRENGTHENING OF RC SLABS

by

KAH YONG TAN

A THESIS

Presented to the Faculty of the Graduate School of the

UNIVERSITY OF MISSOURI-ROLLA

In Partial Fulfillment of the Requirements for the Degree

MASTER OF SCIENCE IN CIVIL ENGINEERING

2003

Approved by

Antonio Nanni, Advisor

John J. Myers, Co-advisor

J. Gustavo Tumialan, Co-advisor

K.Chandrashekhara

© 2003

Kah Yong Tan
All Rights Reserved

ABSTRACT

The use of fiber-reinforced polymer (FRP) composites as externally bonded reinforcement (EBR) to repair and strengthen of deficient structures has taken place since the late 1980's. Continuous efforts in material development and research activities, with strong links to engineering practice, give this application more and more worldwide acceptance. This paper presents an experimental study on flexural strengthening of reinforced concrete (RC) slabs with three different commercially available carbon FRP (CFRP) systems, prefabricated laminate plate, fiber laminate sheet and prefabricated laminate bar, using four different EBR techniques involving cold cured adhesive bonding, prestressing, manual wet lay-up and near surface mounted (NSM) technique. All slabs were tested to failure under simply supported conditions. CFRP EBR increased the flexural strength and reduced the deflections and crack widths of the strengthened slabs. Two modes of failure were observed, debonding and rupture of the CFRP reinforcement. Significant increases in ultimate moment capacity ranging from 63% to 145% were registered in all the strengthening slabs, as compared to the control slab. The slab which was strengthened with NSM laminate bars exhibited the highest efficiency followed by prestressing laminate plates, manual wet lay-up laminate sheet and cold cured adhesive bond laminate plates.

ACKNOWLEDGMENTS

I would like to express my sincere appreciation to the members of my committee, Dr. Antonio Nanni, Dr. John J. Myers, Dr. Jaime Gustavo Tumialan and Dr. K. Chandrashekhara, for their support throughout my research program. It was a tremendous experience to work under the guidance of Dr. Nanni, whose valuable advice and encouragement were very important for the completion of this research. I would also like to show my gratitude to Dr. Tumialan for his continuous guidance and assistance since the commencement of the research program. Their versatility and generous personalities are the qualities that I admire most. In addition, I would like to thank Dr. Pedro Silva for sharing his knowledge with me.

Special thanks to S&P Clever Reinforcement Company, Brunnen, Switzerland for providing financial and material assistance for this research.

A heartfelt thank you is also extended to Mr. Jason Cox for his assistance in preparing experimental specimens and working along with me during numerous testings. I would also like to recognize the contribution of Mr. Sascha Arnold from S&P throughout the process of strengthening the specimens. Special thanks to all the staff and friends at Center for Infrastructure Engineering Studies for caring and sharing many good times with me.

Finally, a very special thanks to my friends and family in Malaysia, for all the love and support they have given me throughout my life.

TABLE OF CONTENTS

	Page
ABSTRACT.....	iii
ACKNOWLEDGMENTS	iv
LIST OF ILLUSTRATIONS.....	viii
LIST OF TABLES.....	x
SECTION	
1. INTRODUCTION.....	1
1.1. BACKGROUND	1
1.2. SCOPE AND OBJECTIVES.....	2
1.3. LAYOUT OF THE THESIS.....	4
2. LITERATURE REVIEW.....	5
2.1. EXTERNALLY BONDED REINFORCEMENT (EBR)	5
2.2. FLEXURAL STRENGTHENING WITH CFRP PLATES	6
2.3. FLEXURAL STRENGTHENING WITH PRESTRESSED CFRP PLATES....	8
2.4. FLEXURAL STRENGTHENING WITH CARBON FIBER SHEET	9
2.5. FLEXURAL STRENGTHENING WITH NSM CFRP BARS	11
2.6. REVIEW OF ANALYTICAL MODELS.....	13
2.6.1. Roberts’ Analytical Model	13
2.6.2. Malek’s Analytical Model.....	15
3. EXPERIMENTAL PROGRAM.....	18
3.1. DESCRIPTION OF RC BEAMS	18
3.2. MATERIAL PROPERTIES	21
3.2.1. Concrete.....	21
3.2.2. Steel.....	21
3.2.3. Prefabricated CFRP Plate.....	22
3.2.4. Carbon Fiber Sheet.....	26
3.2.5. Prefabricated CFRP Bar	26
3.2.6. Adhesive.....	29

3.3. INSTALLATION PROCEDURES	32
3.3.1. Slab A: Cold Cured Adhesive Bonded CFRP Plate	32
3.3.2. Slab B: Prestressed CFRP Plate	33
3.3.3. Slab C: Manual Wet Lay-up Carbon Fiber Sheet.....	36
3.3.4. Slab D: Near Surface Mounted CFRP Bar.....	37
3.4. TIME CONSUMPTION FOR INSTALLATION	38
3.5. TEST SETUP AND TEST PROCEDURE.....	39
4. TEST RESULTS	43
4.1. MODE OF FAILURE.....	43
4.1.1. Control Slab.....	43
4.1.2. Slab A	44
4.1.3. Slab B	45
4.1.4. Slab C	45
4.1.5. Slab D.....	45
4.2. DEFLECTION.....	48
4.3. STRAIN ALONG THE CFRP SYSTEM AND CONCRETE.....	50
4.3.1. Slab A.....	50
4.3.2. Slab B	51
4.3.3. Slab C	52
4.3.4. Slab D.....	53
4.4. THEORETICAL MOMENT CURVATURE.....	54
4.5. EXPERIMENTAL MOMENT CURVATURE.....	58
4.5.1. Control Slab.....	59
4.5.2. Slab A	60
4.5.3. Slab B	61
4.5.4. Slab C	62
4.5.5. Slab D.....	63
5. ANALYTICAL STUDY	66
5.1. ANALYTICAL APPROACH	67
5.2. VALIDATION OF ROBERTS' ANALYTICAL APPROACH	68
5.3. VALIDATION OF MALEK'S ANALYTICAL APPROACH.....	72

6. DESIGN OF EXTERNALLY BONDED FRP SYSTEMS	75
6.1. ACI-440.	75
6.2. CONCRETE SOCIETY TECHNICAL REPORT NO. 55.....	80
7. CONCLUSION	83
7.1. EXPERIMENTAL PHASE	83
7.2. ANALYTICAL PHASE.....	84
7.3. DESIGN PHASE	84
APPENDICES	
A. TENSILE STRESS-STRAIN CURVES FOR CFRP SYSTEMS AND ADHESIVE	84
B. EXPERIMENTAL LOAD-DEFLECTION AND LOAD-STRAIN CURVES.....	100
C. MOMENT CURVATURE CALCULATION.....	108
D. ANALYTICAL SHEAR AND NORMAL STRESSES AT THE PLATE END.....	119
E. FLEXURAL STRENGTHENING OF SLAB A BASED ON ACI 440 AND TECHNICAL REPORT NO.55.....	129
F. RESEARCH PROGRAM VIDEOS ON CR-ROM.....	135
BIBLIOGRAPHY.....	136
VITA.....	141

LIST OF ILLUSTRATIONS

Figure	Page
2.1: Longitudinal Distance.....	16
3.1: Typical Cross Section of Slabs.....	18
3.2: Steel Distribution for A Typical Slab.....	19
3.3: Detailed drawing of Slab A-D (Dimension in meter).....	20
3.4: Test Specimens.....	24
3.5: Tensile Test Failure Modes for CFRP Plate.....	25
3.6: Tensile Test Failure Modes for Carbon Fiber Sheet.....	28
3.7: Tensile Test Failure Modes for CFRP Bar.....	29
3.8: Test Specimen for Epoxy Gel.....	30
3.9: Tensile Test Failure Modes for Epoxy Gel.....	31
3.10: Cold Cured Adhesive Bonded CFRP Plate.....	33
3.11: Prestressing CFRP Plate.....	35
3.12: Strain vs. Time Curves for Prestressed CFRP Plate.....	35
3.13: Strain vs. Time Curves for Prestressed CFRP Plate After 18 Hours.....	36
3.14: Manual Lay-up Carbon Fiber Sheet.....	37
3.15: Near Surfaced Mounted CFRP Bars.....	37
3.16: Gantt Chart for Strengthening Process.....	38
3.17: Test Arrangement (Dimension in meter).....	40
3.18: Test Setup.....	41
3.19: Test Setup Deformation.....	41
3.20: Test Apparatuses.....	42
4.1: Failure Mode of the Control Slab.....	44
4.2: Failure Mode of Slab A.....	46
4.3: Failure Mode of Slab B.....	46
4.4: Failure Mode of Slab C.....	47
4.5: Failure Mode of Slab D.....	47
4.6: Load vs. Deflection Curves.....	49

4.7: Load vs. Strain for Slab A	50
4.8: Load vs. Strain for Slab B.....	51
4.9: Load vs. Strain for Slab C.....	52
4.10: Load vs. Strain for Slab D	53
4.11: Stress-Strain Distribution in the Cross Section of RC Slab.....	54
4.12: Initial Un-factored Load (Dimension in meter).....	59
4.13: Moment vs. Curvature for the Control Slab	60
4.14: Moment vs. Curvature for Slab A.....	61
4.15: Moment vs. Curvature for Slab B.....	62
4.16: Moment vs. Curvature for Slab C.....	63
4.17: Moment vs. Curvature for Slab D.....	64
5.1: Stresses Acting at the Concrete-Adhesive Interface.....	67
5.2: General View of the Test Setup.....	69
5.3: Cross Section of Slab A	69
5.4: Interfacial Shear and Normal Stresses – Roberts’ Analytical Model	71
5.5: Interfacial Shear and Normal Stresses – Malek’s Analytical Model.....	73
6.1: Stress and Strain Distribution in a Section at the Ultimate Limit State.....	76

LIST OF TABLES

Table	Page
3.1: Test Matrix.....	21
3.2: Average Concrete Compressive Strength at 28 days.....	22
3.3: Mechanical Properties of the CFRP Systems	23
3.4: Test Result for Tensile Properties of CFRP Plate.....	25
3.5: Test Result for Tensile Properties of Carbon Fiber Sheet	27
3.6: Test Result for Tensile Properties of CFRP Bar.....	28
3.7: Mechanical Properties of Adhesive	30
3.8: Test Result for Tensile Properties of Epoxy Gel	31
4.1: Test Results.....	43
4.2: The Experimental and Analytical Ultimate Moments	65
5.1: Geometric and Material Properties.....	69

1. INTRODUCTION

1.1. BACKGROUND

Each year, considerable investments made in construction engineering are related to the maintenance, repair and strengthening of existing structures, arising from the social and economic needs for reliable and functional infrastructure. Among several techniques that are available for repair and strengthening is the use of externally bonded reinforcement (EBR). This simple and rapid strengthening technique, developed in the late 1960's, can be attributed to the development of strong structural adhesives. Steel plates were originally used in this technique. EBR technique minimizes disruption of normal operations of the facility during ongoing construction work. When completed, small changes to the overall dimensions of the structural sizes are negligible.

The development of high strength-to-weight ratio, ease of fabrication and bonding, and excellent resistance to electrochemical corrosion of carbon fiber reinforced polymer (CFRP) composites has given this technique even more acceptance worldwide. The use of CFRP composites has distinct advantages over the use of conventional steel plate in terms of many physical characteristics and provides the designer with a unique freedom of designs. However, CFRP is linearly elastic up to its failure and does not exhibit plastic yielding as steel does. This linear elastic behavior could lead to undesirable brittle failures of the strengthened structure and must be accounted for in structural strengthening.

The application and demonstration projects using CFRP EBR that started in the late 1980's through the early 1990's, mainly applied to strengthening reinforced concrete (RC) as well as prestressed concrete (PC) bridges. Most work since then has focused on

the building sector, including the restoration of old buildings. Over the last few years, new CFRP commercial products and EBR techniques have been developed to extend the possibility of implementing CFRP EBR strengthening technique for more complicated situations. The selection of CFRP strengthening materials and technique is a critical process. Every system is unique in the sense that the fibers and the resin components are usually designed to work with each other. This implied that a system for one strengthening system would not automatically work properly for another. Furthermore, a resin system for the fibers will not necessarily provide a good bond to concrete. This implies that only systems that have been tested and applied in full scale on RC structures shall be used in strengthening.

1.2. SCOPE AND OBJECTIVES

The need for strengthening RC floor slabs to the original or higher performance level due to mechanical damage, mistakes in design/construction works, functional changes or reinforcement corrosion has become common and necessary for economic reasons. In the past, RC slabs were strengthened by conventional methods such as concrete overlay, span shortening, and externally bonded steel reinforcement. Today there are several types of CFRP strengthening systems and techniques available to strengthen RC slabs.

The suitability of each system depends on the type of structure that shall be strengthened. Therefore, it is essential for engineers to understand the consequences of the design choice in terms of efficiency and failure mechanism for different systems before further attempts are carried out.

The main objectives of this thesis are to study and compare the efficiencies of different CFRP strengthening systems and techniques for the flexural strengthening of RC slab. Five full-scale RC slabs were cast for this experimental program. Three different CFRP commercial products, which include prefabricated laminate plates, fiber laminate sheets and prefabricated laminate bars were used to strengthen the RC slabs by four installation techniques. The techniques used were wet lay-up, cold cured adhesive bonding, prestressing and near surface mounted (NSM). All slabs were tested to their failure under simply supported conditions, subjected to a 6-point concentrated static loading system. A control slab was used as a baseline to compare the other strengthened slabs.

Two analytical models developed by Roberts and Malek were used to analyze and predict the failure modes of the strengthened slabs. The design guidelines implemented by the American Concrete Institute – Committee 440 in the “*Guide for the Design and Construction of Externally Bonded FRP Systems for Strengthening Concrete Structures*” and the Concrete Society in the “*Design Guidance for Strengthening Concrete Structures Using Fiber Composite Materials*” were used to calculate the ultimate moment of the strengthened slab.

1.3. LAYOUT OF THE THESIS

This thesis is organized as follows:

Section 2 deals with a brief description of the role and effectiveness of CFRP in strengthening and upgrading concrete structures, as well as previous experimentation and analysis models developed by Malek and Roberts for predicting the shear and normal stresses concentration in the adhesive layer of plated reinforced slabs.

Section 3 deals with the description of the experimental program carried out at the High Bay Laboratory at University of Missouri-Rolla. The slab details, material properties, installation procedures and test setup for the experiment are presented.

Section 4 depicts the observations during the tests and discusses the failure modes, deflections, and strain distribution along the FRP systems. The discussion also details the efficiency of each CFRP system and EBR technique. Also included in the section, is a comparison between experimental and analytical moment curvatures.

Section 5 shows the predicted shear and normal stresses in the adhesive layer of cold cured adhesive bonded CFRP plate based on Roberts and Malek's analytical models, as discussed in Section 2.

Section 6 shows the computation of flexural strengthening of Slab A based on strain limitation suggested by ACI-440 and Concrete Society Technical Report No.55 design codes.

Finally, Section 7 provides the concluding remarks for this research program.

2. LITERATURE REVIEW

2.1. EXTERNALLY BONDED REINFORCEMENT (EBR)

EBR is an effective and frequently applied method for repair and strengthening, developed in the late 1960's, and steel plates were originally used. The first recorded case was in Durban, South Africa, in 1964, where epoxy-bonded steel plates were used to strengthen concrete beams in an apartment complex, where part of the reinforcing steel in the building had been accidentally omitted during construction. In 1975 and 1977, externally epoxy-bonded steel plates were used to strengthen four bridges in Swanley, Kent, England. Calculation indicated that the tension reinforcement originally provided was inadequate. The same method was also used to strengthen RC floor slabs and supporting RC beam in several old buildings in Zurich, Switzerland in order to withhold additional live load [1].

Quite naturally, steel plates have been widely used for such rehabilitation works, but more recently non-metallic CFRP are being considered as a contender to replace steel. CFRP materials have many favorable engineering properties that can be used as external plate reinforcement, combined with its lightweight nature and freedom from electrochemical corrosion that occurs to steel. It was recognized early in the work that CFRP is not economically feasible when viewed on the basis of material cost. However, it becomes more attractive because of the reduced time required on site and the considerable reduction in falsework compared with the use of steel plates.

Application and demonstration projects of CFRP EBR started in the late 1980's throughout early 1990's. In Europe, the first application was on the Ibach Bridge in Lucerne, Switzerland, where steel tendons had been severed when the bridge was drilled

to support a sign gantry [2]. Commercial use of CFRP EBR started around 1993 and the amount of CFRP material applied for strengthening increased every year thereafter [3]. There are now numerous CFRP EBR technologies are clearly reaching commercial maturity.

2.2. FLEXURAL STRENGTHENING WITH CFRP PLATES

The use of carbon fiber for structural application in Europe was first studied at the Swiss Federal Testing Laboratories (EMPA). One of the first application considered, which has later proved to be commercially successful, was the use of CFRP plates as externally bonded reinforcement. The CFRP plates are much thinner than its steel counterpart, which allow lap joints to be made between different elements. The reduced eccentricity of the plate also reduces the tendency for peeling failure [2]. Many published test data showed that flexural strengthening with CFRP plates behave very similarly to steel plates [4]. Besides the classical failure modes, such as steel fracture, concrete crushing or shear failure, bond failures could occur in the interface between the externally bonded CFRP plates and the concrete body. This undesirable bond failure resulted in sudden drop in loads and a brittle type of failure due to high concentration of interface shear and normal peeling stress at the cutoff point of the plates. Although substantial increases in load capacity can be achieved with CFRP plates, the possibility of unexpected brittle failure mechanisms needs to be included in design considerations.

Swamy et al., (1988) studied the plate separation and anchorage of RC beams strengthened by epoxy bonded steel plates [5]. He concluded that plate separation is due to high local interface bond stresses and peeling forces at the ends of the plates. The

magnitude of these concentrated shear and normal stresses at the end of the plates depend on the geometry of the plate reinforcement, the engineering properties of the adhesive and the shear strength of the original concrete beam. With careful selection of the geometry of the plate, it is possible to develop ductile failures with the composite beam reaching its full flexural capacity.

Taljsten (1997) used fracture mechanics approach to derive closed-form formula for the case of linear elastic shear slip relationship [6]. The results from both theory and finite-element analysis showed that the stresses are very large at the end of the plate, but they quickly diminish as we move nearer to the center of the beam. The magnitude of the stresses is influenced not only by the geometrical and material parameters of the beam, but also by the adhesive and the strengthening material. To minimize these stresses, the distance from the support to the cutoff point of the plate should be kept as short as possible. Furthermore, the parameter study indicates that with increasing stiffness of the adhesive that the shear and peeling stresses also increase. This is also the fact with decreasing thickness of the adhesive layer or if the thickness of the plate is increased. In addition, if the Young's modulus of the plate is increased, then the shear and peeling stresses increase as well.

Blaschko (1998) studied the bond failure modes of flexural member strengthened with CFRP plates [7]. He found that bond failures can occur in the interface between the externally bonded reinforcement and the concrete body caused by flexural cracks along the tension face of the concrete, shear cracks and unevenness of the concrete surface. Each of these failures can cause the total high interface shear and normal stresses to concentrate at the end of the plate.

2.3. FLEXURAL STRENGTHENING WITH PRESTRESSED CFRP PLATES

Post-strengthening of structures with prestressed CFRP plates is a cutting edge technique in EBR. To take full advantage of this expensive material, it is beneficial to apply the plates in a prestressed state. This reinforcement technique increases the composite strain level but reduces the steel strain level under structure loading. This effect is beneficial for structure serviceability conditions. The Giuliana Bridge in Libya and several RC slabs for housing in Zurich, Switzerland had been strengthened with this technique. Due to the limited shear strength of concrete and the high shear stresses at the ends of the system, the plates have to be anchored with special anchorage devices. A failure of the anchorage would cause a total failure of the strengthening system.

To overcome anchorage problems, Stocklin and Meier (2001) custom fabricated a prestressing device to gradually prestress the CFRP plates using a stepwise approach [8]. The result was an increased development length of the prestressing force such that the occurring shear stresses are within the limitation of the shear strength of concrete. There was no measurable loss of prestressing force in the CFRP plate over a period of 125 days. This method enables prestressing of a CFRP without the need of a preliminary anchorage device on the CFRP plates.

Ferrier (2001) studied the mechanical behavior of an RC element strengthened with externally prestressed CFRP plates [9]. His test results showed that this reinforcement technique allows for increasing the composite strain level to be increased under structure loading. It also contributed to reducing the strain level in steel rebars. This effect is beneficial for structure serviceability conditions.

A series of RC slabs strengthened with non-tensioned and prestressed laminate plates was tested at the University of Freiburg, Switzerland. The prestressing method used for strengthening in the University of Freiburg tests are the same as the method used for strengthening Slab B in this research. However, the University of Freiburg used greater cross-section areas of CFRP plates [10]. The serviceability condition of the test specimens strengthened with prestressed laminate plates exhibit a high reduction in the deflection and crack widths. The failure condition showed a high increase in the ultimate load. Specimen with untensioned laminate plates showed an increase in the ultimate load of 32%, while the prestressed laminate plates raised the ultimate load by 82% at an initial prestressed condition of 4% and by 93% at an initial prestressed condition of 6%.

2.4. FLEXURAL STRENGTHENING WITH CARBON FIBER SHEET

Carbon Fiber sheets have been developed primarily in Japan and used for seismic retrofitting of existing RC structures. More than 1000 strengthening projects have been performed there in a manner similar to bonded steel plates [11]. Currently, many grades of carbon fiber sheets are available, offering elastic modulus values from 230 kN/mm² (33 Msi) to 640 kN/mm² (93 Msi). Moreover, the carbon fiber can be aligned and woven in uni-directional and bi-directional ways to produce a fine mesh sheet of fiber. Thus, the designers have freedom of design when considering structural strengthening with CFRP sheets. CFRP sheets are easy to handle and install and also can be used in a variety of applications. They are ideal for complex shapes where strengthening is required.

Yoshizawa (1996) carried out a series of experiments to clarify the influence of bonding conditions between CFRP sheet and concrete members [12]. By changing the method of concrete surface preparation (water jet and sander), type of carbon fiber and debonding area rate, bonding strength tests were performed through a four point bending test. It revealed that when epoxy was used, surface treatment with a water jet was more effective for increasing bonding strength compared to an ordinary sander. The bonding strength of high modulus CFRP sheets was higher than low modulus, high tensile strength CFRP sheet. As for artificial debonding of CFRP sheet up to 10% in area ratio, no significant influence on bonding strength was found.

Tumialan (1998) studied the concrete cover delamination in RC beam strengthened with CFRP sheets [13]. Six RC beams strengthened in flexural with varied plies of CFRP sheets were tested. Two types of failure modes were observed, concrete cover delamination starting at the cutoff point of the sheets and cover delamination starting at the intermediate flexural cracks and developed towards the beam mid span. The former failure might have occurred when more than one ply of CFRP sheet was attached to the concrete surface. During the test, it was observed that the employment of CFRP sheets delayed the presence of the first visible cracks. Similarly, the flexural crack spacing was reduced when the number of plies of CFRP sheets was increased. In addition, important increases in flexural stiffness and ultimate capacity were achieved despite the ductility losses.

Alkhrdaji and Nanni (1999) investigated the behavior of an existing bridge strengthened with CFRP systems in order to provide the necessary field verification of design method, structural performance, and failure mode [14, 15]. The bridge consisted

of three simply supported solid RC decks having a thickness of 460 mm (18 in.) and a roadway width of 7.6 m (25 ft). Each of the three decks spanned 7.9 m (26 ft). Two of the three decks were strengthened with externally bonded CFRP sheets and NSM CFRP bars respectively, while the third deck was left as a benchmark. The failure mode of the deck strengthened with CFRP sheets was a combination of rupture and peeling of the sheets. The CFRP sheets strengthened decks had smaller deflection and 17% higher moment capacity at their ultimate point than the unstrengthened deck. The contribution of the strengthening system to the nominal capacity was less than originally predicted due to the significantly higher strength of the benchmark. The deck strengthened with NSM CFRP bars are described in the following section.

2.5. FLEXURAL STRENGTHENING WITH NSM CFRP BARS

CFRP is sensitive to impact and fire. It is also vulnerable to vandalism since it is often in an exposed environment and has no protection on the surface of the structure. To preclude this from happening, the composite can be inserted into the concrete cover in specially sawed slots or grooves. This method is called near surface mounted (NSM) reinforcement. Furthermore, the insertion of the composite should vouch for a better quality since it is less dependent on installation. The bond surface will increase compared to plate bonding, which most likely gives a higher strengthening capacity. However, a drawback with this technique is that the placements of the CFRP bars are dependent on the concrete clear cover. For very thin concrete covers, the method will unlikely be possible without damaging the existing steel reinforcement.

Taljsten and Carolin (2001) investigated the strengthening effects of RC beams strengthened by CFRP NSM bars [16]. Results from several tests showed that a considerable strengthening effect could be achieved together with more ductile behavior and large deformation at failure. A comparison between the theory and test showed that the theory somewhat overestimates the ultimate load at failure. The reasons for this are still under investigation.

De Lorenzis (2000) studied the structural performance of a full-scale, simply supported RC T-beams strengthened with FRP NSM bars [17]. FRP bars of different sizes were used for flexural strengthening. The failure mode of the strengthened beams was the debonding of the NSM bars. However, the test results showed that the beams strengthened in bending increased in capacity ranging from 25.7% to 44.3% over the control beam.

Alkhrdaji and Nanni (1999) carried out full-scale strengthening and testing to the failure on Bridge J857 located at Phelps County, Missouri, USA. As mentioned in section 2.4, one of the three solid RC decks was strengthened using CFRP NSM bars [14, 15]. Preliminary examination of the test results clearly indicated the successful performance of CFRP NSM bars. Smaller deflection and higher load capacity at the point of maximum deflection than unstrengthened deck were observed. The final failure was initiated by the rupture of some CFRP rods at the location of the widest crack. The ultimate moment capacity of the strengthened deck was 28.3% higher than the unstrengthened deck.

2.6. REVIEW OF ANALYTICAL MODELS

A number of strength models have been developed by Swamy (1988), Robert (1989) to predict the shear and normal stress concentrations in the adhesive layer of steel plated RC structures over the last decade. Since the failure modes of a steel plated RC structure behave similarly to a FRP plated structure, the strength models may well be applied to FRP plated structure, with modification if necessary. Taljsten (1997), Saadatmanesh (1998), Malek (1998) and Tumialan (1999) had developed several analytical models to predict shear and normal stresses for FRP plated structures.

Smith and Teng (2001) reviewed several existing models for plate end debonding in FRP strengthened RC beams using available test data and identified most of the models developed for steel plated beams to be the more accurate ones, while those specially developed for FRP plated beams give poorer predictions [18]. To verify the statement above, a steel plate analytical model developed by Robert and a FRP plate analytical model developed by Malek were reviewed and verified with experimental results of cold cured adhesive bonding laminate plate in Section 5. The same terminology and notations have been used for all the above analytical models to facilitate their application.

2.6.1. Roberts' Analytical Model. Robert (1989) developed an analytical model based on partial interaction theory to predict the shear and normal stresses concentrations in adhesive joints for steel plate [19, 20]. His analytical model was developed in three stages. During the first stage, stresses were determined assuming full composite action between the reinforcement concrete beam and adhesive bonded steel plate. During the second and third stages, the analysis was modified to take into account the actual

boundary condition at the ends of the steel plate. The complete solution was then obtained by superposition. Roberts found that the shear and normal stress concentrations in the adhesive layer at the end of the steel plate depend significantly on the shear and normal stiffness of the adhesive and on the thickness and point of termination of the steel plate. He simplified further and omitted terms of minor significance in his analytical model to an acceptable level for predicting shear and normal stress concentration in the adhesive layer of plated RC structure. Considering the employment of CFRP plate instead of steel plate, the simplified maximum shear stress, τ_{max} , and normal stresses, σ_{max} , at the cutoff point of the plate were modified as showed below:

$$\tau_{max} = \left(F_0 + \left\{ \frac{K_s}{E_f b_f t_f} \right\}^{1/2} M_0 \right) \frac{b_f t_f}{I_{fr} b_a} (\bar{y}) \quad (2.1)$$

and

$$\sigma_{max} = \tau_{max} t_f \left(\frac{K_n}{4E_f I_f} \right)^{1/4} \quad (2.2)$$

where

$$K_s = G_a \frac{b_a}{t_a} \quad K_n = E_a \frac{b_a}{t_a} \quad (2.3)$$

in which F_0 = shear force at the end of laminate plate; M_0 = bending moment at the end of the laminate plate; K_s = shear stiffness per unit length of adhesive ; K_n = normal stiffness per unit length of adhesive; t_f = thickness of laminate plate; t_a = thickness of the adhesive layer; b_f = the width of steel plate; b_a = the width of adhesive; G_a = shear modulus of elasticity of the adhesive layer; E_f = elastic modulus of laminate plate; E_a = elastic

modulus of adhesive; I_{fr} = moment of inertia of transformed section based on laminate plate; \bar{y} = distance from neutral axis of the strengthened section to center of plate.

2.6.2. Malek's Analytical Model. Malek et al. (1998) developed an analytical model to predict the shear and normal stresses at the cutoff point of the FRP plate based on the following assumptions [21, 22]:

- (a) Linear elastic and isotropic behavior for FRP, epoxy, concrete and steel reinforcement;
- (b) Complete composite action between plate and concrete (no slip); and
- (c) Linear strain distribution through the full depth of the section.

The above assumptions did not oversimplify the behavior of this system since the plate cutoff point was usually taken near the inflection point or points of zero moments where the normal stresses are generally low. This justifies the assumption of linear elasticity for the materials. The predicted results of the analytical model indicated a good agreement with both the finite element method and the experimental results. His analytical models provided closed form solution for the maximum shear stress, τ_{max} , at the FRP plate end and can easily be incorporated into design equations.

$$\tau_{max} = t_f (b_3 \sqrt{A} + b_2) \quad (2.4)$$

where

$$A = \frac{G_a}{t_a t_f E_f} \quad (2.5a)$$

$$b_1 = \frac{\bar{y} a_1 E_f}{I_{tr} E_c} \quad (2.5b)$$

$$b_2 = \frac{\bar{y}E_f}{I_{tr}E_c}(2a_1L_0 + a_2) \quad (2.5c)$$

$$b_3 = E_f \left[\frac{\bar{y}}{I_{tr}E_c}(a_1L_0^2 + a_2L_0 + a_3) + 2b_1 \frac{t_a t_f}{G_a} \right] \quad (2.5d)$$

In the above expression, E_c = elastic modulus of concrete; I_{tr} = moment of inertia of transformed section based on concrete; and L_0 = distance between the support and the cutoff point (see Figure 2.1). In developing the above solution, the origin of the x has been assumed at the cutoff point of the plate. Furthermore, the equation of bending moment was assumed to be quadratic in the development of the previous equations

$$M(x_0) = a_1x_0^2 + a_2x_0 + a_3 \quad (2.6)$$

Parameter a_1 , a_2 and a_3 are derived from (6); furthermore, the origin of x_0 is arbitrary, and can be assumed at any convenient point at a distance L_0 from the cutoff point. In other words, $x_0 = x + L_0$ where x = longitudinal axis of FRP plate (see Figure 2.1).

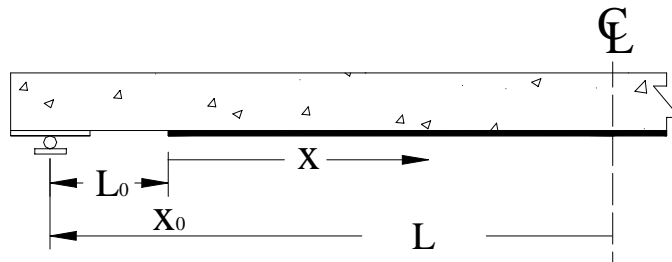


Figure 2.1: Longitudinal Distance

The maximum normal interfacial stress also occurs at the cutoff point ($x = 0$) and is expressed by:

$$\sigma_{\max} = \frac{E_a}{2b_a\beta^3t_a} \left(\frac{V_f}{E_fI_f} - \frac{V_c + \beta M_0}{E_cI_c} \right) + \frac{qE_fI_f}{b_fE_cI_c} \quad (2.7)$$

where
$$V_c = V_0 - b_f \bar{y}_c t_f (b_3 \sqrt{A} + b_2) \quad (2.8a)$$

$$V_f = -\frac{1}{2} b_f t_f^2 (b_3 \sqrt{A} + b_2) \quad (2.8b)$$

and

$$\beta = \left(\frac{E_a b_f}{4E_f I_f t_a} \right)^{0.25} \quad (2.8c)$$

in which M_0 = bending moment in the concrete beam at the cutoff point due to external load; q = external distributed load applied on concrete beam; V_c = shear force in the concrete beam; V_f = shear force in the plate beam; V_0 = shear force in the concrete beam at the cutoff point due to external load; \bar{y}_c = distance between the centroid and the bottom of concrete beam.

The results of the analytical study and finite-element analysis have shown very high shear stress at the location of the cracks. Therefore, debonding around the cracks cannot be avoided and the effect of the debonded length on the nominal moment needs to be investigated further.

3. EXPERIMENTAL PROGRAM

3.1. DESCRIPTION OF RC BEAMS

A total of five slabs having nominal dimensions: 1000 x 220 x 6300 mm (39.4 x 8.6 in x 20.8 ft) were cast with ready-mix concrete and cured under normal laboratory condition. All the slabs were reinforced in the longitudinal with four $\phi 13$ mm (#4) deformed steel bars at the interior and two $\phi 10$ mm (#3) grade 420 (60) deformed steel bars at both edges. The reinforcing steel bars were tied with $\phi 10$ mm (#3) steel bars, spaced at 200 mm (7.9 in.) center-to-center. The total reinforcement corresponded to the minimum reinforcement as specified by the European (EC2) and North American standards (ACI 318-02). The minimum clear cover for the slabs was 0.03 m (1.2 in.). Details of the slab reinforcement are given in Figure 3.1. Four foil strain gages were attached to the interior steel bars before the concrete was poured (see Figure 3.2).

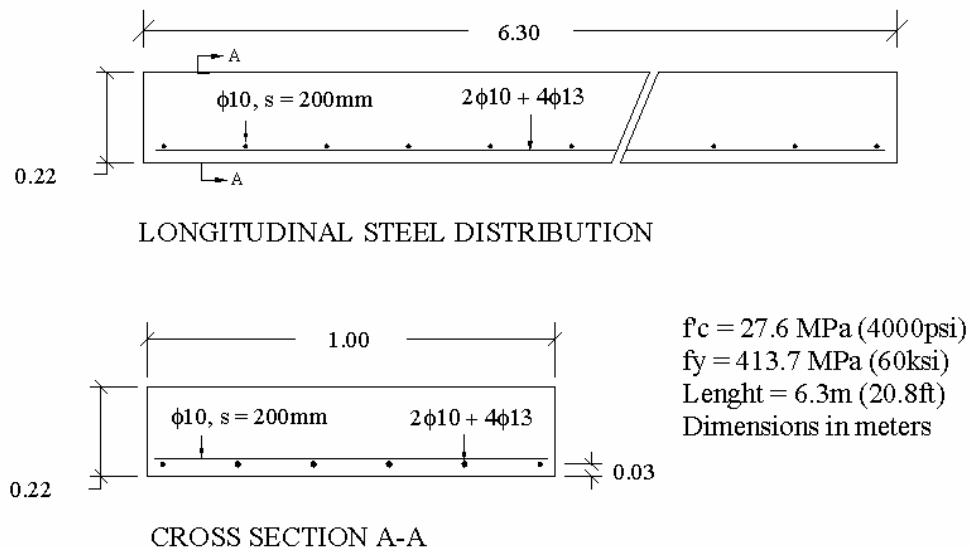


Figure 3.1: Typical Cross Section of Slabs

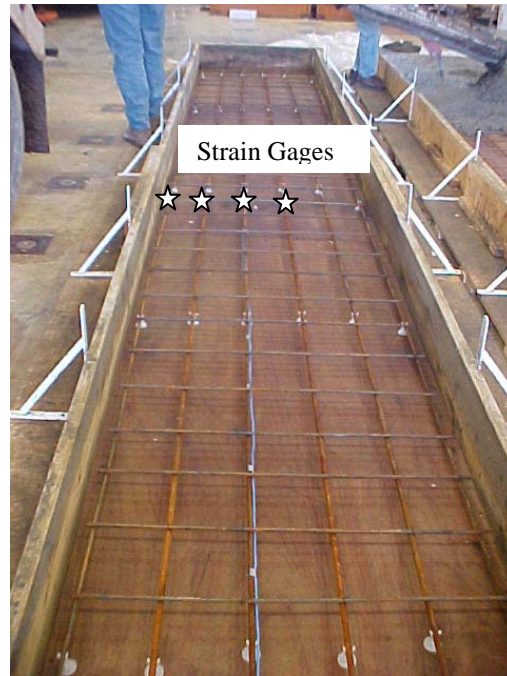
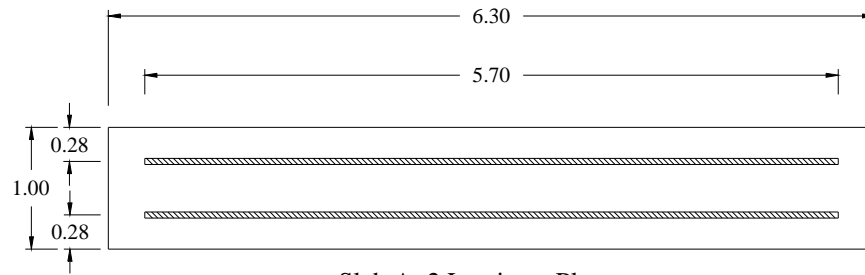
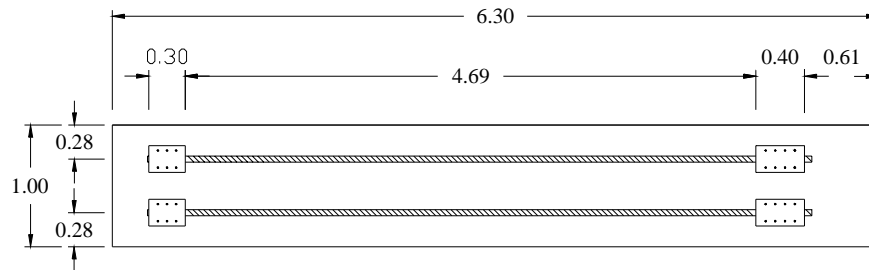


Figure 3.2: Steel Distribution for A Typical Slab

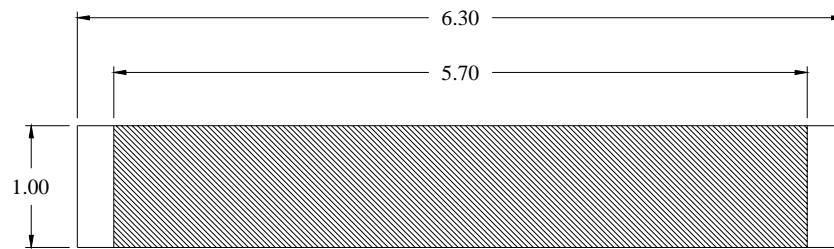
Three different available CFRP strengthening systems, which include prefabricated CFRP plates, carbon fiber sheets and prefabricated CFRP bars fabricated by S&P Clever Reinforcement Company of Switzerland were used for the research. The first slab was used as the control slab and the others, which were identified as Slabs A, B, C and D, were strengthened with different CFRP EBR techniques. Slab A was strengthened with 2 strips of cold cured adhesive bonding CFRP plates, Slab B was strengthened with 2 strips of prestressed CFRP plates, Slab C was strengthened with one ply of manual lay-up carbon fiber sheet and Slab D was strengthened with 8 strips of near surface mounted (NSM) CFRP bars. The detailed drawings of the strengthened slabs are given in Figure 3.3 and summarized in Table 3.1. All strengthened slabs were tested after a curing period, under normal laboratory conditions, of 7 days of the adhesive.



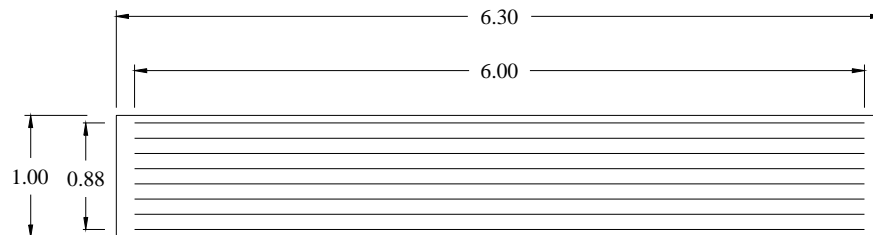
Slab A: 2 Laminate Plates



Slab B: 2 Prestressing Laminate plates



Slab C: 1 Ply Fiber Laminate Sheet



Slab D: 8 Laminate Bars

Figure 3.3: Detailed drawing of Slab A-D (Dimension in meter)

Table 3.1: Test Matrix

<i>Slab</i>	<i>EBR Techniques</i>	<i>Strengthening</i>
<i>Control</i>	<i>N/A</i>	<i>N/A</i>
<i>A</i>	<i>Cold cured adhesive bonding</i>	<i>2 strips of CFRP plates</i>
<i>B</i>	<i>Prestressing</i>	<i>2 strips of CFRP plates</i>
<i>C</i>	<i>Manual wet lay-up</i>	<i>1 ply of carbon fiber sheet</i>
<i>D</i>	<i>Near surface mounted</i>	<i>8 strips of CFRP bars</i>

3.2. MATERIAL PROPERTIES

3.2.1. Concrete. All slabs were cast at different periods with ready-mix concrete. The slabs were maintained above 10 °C (50 °F) in a moist condition for the first 7 days and cured under normal laboratory conditions for 28 days after being cast. Three cylindrical concrete specimens measuring 150 mm (6 in.) in diameter and 300 mm (12 in.) long for each batch of ready-mix concrete were cast and tested on the 28th day. The compressive strength of the cylindrical concrete specimens was tested based on ASTM C39-96. During the compression test, the load was maintained at 1000 pounds/sec until the maximum compressive strength, f'_c , was reached in 2 to 3 minutes. Table 3.2 shows the compressive strength for each slab at the 28th days.

3.2.2. Steel. Three coupons of each ϕ 10 mm (#3) and ϕ 13 mm (#4) deformed steel bars were tested under uniaxial tension in accordance with ASTM A370-90A. The yield stress for ϕ 13 mm (#4) deformed steel bars was 427.5 MPa (62 ksi) and the ultimate stress was 586 MPa (85 ksi). In the case of ϕ 10 mm (#3) deformed steel bars, the yield

stress was 358.5 MPa (52 ksi) and the ultimate stress was 489.5 MPa (71 ksi). An average yield stress of 413.7 MPa (60 ksi) and a modulus of elasticity of 200 GPa (29000 ksi) were used for the analytical study in Section 5.

Table 3.2: Average Concrete Compressive Strength at 28 days

<i>Slab</i>	<i>Average Concrete Compressive Strength, MPa (psi)</i>
<i>Control Slab</i>	30.2 (4380)
<i>A</i>	33.8 (4900)
<i>B</i>	33.8 (4900)
<i>C</i>	42.4 (6140)
<i>D</i>	42.3 (6130)

3.2.3. Prefabricated CFRP Plate. The CFRP plate was fabricated a in cross-section of 50 x 1.2 mm (2.0 x 0.047 in.) by pultrusion. For technical reasons, the pultrusion method is limited to 70% carbon fiber content. The elastic properties of a unidirectional layer can be calculated from the performance of the fiber and the matrix. According to the manufacturer, the modulus of elasticity for the laminate plate is 164 kN/mm² (23 Msi) and the ultimate tensile strength is 2900 N/mm² (420 ksi). The ultimate elongation is 1.6% (see Table 3.3).

An independent test was performed to characterize the tensile properties of the CFRP laminate plate based on the ASTM D3039-00. The CFRP laminate plate was cut into a 300 mm (12 in.) length and tabbed with aluminum plates using epoxy gel (see

Figure 3.4). An active foil strain gage length of 12.7 mm (0.5 in.) was attached to the specimen, symmetrically about the mid-span, mid-width location. A total of five specimens were prepared and tested with the MTS machine under normal laboratory conditions. The speed of testing was set at 17.8 kN/min (4000 lb/min). Table 3.4 summarizes the test results and Figure 3.5 shows the failure mode of the specimens. Due to the bond failure at the grip, the test results for the third specimen were not taken into consideration. The plots of stress versus strain curves for determination of elastic modulus are shown in Appendix A.

The average E-modulus and tensile strength of the test specimens were 179 kN/mm² (25.9 Msi) and 2580 N/mm² (375 ksi), which were higher than the numbers given by the manufacturer. However, the average ultimate strain was 1.51%, lower than the ultimate strain given by the manufacturer.

Table 3.3: Mechanical Properties of the CFRP Systems

<i>CFRP System</i>	<i>Thickness mm (in.)</i>	<i>E_f kN/mm² (Msi)</i>	<i>Tensile strength, N/mm² (Ksi)</i>	<i>Ultimate strain, %</i>
<i>CFRP Plate</i>	1.2 (0.047)	164 (23.8)	2500 (360)	1.60
<i>Carbon Fiber sheet</i>	0.117 (0.005)	240 (34.8)	3800 (550)	1.55
<i>CFRP Bar</i>	1.4 (0.055)	164 (23.8)	2900 (420)	1.80

* Provided by S&P Clever Reinforcement Company, Brunnen, Switzerland

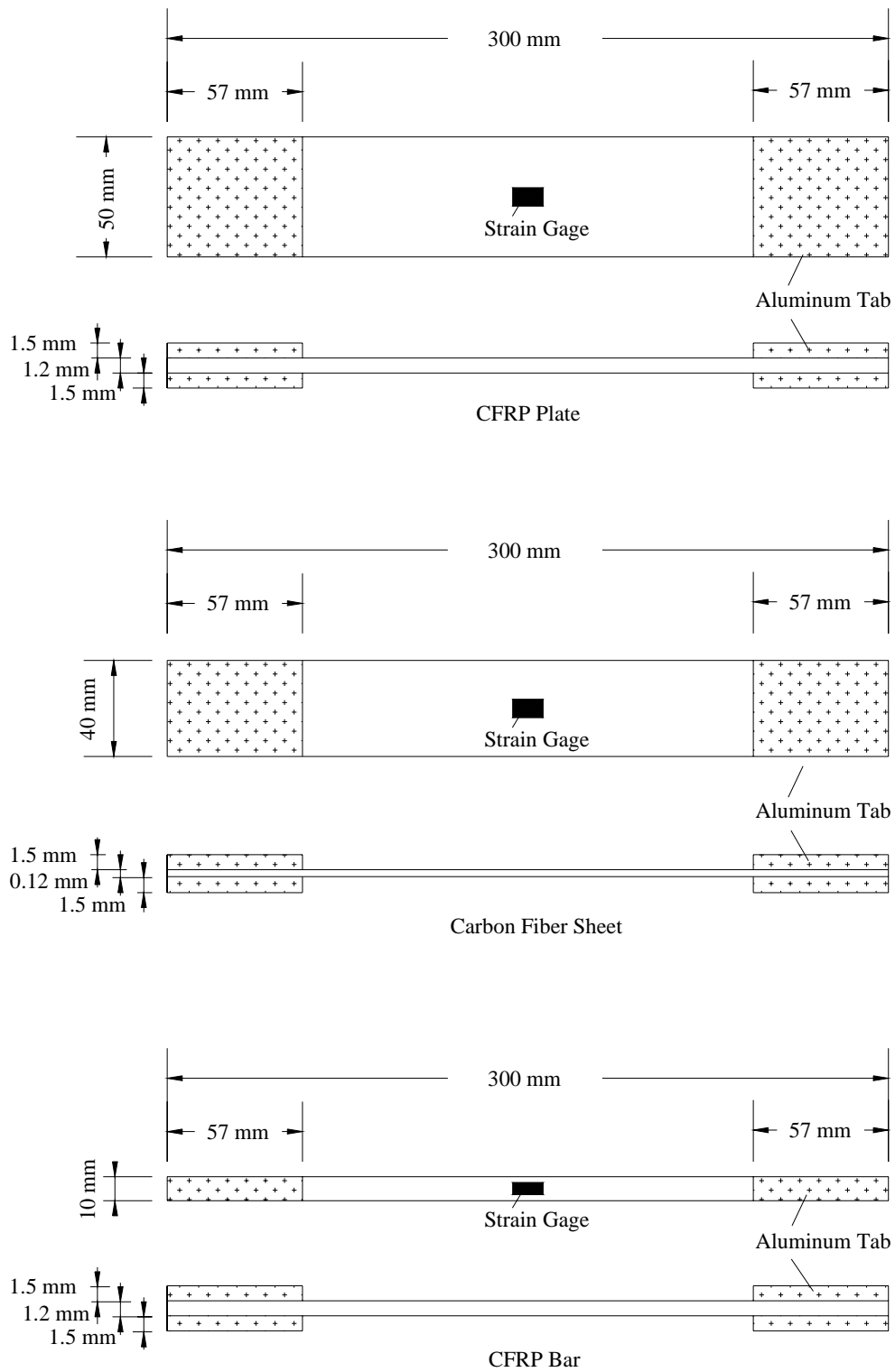


Figure 3.4: Test Specimens

Table 3.4: Test Result for Tensile Properties of CFRP Plate

<i>Specimen</i>	E_f <i>kN/mm²</i> <i>(Msi)</i>	<i>Tensile strength,</i> <i>N/mm² (Ksi)</i>	<i>Ultimate strain, %</i>	<i>Failure Type / Area / Location</i>
1	180 (26.1)	2560 (371)	1.58	<i>Explosive / Gage / Middle</i>
2	187 (27.1)	2960 (430)	1.64	<i>Lateral / At grip / Top</i>
3	--	--	--	<i>Grip / At grip / Bottom</i>
4	179 (25.9)	2520 (365)	1.44	<i>Splitting / At grip / Top</i>
5	172 (25.0)	2300 (333)	1.39	<i>Splitting / At grip / Bottom</i>
<i>Average</i>	179 (25.9)	2580 (375)	1.51	<i>N/A</i>
S_{n-1}	5.32	241	0.10	<i>N/A</i>
<i>CV (%)</i>	3.11	9.34	6.62	<i>N/A</i>

S_{n-1} : Standard deviation; CV: Coefficient of variation;

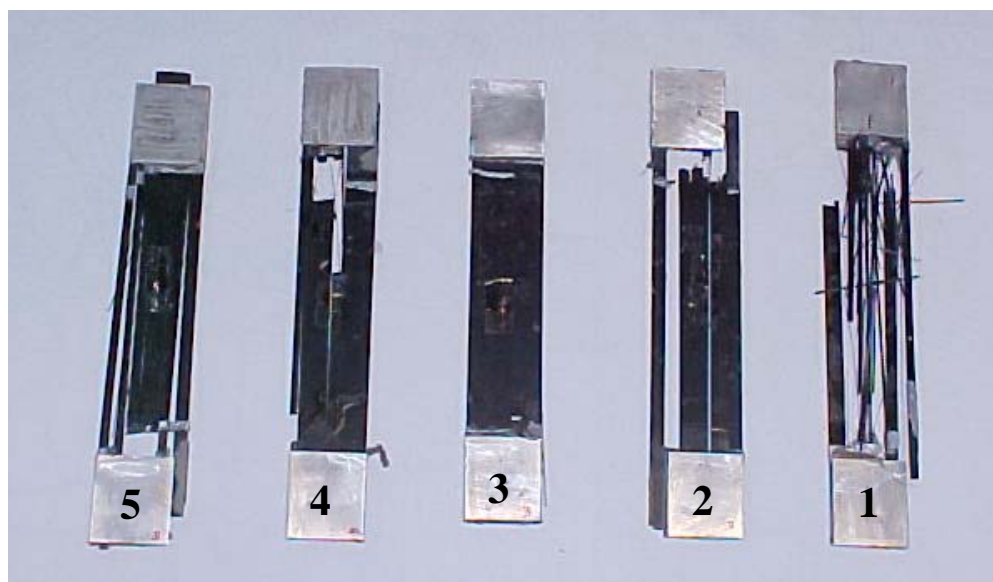


Figure 3.5: Tensile Test Failure Modes for CFRP Plate

3.2.4. Carbon Fiber Sheet. The unidirectional carbon fiber sheet was fabricated in widths of 300 mm (12 in.). The theoretical thickness (C fiber only) of the carbon sheet is 0.117 mm (0.005 in.) and the density is 200g/mm^3 . According to the manufacturer, the modulus of elasticity for the laminate sheet is 240 kN/mm^2 (34.8 Msi) and the tensile strength is 3800 N/mm^2 (550 ksi). The ultimate elongation is 1.55%.

The tensile properties of the carbon fiber sheet were tested based on ASTM D3039-00. A ply of carbon fiber laminate sheet was impregnated with saturant and cured under normal laboratory condition. After curing for 24 hours, the carbon fiber laminate sheet was cut into a size of 300 x 40 mm (12 x 1.6 in.) and tabbed with aluminum plates using epoxy gel (see Figure 3.4). An active foil strain gage length of 12.7 mm (0.5 in.) was attached to the specimen, symmetrically about the mid-span, mid-width location. A total of five specimens were prepared and tested with the MTS machine. The speed of testing was set at 24.5 kN/min (5500 lb/min). Table 3.5 summarizes the test results and Figure 3.6 shows the failure modes of the specimens. The average E-modulus, tensile strength and ultimate strain of the test specimens were 216 kN/mm^2 (31.4 Msi), 2390 N/mm^2 (347 ksi) and 1.28%, respectively. All the test results were lower than the numbers given by the manufacturer.

3.2.5. Prefabricated CFRP Bar. The CFRP bar was fabricated in a cross-section of 10 x 1.4 mm (0.4 x 0.06 in.) by pultrusion, with 70% fiber content. According to the manufacturer, the modulus of elasticity for the laminate bar is 164 kN/mm^2 (23 Msi) and the ultimate tensile strength is 2900 N/mm^2 (420 ksi). The ultimate elongation is 1.8%.

The tensile properties of the CFRP bar was tested based on ASTM D3039-00. The CFRP laminate bar was cut into a 300 mm (12 in.) length and tabbed with aluminum plates as shown in Figure 3.4. An active foil strain gage length of 12.7 mm (0.5 in.) was attached to the specimen, symmetrically about the mid-span, mid-width location. A total of five specimens were prepared and tested with the MTS machine. The speed of testing was set at 24.5 kN/min (5500 lb/min). Table 3.6 summarizes the test results and Figure 3.7 shows the failure mode of the specimens. All the test specimens ruptured at the mid span during the tests. The average E-modulus, tensile strength and ultimate strain of the test specimens were 2490 N/mm² (361 ksi) and 1.49%, respectively. The average E-modulus from the test results showed higher values compared to the numbers given by the manufacturer. The tensile strength and ultimate strain, however, were lower than the manufacturer's numbers.

Table 3.5: Test Result for Tensile Properties of Carbon Fiber Sheet

<i>Specimen</i>	E_f <i>kN/mm² (Msi)</i>	<i>Tensile strength,</i> <i>N/mm² (Ksi)</i>	<i>Ultimate</i> <i>strain, %</i>	<i>Failure</i> <i>Type / Area / Location</i>
1	216 (31.1)	2350 (341)	1.32	<i>Lateral / At grip / Top</i>
2	237 (34.3)	2730 (396)	1.20	<i>Lateral / At grip / Top</i>
3	226 (32.7)	2460 (356)	1.31	<i>Lateral / Gage / Middle</i>
4	197 (28.6)	2150 (312)	1.32	<i>Lateral / At grip / Top</i>
5	206 (29.8)	2270 (329)	1.23	<i>Lateral / Gage / Middle</i>
<i>Average</i>	216 (31.4)	2390 (347)	1.28	<i>N/A</i>
S_{n-1}	15.8	220	0.06	<i>N/A</i>
<i>CV (%)</i>	7.31	9.21	4.45	<i>N/A</i>

S_{n-1} : Standard deviation; CV: Coefficient of variation

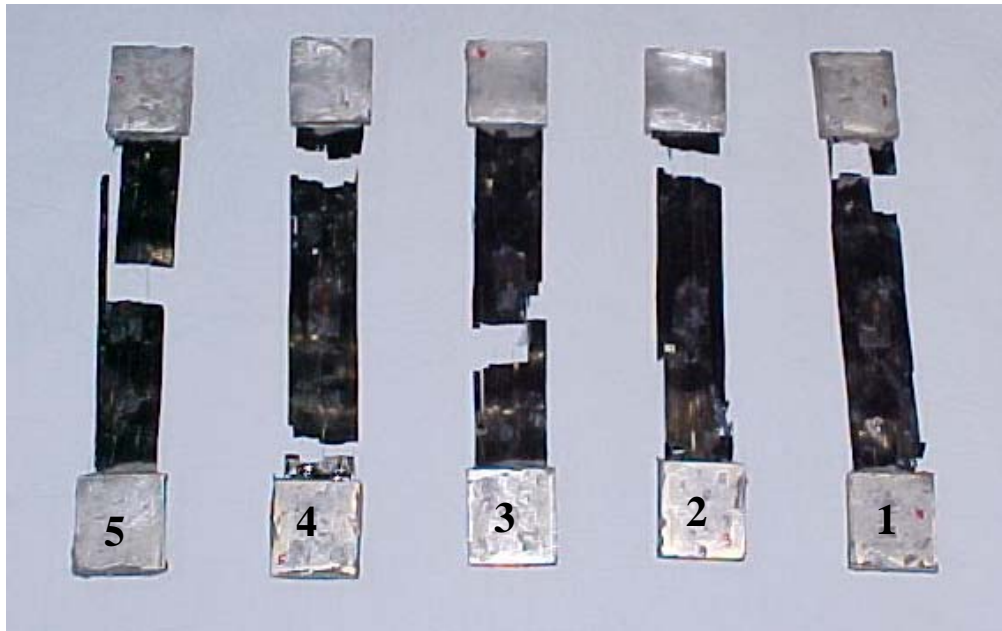


Figure 3.6: Tensile Test Failure Modes for Carbon Fiber Sheet

Table 3.6: Test Result for Tensile Properties of CFRP Bar

<i>Specimen</i>	E_f <i>kN/mm² (Msi)</i>	<i>Tensile strength,</i> <i>N/mm² (Ksi)</i>	<i>Ultimate</i> <i>strain, %</i>	<i>Failure</i> <i>Type / Area / Location</i>
1	179 (25.9)	2920 (424)	1.70	<i>Explosive / Gage / Middle</i>
2	178 (25.8)	2680 (388)	1.55	<i>Explosive / Gage / Middle</i>
3	170 (24.6)	2460 (357)	1.44	<i>Explosive / Gage / Middle</i>
4	169 (24.5)	2080 (302)	1.29	<i>Explosive / Gage / Middle</i>
5	170 (24.6)	2290 (332)	1.47	<i>Explosive / Gage / Middle</i>
<i>Average</i>	173 (25.1)	2490 (361)	1.49	<i>N/A</i>
S_{n-1}	4.87	328	0.15	<i>N/A</i>
<i>CV (%)</i>	2.81	13.2	10.1	<i>N/A</i>

S_{n-1} : Standard deviation; CV: Coefficient of variation

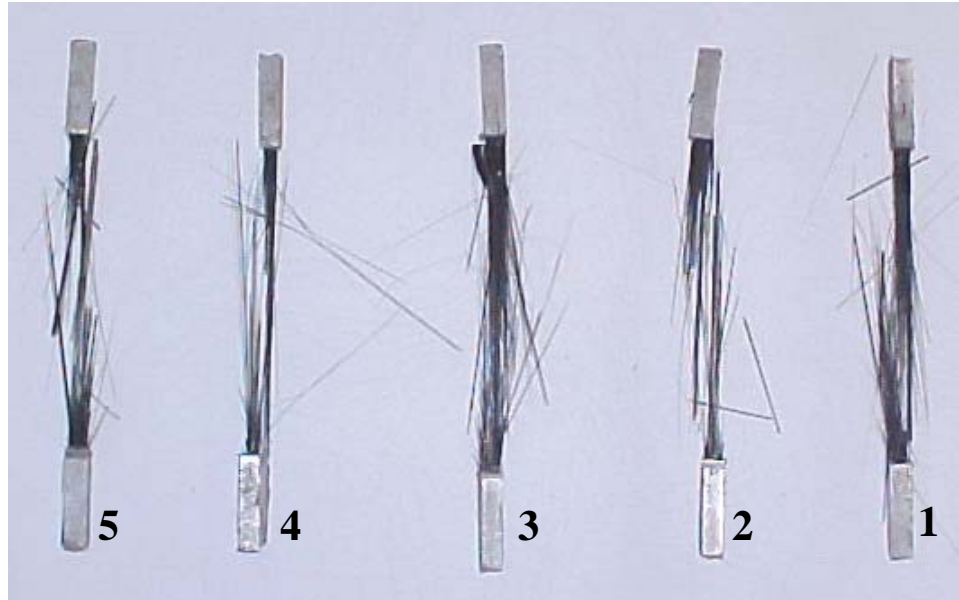


Figure 3.7: Tensile Test Failure Modes for CFRP Bar

3.2.6. Adhesive. Two types of adhesive, epoxy gel and saturant, were used in this experimental program. The epoxy gel is a 100% solid, high modulus, high strength, and moisture insensitive system and the saturant is a standard viscosity epoxy priming resin. Both are two-component systems. After mixing, the epoxy gel adhesive has a paste like consistency while the saturant has a liquid form. Application at ambient temperature below 40 °F is not recommended. Table 3.7 summaries the adhesive properties provided by the manufacturer.

An independent test was performed to characterize the Poisson's ratio of the epoxy gel based on ASTM E132-97. The epoxy gel was mixed and cured at room temperature for 7 days before it was cut into a 250 mm (12 in.) length and 40 mm (1.25 in.) width. The average thickness for the specimens was 3.8 mm (0.15 in.). (See Figure 3.8.) An active Stacked Rosettes was attached to the specimen, symmetrically about the

mid-span, mid-width location. A total of five specimens were prepared and tested with the MTS machine under normal laboratory conditions. The speed of testing was set at 580 N/min (130 lb/min). Table 3.8 summarizes the test results and Figure 3.9 shows the failure modes of the specimens. The plots of strain versus load for determination of elastic modulus and Poisson's ratio are showed in Appendix A. The average tensile strength and ultimate strain of the test specimens were considerably lower than the numbers given by the manufacturer.

Table 3.7: Mechanical Properties of Adhesive

<i>Adhesive</i>	<i>Tensile Strength, N/mm² (ksi)</i>	<i>Compression Strength, N/mm² (ksi)</i>	<i>Bond Strength*, N/mm² (Psi)</i>	<i>Elongation at 77⁰F, %</i>
<i>Epoxy gel</i>	69 (10)	96.5 (14)	4.1 (600)	2
<i>Saturant</i>	69 (10)	82.8 (12)	3.4 (500)	2

*Provided by the manufacturer; * After 24 hour*

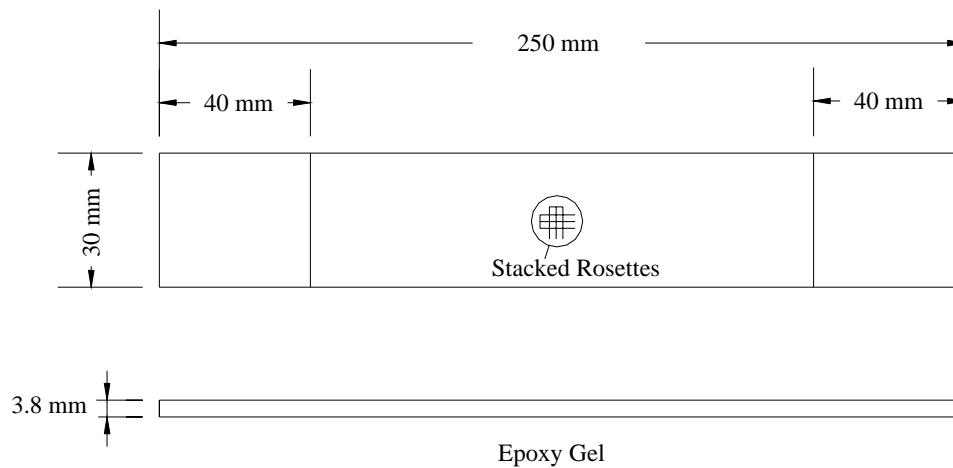


Figure 3.8: Test Specimen for Epoxy Gel

Table 3.8: Test Result for Tensile Properties of Epoxy Gel

<i>Specimen</i>	E_f <i>kN/mm² (ksi)</i>	<i>Tensile strength,</i> <i>N/mm² (psi)</i>	<i>Ultimate</i> <i>strain, %</i>	<i>Poisson's</i> <i>Ratio</i>
1	1.75 (254)	16.1 (2330)	0.97	0.44
2	1.81 (263)	17.2 (2500)	1.07	0.42
3	1.51 (219)	16.7 (2420)	1.21	0.46
4	1.76 (256)	20.2 (2930)	1.36	0.41
5	1.70 (247)	19.3 (2800)	1.32	0.43
<i>Average</i>	1.71 (247)	17.9 (2600)	1.19	0.43
S_{n-1}	0.12	1.76	0.16	0.02
<i>CV (%)</i>	7.02	9.83	13.4	4.65

S_{n-1} : Standard deviation; CV: Coefficient of variation

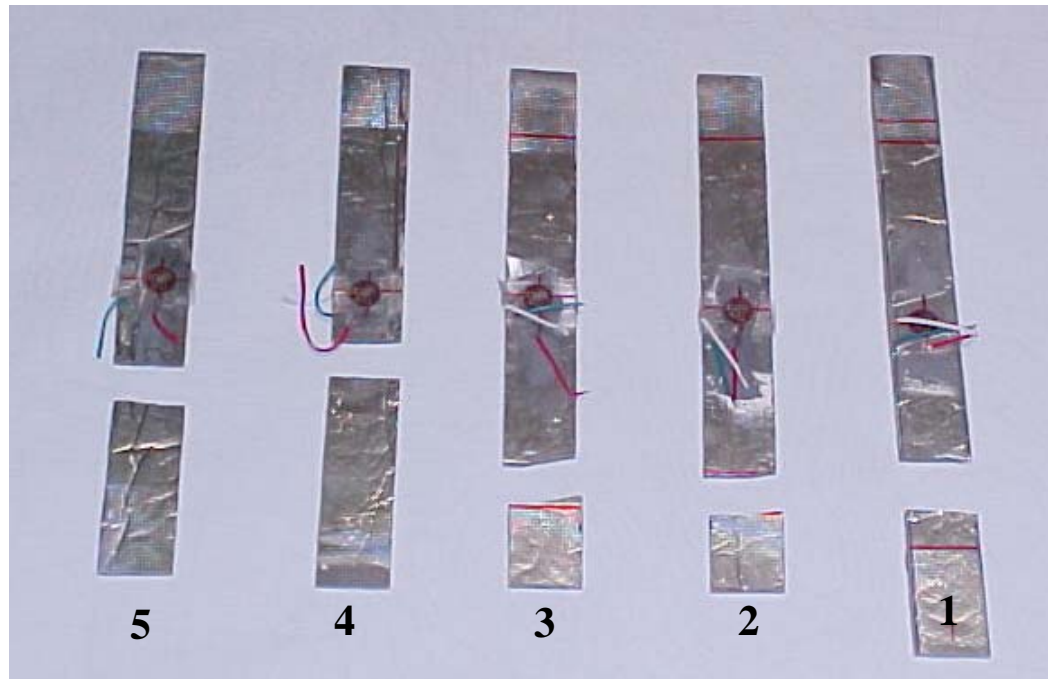


Figure 3.9: Tensile Test Failure Modes for Epoxy Gel

3.3. INSTALLATION PROCEDURES

All concrete surfaces were sandblasted and cleaned to ensure good bonding before strengthening. The adhesive was mixed in a 2:1 ratio by volume until it was uniform and complete mixing was observed.

3.3.1. Slab A: Cold Cured Adhesive Bonded CFRP Plate. The epoxy gel was spread to areas where the CFRP plate has contact. The CFRP plate was cut into the design length, cleaned with acetone and pressed into the wet epoxy gel. Trapped air was released by rolling. The thickness of the epoxy gel was maintained at approximately 1.5 mm (0.06 in.). (See Figure 3.10.)



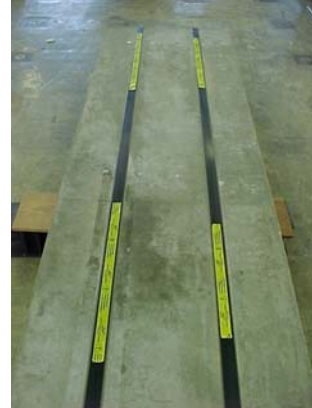
(a) Two component epoxy gel



(b) Press with hard roller



(c) 1.5 mm thickness of Epoxy.



(d) Installation accomplished

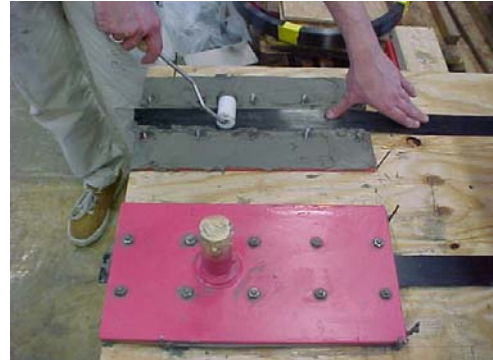
Figure 3.10: Cold Cured Adhesive Bonded CFRP Plate

3.3.2. Slab B: Prestressed CFRP Plate. The installation of prestressed CFRP plate is illustrated in Figure 3.11. It started with the preparation of the moveable anchorage. This consists of gluing one end of the CFRP plate between two steel plates, held in place by means of screws. After the moveable anchorage was cured for 24 hours, the first fixed anchorage was installed and the CFRP plate was glued between the steel plate and the concrete surface. The steel plate was fastened to the concrete surface with six Hilti HSA-M12 anchor bolts. The anchor bolt was 12 mm (0.3 in.) in diameter and 100 mm (2.5 in.) in length, respectively. The penetration depth was 70 mm (1.78 in.). The recommended tensile and shear force for the anchor bolt in un-crack concrete are 9.5 kN (2.1 kips) and 10.8 kN (2.4 kips), respectively. The fixed anchorage was cured for another 24 hours before the CFRP plate could be stressed. While waiting for the fixed-end anchorage to cure, another fixed anchorage was attached from the other end of the slab, to the concrete surface with eight anchor bolts. After both fixed anchors have been installed, the system was ready for prestressing. During the prestressing process, an epoxy gel was spread uniformly on all areas of the concrete surface where the laminate has contact. The thickness of the epoxy gel was approximately 1.5 mm (0.06 in.). Trapped air was released by rolling. The CFRP plate was stressed by programmed

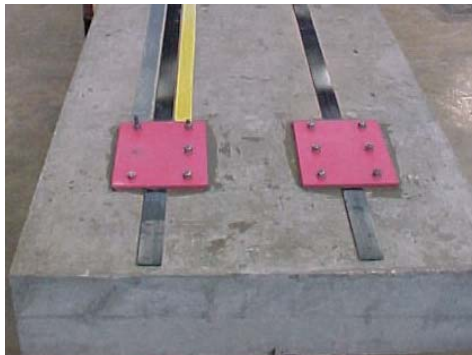
hydraulic machinery in a time interval pattern until it reached an initial elongation of 5% , which represented 31% of the ultimate strain (see Figure 3.12). Based on the elastic modulus given by the manufacturer, the total prestressed force for two strips of CFRP plates was 98 kN (22 kip). After the epoxy gel cured, the moveable anchors were removed while the fixed anchors remained in place.



(a) Clean with acetone



(b) Sandwich the CFRP plate



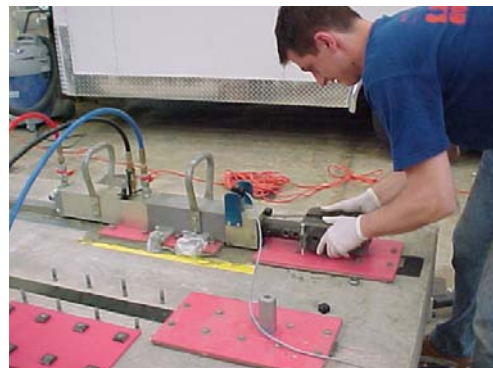
(c) Six bolts fixed anchorage



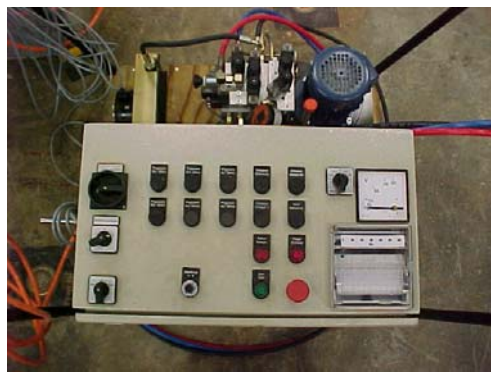
(d) Eight bolts fixed anchorage



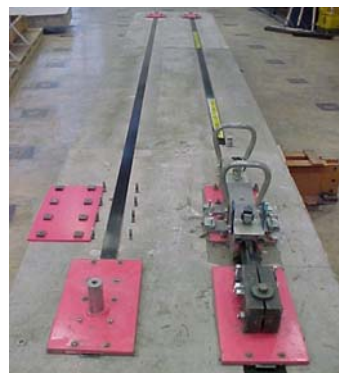
(e) Apply epoxy before prestressing



(f) Fix the prestressing kit



(g) Programmed hydraulic machinery



(h) Curing after prestressing

Figure 3.11: Prestressing CFRP Plate

Figure 3.13 shows the strain versus time curves 18 hours after prestressing. The strains showed noticeable losses in the first hour after prestressing and they stabilized thereafter. The total losses after 18 hours was 6%.

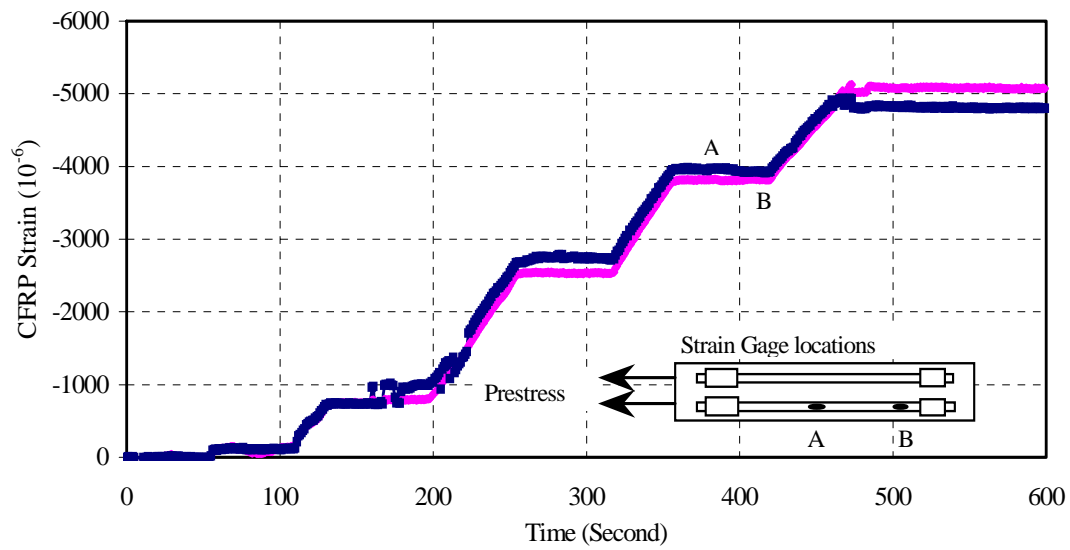


Figure 3.12: Strain vs. Time Curves for Prestressed CFRP Plate

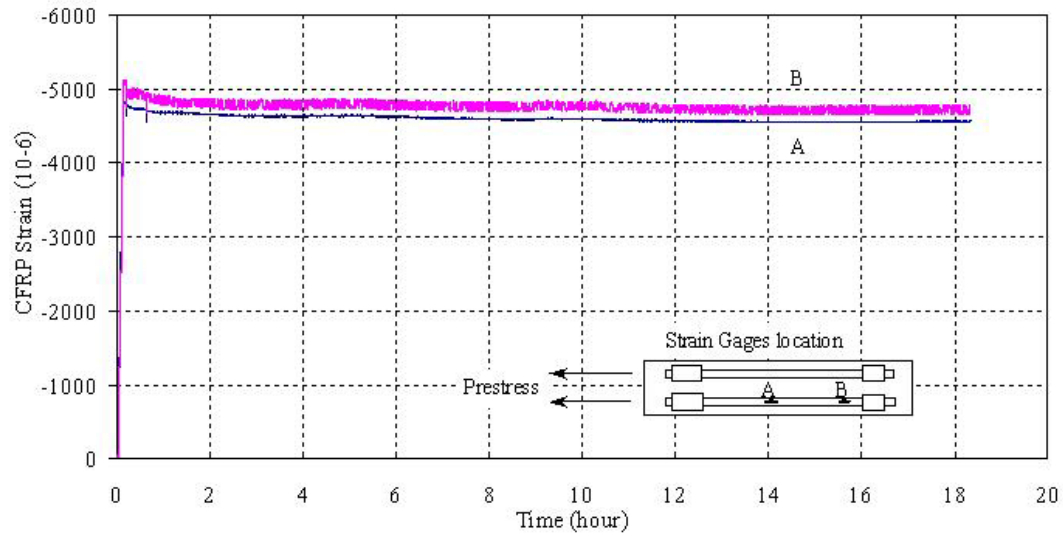


Figure 3.13: Strain vs. Time Curves for Prestressed CFRP Plate After 18 Hours

3.3.3. Slab C: Manual Wet Lay-up Carbon Fiber Sheet. An adequate layer of saturant was spread uniformly on all areas where the carbon fiber sheet was to be placed. A single layer of CFRP laminate sheet was cut into design length and pressed down with a “bubble roller” to eliminate the trapped air and impregnate the laminate sheet with saturant. A second layer of saturant was reapplied to obtain complete impregnation prior to curing of the first layer of saturant (see Figure 3.14).



(a) Start at 11 in. from the edge. (b) Installation accomplished

Figure 3.14: Manual Lay-up Carbon Fiber Sheet

3.3.4. Slab D: Near Surface Mounted CFRP Bar. A total of eight 3mm (1/8 in.) wide and 15 mm (5/8 in.) deep slots were sawed 126 mm (5.0 in.) center-to-center at the substrate of the Slab D. The slots were vacuum cleaned and filled with saturant. The CFRP bars were cut into design length, cleaned with acetone and lightly pressed into the slots. The slots were refilled after part of the saturant was absorbed by the micro-cavities of the concrete (see Figure 3.15).



(a) 3 mm wide x 15 mm deep slots



(b) Filling slots with saturant



(c) Press down the CFRP bar



(d) Refill the slots with saturant

Figure 3.15: Near Surfaced Mounted CFRP Bars

3.4. TIME CONSUMPTION FOR INSTALLATION

Figure 3.16 shows the Gantt chart for each strengthened slab. The cold cured adhesive bonding (Slab A) and manual lay-up (Slab C) seems to be easy and fast compared to the other two strengthening techniques. However, surface preparation for site condition is usually more complicated and often more time consuming.

A total of 76 hours was needed to accomplish the entire prestressing process (Slab B). However, the labor-intensive portion of the process was low since most of the time was used to cure the epoxy gel. The near surface mounted reinforcement (Slab D) can be expedited if a suitable tool was used to saw the concrete. NSM reinforcement usually involves less surface preparation and is less time consuming when strengthening deteriorated structures.

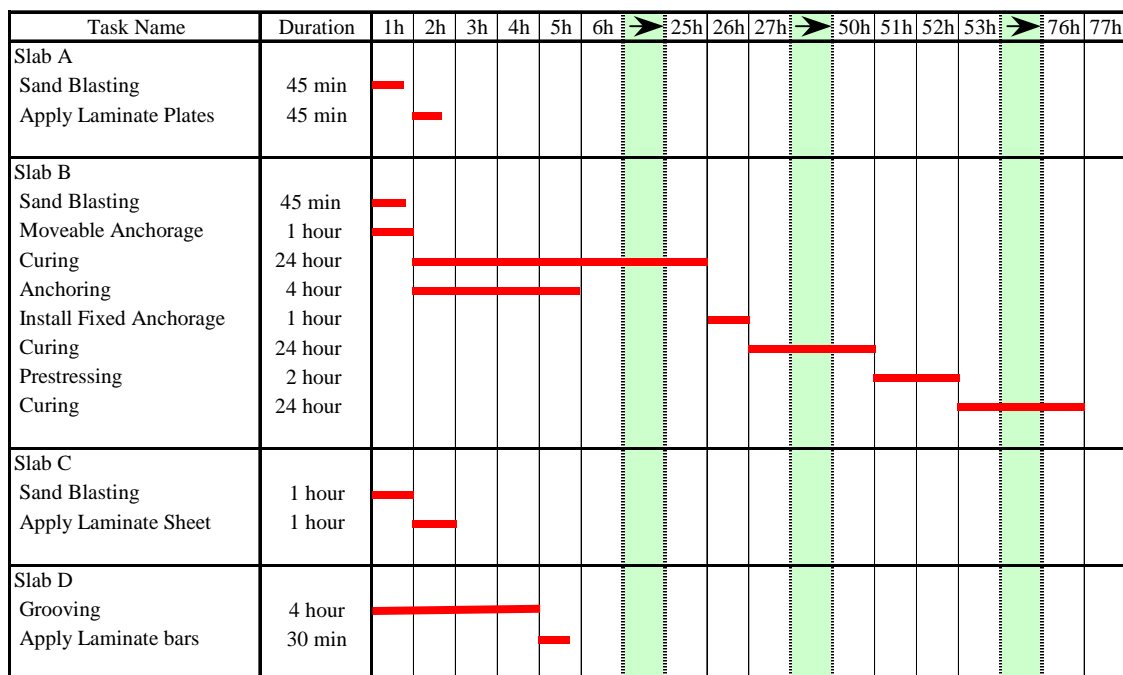


Figure 3.16: Gantt Chart for Strengthening Process

3.5. TEST SETUP AND TEST PROCEDURE

Two heavy-duty pin rollers were used to support the slab on a span of 6.0 m (20 ft). These pin rollers provided bearing and frictionless rotational action during the test. All slabs were tested to failure under a symmetric 6-point concentrated static loading system. The distance between each point load was 1.2 m (4 ft). (See Figure 3.17 and 3.18).

Two 445 kN (100 kip) and 89 kN (20 kip) capacity load cells were placed between the 1334 kN (300 kip) capacity hydraulic jack and top supporting beam on both side of the racks to record the applied load. During the test, the loads were applied in cycles: one cycle before cracking of the concrete and two cycles before yielding of the steel. The total number of cycles depended on the maximum predicted load. By applying the load in cycles, the stability of the system could be checked. The 89 kN (20 kip) load cell was used as the main reference source of data collection because it provided more accurate results. The 445 kN (100 kip) load cell was used to countercheck the readings of the first load cell and ensure that both hydraulic jacks applied equal pressure. The test results presented in the next section will only refer to the readings collected by the 89 kN (20 kip) load cell.

Strain gages were attached to the center of the concrete top surface, steel and along the CFRP systems. An array of five Linear Variable Differential Transducers (LVDTs) was placed at 1.5 m (5 ft) from each other, starting from the supporting edge, for displacement readings. The strain distribution on CFRP systems as well as steel and

concrete, and the flexural behavior of the test specimens were examined experimentally. The data was collected by a data acquisition system at a frequency of 1Hz.

The loading set-up was designed to accommodate large deflection without generating undesirable forces on equipments or specimen. In fact, the loading jacks reacted against spreader beams anchored to the structural floor by means of DYWIDAG rods. The stiffness of such rods was sufficiently low to allow rotation of the loading apparatus to follow the contour of the specimen. Figure 3.19 clearly illustrates the situation described above. Figure 3.20 illustrates all apparatus that were used to test the slabs.

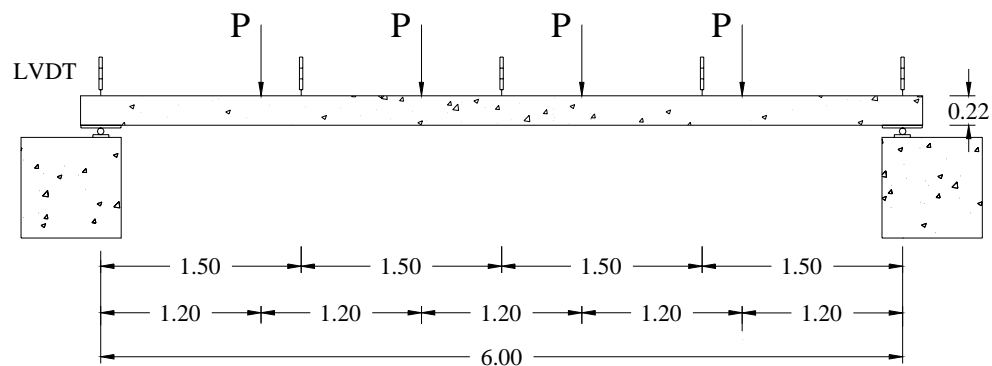


Figure 3.17: Test Arrangement (Dimension in meter)

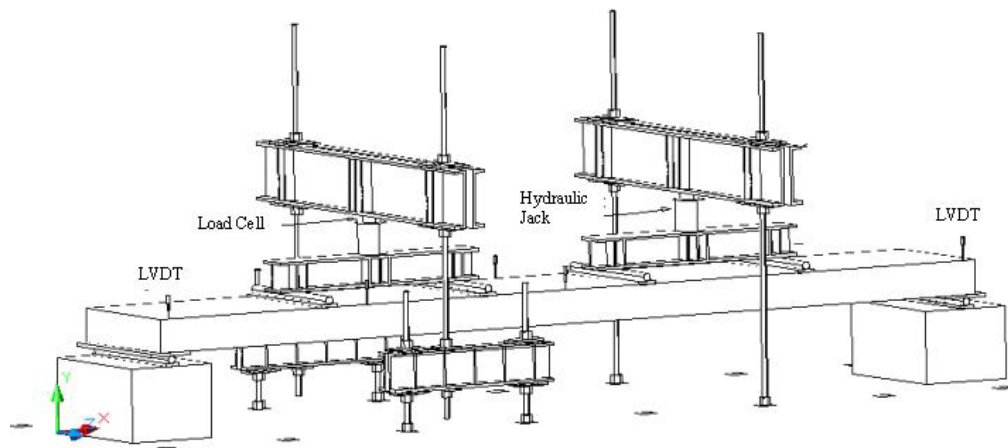


Figure 3.18: Test Setup

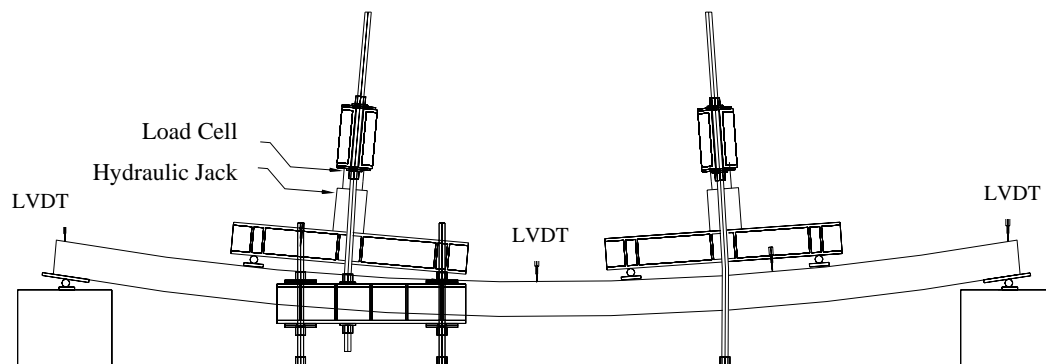


Figure 3.19: Test Setup Deformation



(a) Test setup



(b) Hydraulic jack and load cell



(c) Heavy-duty pin roller support



(d) LVDT

Figure 3.20: Test Apparatuses

4. TEST RESULTS

4.1. MODE OF FAILURE

A measure of the efficiency of the different systems can be obtained by considering the modes of failure and the failure loads of the slabs. Results are presented in Table 4.1. The normalized increment is calculated by dividing the moment increment in column 5 by the axial stiffness ratio of CFRP over steel reinforcement in column 2. Figures 4.1 to 4.5 illustrate the specimens after failure.

Table 4.1: Test Results

<i>Slab</i>	$E_f A_f / E_s A_s$, (%)	<i>Failure load, P</i> <i>kN (Kip)</i>	<i>Failure moment*</i> , <i>kN-m (k-ft)</i>	<i>Moment Increment</i> , (%)	<i>Normalized Increment</i> **
(1)	(2)	(3)	(4)	(5)	(6)
<i>Control</i>	--	5.6 (1.26)	46.8 (34.5)	--	--
<i>A</i>	15.3	13.7 (3.08)	76.3 (56.3)	63	4.1
<i>B</i>	15.3	20.8 (4.65)	102.2 (75.4)	118	7.7
<i>C</i>	21.8	21.3 (4.78)	104.0 (76.6)	122	5.6
<i>D</i>	14.2	24.1 (5.43)	114.6 (84.5)	145	10.2

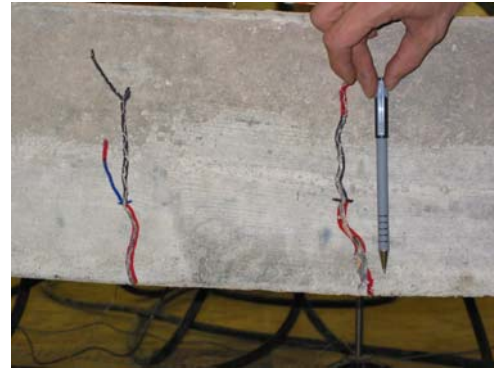
*Include slab self-weight; ** Column 5 divided by column 2

4.1.1. Control Slab. The Control Slab behaved in expected fashion under flexural loading. As loads increased, flexural cracks increased in number, width and depth. The first crack was observed immediately after applying the load. The flexural cracks were distributed equally between 10-16 cm (4-6 in.) at the constant moment region (see

Figure 4.1). The test was discontinued after the steel yielded before the concrete crushed at a load of 5.60 kN (1.26 kips) due to excessively large cracks at the tension zone. The Control Slab was used as a baseline to compare the remaining strengthened slabs (see Table 4.1).



(a) Flexural failure



(b) Crack width opening under load

Figure 4.1: Failure Mode of the Control Slab

4.1.2. Slab A. Slab A showed a reduction of deflection compared to the Control Slab. The formation of flexural cracks that occurred as a result of the yielding of the embedded steel reinforcement generated high stresses in the CFRP plate across the crack. Since the concrete could not maintain the interface shear and normal stresses, the CFRP plates snapped from the substrate at a point load of $P = 13.7$ kN (3.08 kips). A relatively thin layer of concrete was attached to the CFRP plates (see Figure 4.2). No sign of concrete crushing was observed. The failure moment (includes slab self-weight) was 76.3 kN-m (56.3 k-ft), which was 63% higher than that of the Control Slab. After normalization the increment was 4.1 (see Table 4.1).

4.1.3. Slab B. The introduction of initial prestressing provided Slab B with the ability to resist high loads prior to cracking. The cracks that developed in Slab B were fewer and finer as compared to Slab A. At a load of 20.7 kN (4.67 kips), sudden slippage took place at the anchor fixed with six bolts. Due to the sudden release of axial force, the CFRP laminate plate split and ruptured into pieces (see Figure 4.3). There was no evidence of concrete crushing. The failure load and moment for Slab B were 22.7 kN (5.10 kips) and 102.2 kN-m (75.4 k-ft), respectively. The failure moment was 118% higher than the Control Slab. After normalization, the increment was 7.7 (see Table 4.1).

4.1.4. Slab C. Slab C failed in a sudden and brittle manner caused by rupture of the carbon fiber sheet at the constant moment region. The ruptured remains of carbon fiber sheet at both ends of the slab were still attached firmly to the substrate. Examination of the concrete substrate after the load was removed showed wide-open cracks propagating transversely at the substrate of the slab (see Figure 4.4). Growth in the amount and width of cracks might have caused the carbon fiber sheet to delaminate and create local stress concentration. No sign of concrete crushing was observed. The failure load was 21.3 kN (4.78 kips) and the failure moment was 122% higher than that of the Control Slab. After normalization, the increment was 5.6 (see Table 4.1).

4.1.5. Slab D. During the test, no sign of debonding was observed. The CFRP laminate bars at the center of the slab ruptured at a load of 24.1 kN (5.43 kips). The failure arose suddenly and in a brittle mode. No sign of concrete crushing was observed. The failure moment was 114.6 kN-m (84.5 k-ft), which was 145% higher than the Control Slab. After normalization, the increment was 10.2, which was the highest compared to other strengthened slabs (see Table 4.1).



(a) Interfacial debonding



(b) A relatively layer of concrete attached to the plates

Figure 4.2: Failure Mode of Slab A



(a) Anchorage failure



(b) Sign of slippage



(c) Rupture of CFRP plates



(e) Rupture of CFRP plate

Figure 4.3: Failure Mode of Slab B



(a) Rupture of Carbon fiber sheet



(b) Cracks at the substrate of the slab

Figure 4.4: Failure Mode of Slab C



(a) Large Deflection



(b) No sign of concrete crushing



(c) Rupture of CFRP bars



(d) Rupture of CFRP bars

Figure 4.5: Failure Mode of Slab D

4.2. DEFLECTION

The Load vs. Deflection Curves for all the slabs is shown in Figure 4.6. It is observed that up to a load of approximately 4.4 kN (1.0 kips), all strengthened slabs behaved similarly, with roughly linear responses and stiffnesses about 84% greater than the Control Slab. The Control Slab started to crack at 1.25 kN (0.28 kips) and yielded after a load of 4.4 kN (1.0 kips) was placed. The Control Slab continued to deform thereafter.

At 13.7 kN (3.08 kips), Slab A failed suddenly and exhibited no ductility. The maximum deflection prior to failure was 7.7 cm (3.04 in.). Slab B exhibited a lower deflection as compared to Slab A at the same load level. Above 17.8 kN (4.0 kips) the curve for Slab B was much flatter and could be attributed to the yielding of the internal steel reinforcement. The maximum deflection prior to failure was 21.2 cm (8.37 in.).

The carbon fiber sheet, which was used to strengthen Slab C, had an axial stiffness, $E_f A_f$, approximately 1.5 times larger than the CFRP plate and bar. The influence of a high amount of $E_f A_f$ on the stiffness of the slab was clearly observed in Slab C. Slab C showed similar stiffness to Slab B until it reached 13.5 kN (3.04 kips), at which point the internal steel reinforcement started to yield. The maximum deflection for Slab C prior to failure was 14.5 cm (5.71 in.).

The CFRP laminate bar had an $E_f A_f$ similar to that of the CFRP laminate plate; hence Slab D and Slab A had a similar stiffness. As was the case with Slab C, the internal steel reinforcement of Slab D started to yield at a lower load level as compared to Slab B. The maximum deflection prior failure for Slab D was 24.5 cm (9.66 in.).

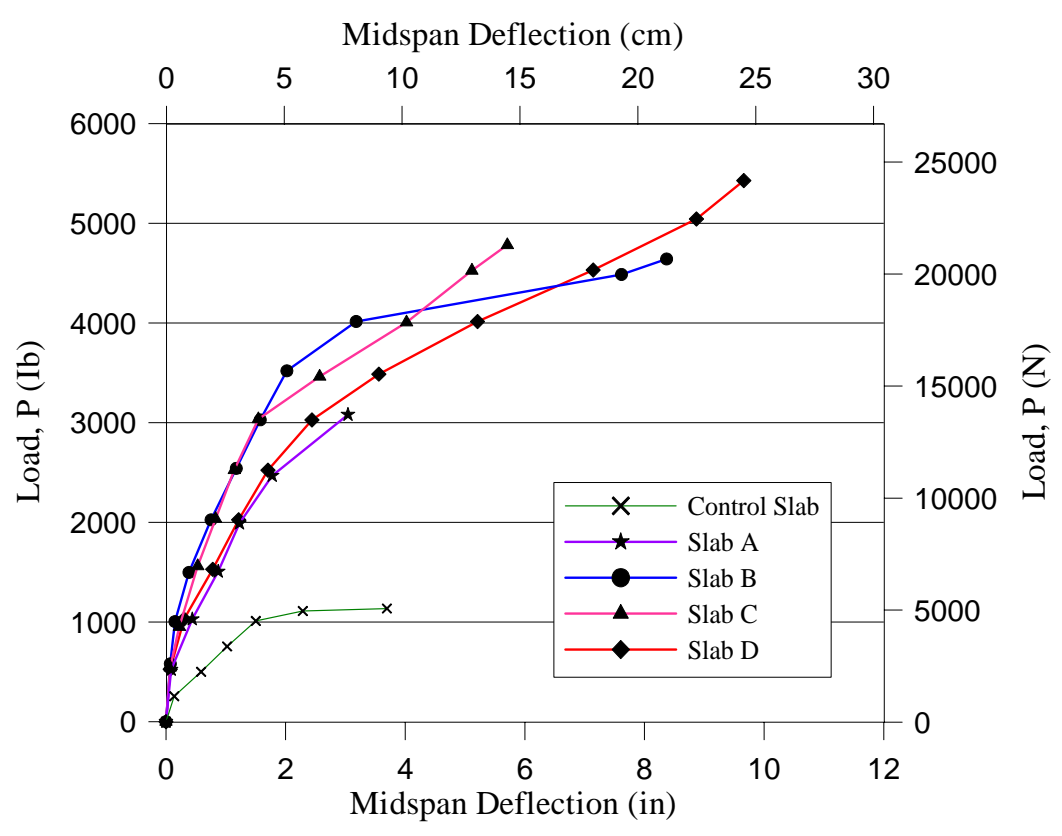


Figure 4.6: Load vs. Deflection Curves

4.3. STRAIN ALONG THE CFRP SYSTEM AND CONCRETE

Strain of the CFRP systems along the tensile zone and the concrete at the mid-span of compression zone were measured with foil strain gages. Figure 4.7 to 4.10 show the Load versus Strain Curves for Slab A to D, respectively.

4.3.1. Slab A. The strain at the mid span (location A) of the CFRP plate gradually increased during the test. A significant change in the slope of the curve occurred at a load of 11 kN (2500 lb). This phenomenon indicated that the internal steel reinforcement started to yield and most of the forces was transferred from the steel reinforcement to the CFRP laminate plates. At a location near to the support (location B), a stiffer curve was recorded. The CFRP plates snapped off from the substrate when the strain at the mid span reached 5.7‰, which was 35% of the ultimate strain. The strain near the support was only 1.5‰ and the concrete strain was 1.0‰ when the failure occurred.

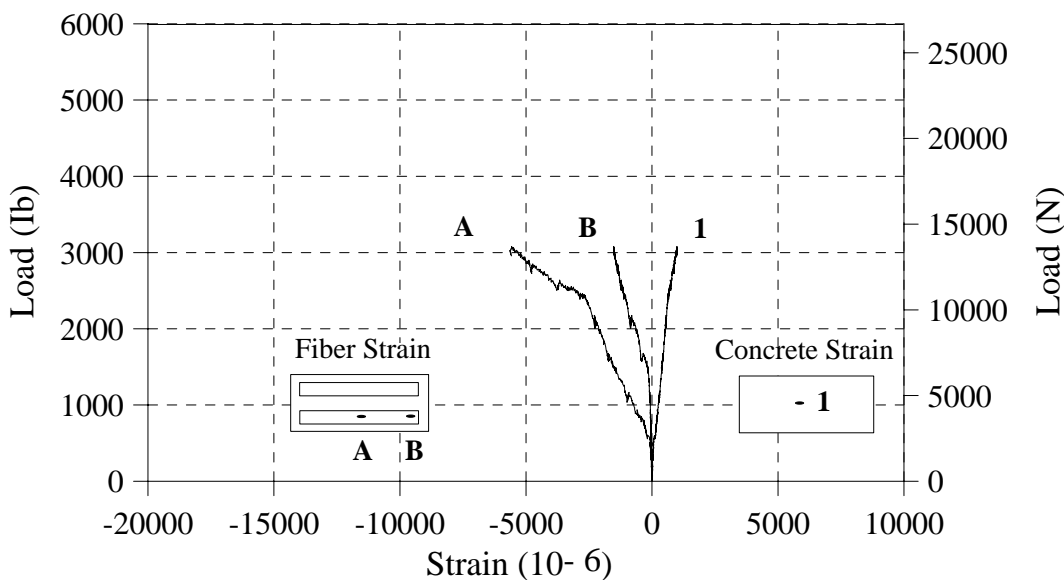


Figure 4.7: Load vs. Strain for Slab A

4.3.2. Slab B. The strain along the CFRP plates started with an initial elongation of $5‰$ after taking into account initial prestressing of the CFRP plates. The strain curve at location B (mid-span) diverges from the strain curves at location A and C (close to fixed anchorages) at a load of 6.2 kN (1.39 kips). This divergence was interpreted as debonding that began at the mid span, which later propagated towards the fixed anchorage. Strains at location A and C showed a dramatic increment at 18.5 kN (4.15 kips), indicating that debonding had reached the edge of the fixed anchorages. The fixed anchorages held the CFRP plates and enable the slab to carry more loads. Failure eventually took place due to slippage from the fixed anchors with six bolts at a load of 20.6 kN (4.64 kips). The average maximum strain prior to the slippage was 1.33%, which was 83% of the ultimate strain given by the manufacturer. The maximum concrete strain was $2.5‰$.

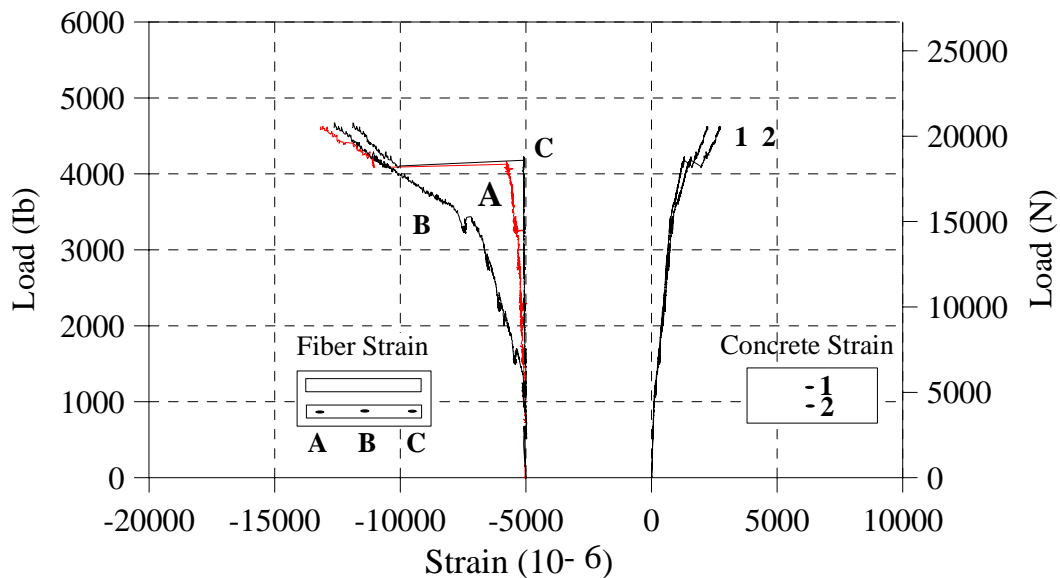


Figure 4.8: Load vs. Strain for Slab B

4.3.3. Slab C. Slab C had strain patterns similar to Slab A. The carbon fiber sheet at location B started to delaminate at a load of 2.1 kN (0.47 kips). The sudden change in slope at a load of 14.3 kN (3.2 kips) was due to yielding of steel reinforcement. The formation of wide flexural cracks after the steel yielded generated high stress in the fiber across the crack. This concentrated stress can only dissipate by debonding. The maximum strain at location B (mid-span) prior to failure was 1.0%, which was 65% of the ultimate strain given by the manufacturer. This significant difference might be caused by the strain at the crack location reaching the ultimate strain before the strain at the mid-span was recorded by the strain gage. The average maximum strain at locations A and C were only $4‰$ and the average concrete strain at the compression zone was $1.5‰$.

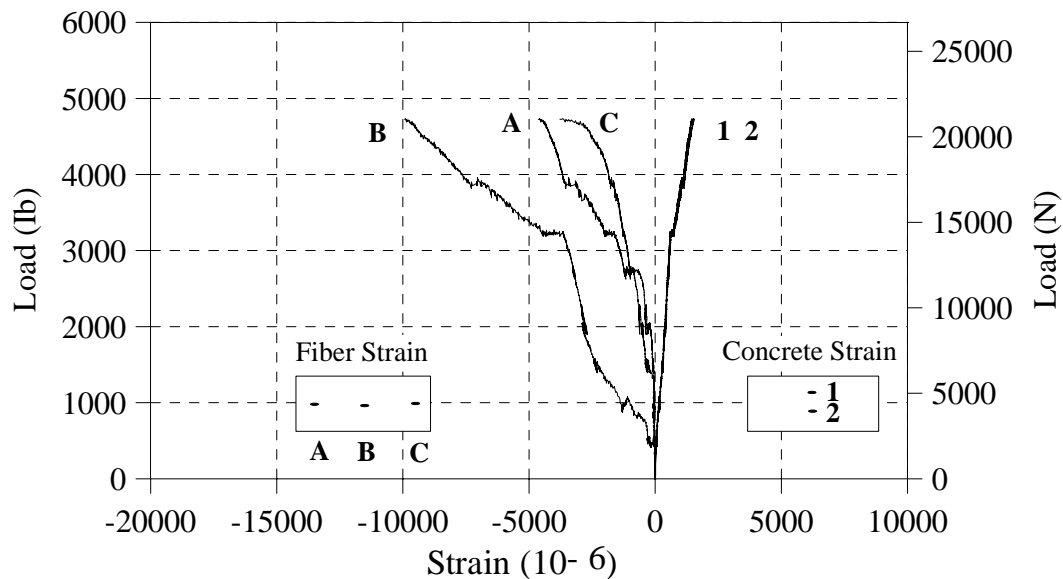


Figure 4.9: Load vs. Strain for Slab C

4.3.4. Slab D. Three foil stain gages were attached to the mid-span of the second, third and fourth CFRP bars. The stain curves showed that the CFRP bars were uniformly stressed until failure occurred. The maximum strain at location C prior to failure was 1.82%, which was slightly higher than the ultimate strain provided by the manufacturer. The maximum strains at locations A and B were 1.45% and 1.58%, respectively. No anchorage failure was observed. The test positively proved that a good and uniform bond existed between the laminate and the concrete. The high tensile strength of the CFRP bars was fully utilized. The maximum concrete strain at the compression zone was 2.9%, which was very close to the crushing strain of concrete.

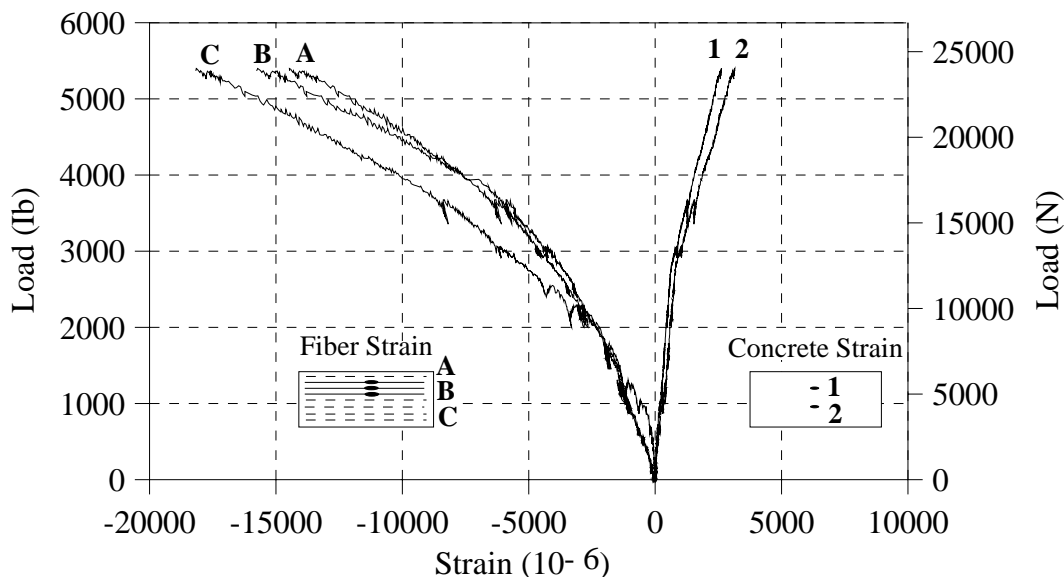


Figure 4.10: Load vs. Strain for Slab D

4.4. THEORETICAL MOMENT CURVATURE

A modified analytical model based on Bernoulli's hypothesis was developed to calculate the theoretical moment curvature of the strengthened slabs. The compatibility of deformation and equilibrium of forces in the cross section were always maintained. The principles for strengthening in bending are showed in Figure 4.11.

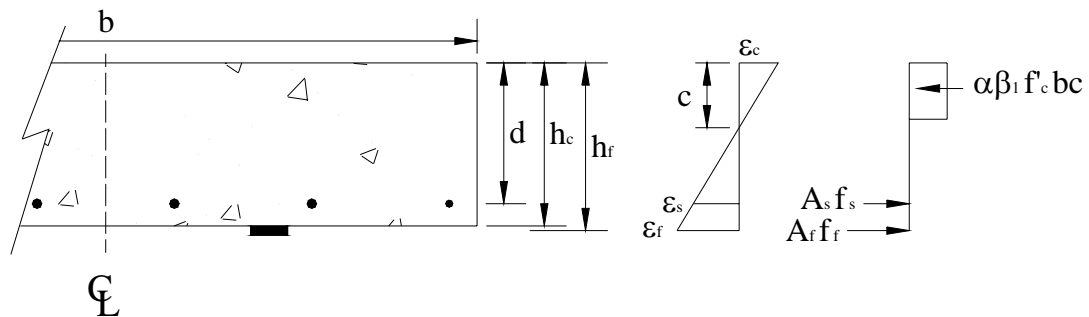


Figure 4.11: Stress-Strain Distribution in the Cross Section of RC Slab

The following assumptions were taken into consideration while developing the analytical model:

- (a) The maximum usable concrete compression strain is assumed to be 0.003;
- (b) The tensile behavior of the CFRP reinforcement is linearly elastic until failure;
- (c) Strain in the concrete and the CFRP reinforcement is proportional to the distance from the neutral axis;
- (d) Plane section before loading remains plane after loading;
- (e) Perfect bond exists between the concrete and the CFRP reinforcement. No premature failure such as debonding will occur;

- (f) No initial strain exists at the bottom face of the cross section;
- (g) CFRP system does not contribute any capacity prior to concrete crack.

Two theoretical moment curvature diagrams were plotted based on the mechanical properties of CFRP systems that were given by the manufacturer and the results obtained from the ASTM tests. The theoretical moment curvature diagrams were subsequently compared with the experimental moment curvature diagram to evaluate the efficiency of the CFRP EBR technique. Detailed calculations were implemented in Mathcad to ease the calculations (see Appendix C). All the units in the calculation sheets were based on US customary unit.

In this model, the concrete is assumed to be linearly elastic prior to cracking. The cracking moment, M_{cr} , and curvature, ϕ_{cr} , of the specimen due to externally applied load are expressed as:

$$M_{cr} = \frac{\sigma I_c}{y_t} \quad (4.1)$$

$$\phi_{cr} = \frac{\varepsilon_{cr}}{y_t} \quad (4.2)$$

where

$$\sigma = 7.5\sqrt{f'_c} \quad (\text{ACI 318-02}) \quad (4.3)$$

$$E_c = 57000\sqrt{f'_c} \quad (\text{ACI 318-02}) \quad (4.4)$$

$$\varepsilon_{cr} = \frac{\sigma}{E_c} \quad (4.5)$$

in which σ = modulus of rupture of concrete; f'_c = specified compressive strength of concrete; E_c = modulus of elasticity of concrete; ε_{cr} = concrete cracking strain; I_c = moment of inertial of RC Slab before cracking; b = width of compression face of slab; h = overall thickness of the RC slab; and y_t = distance from centroidal axis of gross section, neglecting reinforcement, to extreme fiber in tension.

After the concrete crack, the moment and curvature over the cross section with a given concrete compressive stress, ε_c , were calculated. Instead of using actual nonlinear stress distribution for concrete in compression, equivalent uniform stress distribution, whose integral could be evaluated by inspection, were employed. Thus, the stress-block factors α and β_l were determined so that the magnitude and location of the resultant compressive force were the same as in the equivalent uniform stress distribution as in the actual distribution [25]. The requirement that the magnitude of the resultant force remain the same is:

$$\int_0^c f_c b dy = \alpha \beta_l f'_c b c \quad (4.6)$$

For a parabolic stress-strain curve and a constant width, b , Equation 4.6 reduces to

$$\alpha \beta_l = \frac{\varepsilon_c}{\varepsilon'} - \frac{1}{3} \left(\frac{\varepsilon_c}{\varepsilon'} \right)^2 \quad (4.7)$$

and

$$\beta_l = \frac{4 - \varepsilon_c / \varepsilon'}{6 - 2\varepsilon_c / \varepsilon'} \quad (4.8)$$

in which ε_c = concrete compressive strain and ε' = peak concrete compressive strain, which was set as 0.002 [26].

Under a balance condition, before the steel reinforcement yield and CFRP system rupture, the equilibrium of compression force in concrete and tensile force in the steel reinforcement and CFRP system is expressed as 4.9a.

$$\alpha\beta_1 f'_c b c = A_s E_s \varepsilon_c \left(\frac{d-c}{c} \right) + A_f E_f \varepsilon_c \left(\frac{h_f - c}{c} \right) \quad (4.9a)$$

After the steel yields, the equation is expressed as 4.9b.

$$\alpha\beta_1 f'_c b c = A_s f_y + A_f E_f \varepsilon_c \left(\frac{h_f - c}{c} \right) \quad (4.9b)$$

By solving Equation 4.9, the compression depth, c (distance from extreme compression fiber to neutral axis), is determined and carried forward to determine the moment and curvature of the predetermined concrete compression strain, ε_c . The moment, M , and curvature, ϕ , are expressed as:

$$M = A_s f_s (d - \frac{1}{2} \beta_1 c) + A_f f_f (h_f - \frac{1}{2} \beta_1 c) \quad (4.10)$$

$$\phi = \frac{\varepsilon_c}{c} \quad (4.11)$$

where

$$f_s = E_s \varepsilon_c \left(\frac{d-c}{c} \right) \leq f_y \quad (4.12a)$$

and

$$f_f = E_f \varepsilon_c \left(\frac{h_f - c}{c} \right) \leq f_{fu} \quad (4.12b)$$

in which f_s = stress in steel reinforcement; and f_f = stress in CFRP system.

Once the CFRP system exceeds its ultimate strain (CFRP rupture) or the concrete exceeds its ultimate compression strain (concrete crushing), the slab was considered failed. The model predicts that all strengthened slabs would fail by the CFRP rupture. The model needs further improvement to incorporate debonding of anchorage failure.

4.5. EXPERIMENTAL MOMENT CURVATURE

During the computation of the experimental moment curvature diagram, the substantial slab self weigh, 5.0 kN/m (0.34 kip/ft), and the weight of steel racks from the test setup, 0.78 kN (0.175 kip), were taken into consideration (see Figure 4.12). The initial moment and curvature due to these initial sustained loads was 26.2 kN-m (19.3 kip-ft) and $1.06 \times 10^{-3} \text{ 1/m}$ ($2.7 \times 10^{-5} \text{ 1/in}$), respectively.

Based on a free body diagram, the mid span moment due to the imposed static point load, P , can be derived as Equation 4.13. The resulting moment was eventually added to the initial moment to obtain the total mid span moment.

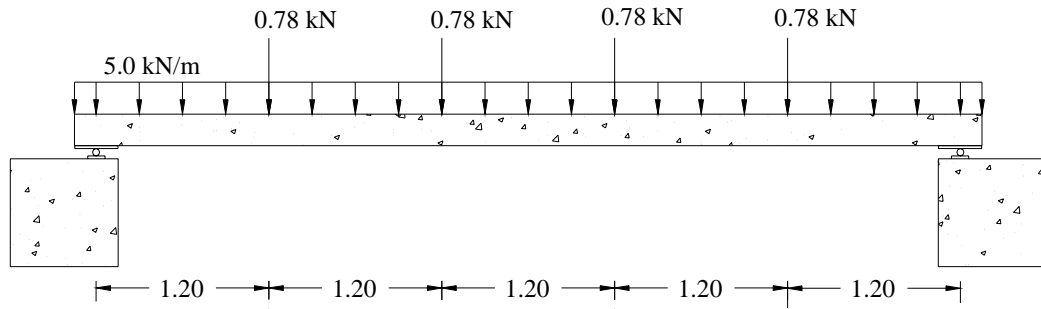


Figure 4.12: Initial Un-factored Load (Dimension in meter)

$$M_{test} = 3.6P_{kN} \text{ kN} \cdot m \quad (4.13a)$$

$$M_{test} = 12P_{kip} \text{ k} \cdot ft \quad (4.13b)$$

The recorded compression strain of the concrete, ε_c , and tensile strain of the CFRP system, ε_f , at the mid span are used to compute the curvature of the slab. It was assumed plane sections remained plane and perfect bond exists. The equation to compute the experimental curvature is expressed as:

$$\phi = \frac{\varepsilon_c + \varepsilon_f}{h} \quad (4.14)$$

4.5.1. Control Slab. Due to the significant slab self weight and steel racks, the Control Slab almost reached its theoretical cracking moment 29 kN-m (21.4 k-ft) before loading. During the test, the Control Slab reached the cracking moment at 28 kN-m (20.9 k-ft) and started to yield at 47 kN-m (34.5 k-ft) (see Figure 4.13).

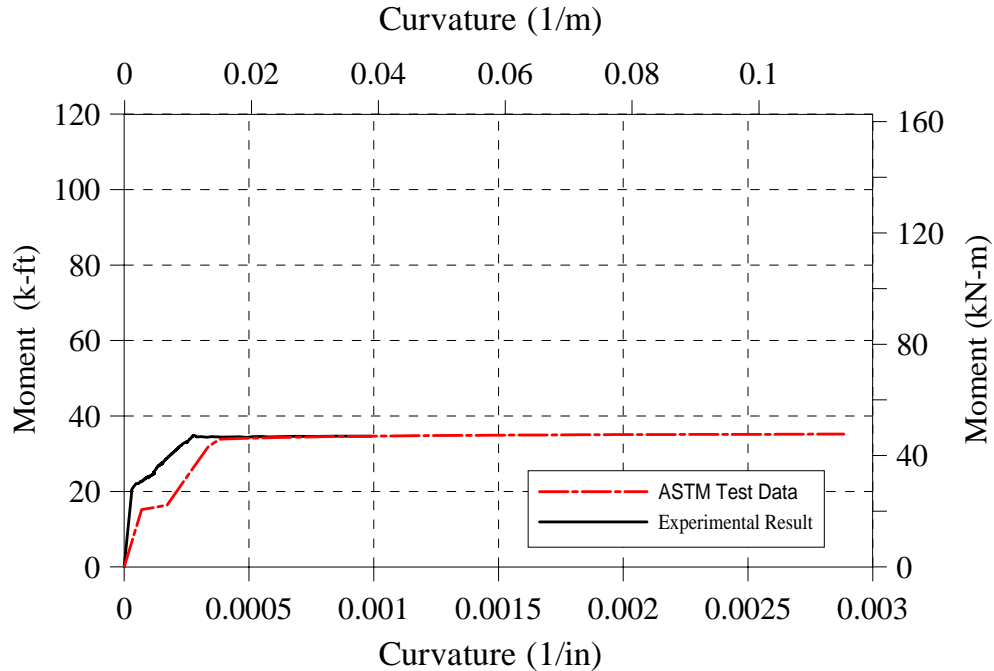


Figure 4.13: Moment vs. Curvature for the Control Slab

4.5.2. Slab A. Slab A reached the cracking moment at 31 kN-m (23.0 k-ft) and started to yield at 67 kN-m (49.5 k-ft). The ultimate moment for Slab A was 77.5 kN-m (57.2 k-ft). The moment curvature diagram derived from the ASTM test results was stiffer than the moment curvature diagram derived from the manufacturer data. The analytical ultimate moment based on the ASTM test results and the manufacturer data were 112 kN-m (82.7k-ft) and 110 kN-m (81.0 k-ft), respectively (see Figure 4.14). Both the analytical ultimate moments were about 42% higher than the experimental ultimate moment. The experimental ultimate curvature prior to failure was $0.03 \frac{1}{m}$ ($1 \cdot 10^{-4} \frac{1}{in}$) and showed no ductility. The analytical ultimate curvatures based on the ASTM test results and the manufacturer data were $0.07 \frac{1}{m}$ ($1.9 \cdot 10^{-3} \frac{1}{in}$) and $0.08 \frac{1}{m}$ ($2 \cdot 10^{-3} \frac{1}{in}$), respectively.

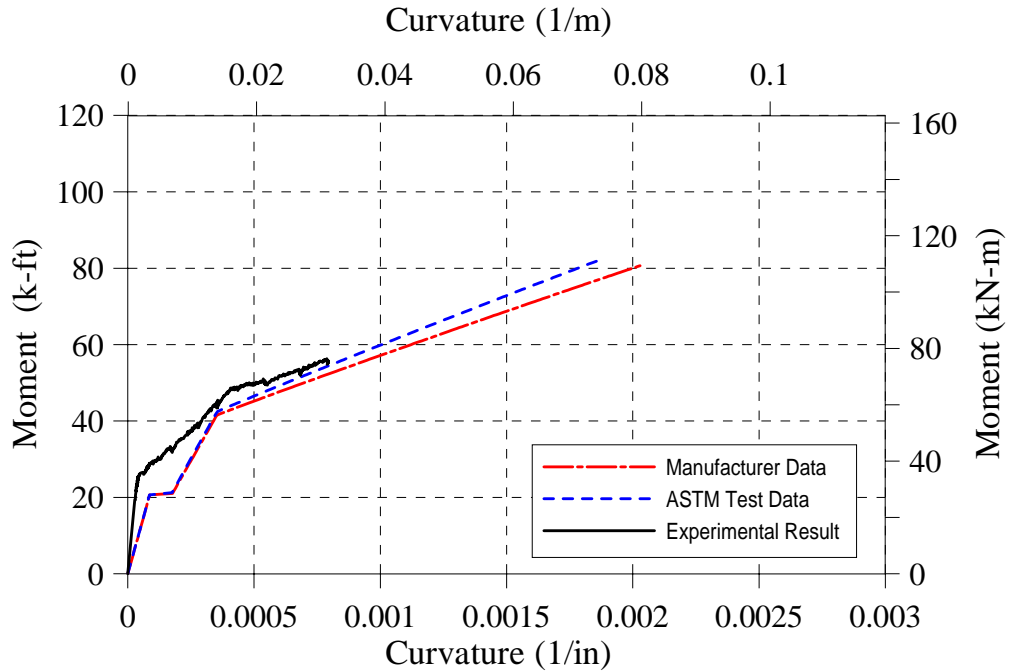


Figure 4.14: Moment vs. Curvature for Slab A

4.5.3. Slab B. Slab B reached the cracking moment at 49 kN-m (36.0 k-ft) and started to yield at 102 kN-m (75.4 k-ft). The ultimate moment of the slab was 103 kN-m (75.6 k-ft). The analytical ultimate moment based the ASTM test results was 111 kN-m (82.0 k-ft), which was 9% higher than experimental ultimate moment. The analytical ultimate moment based on manufacturer data was 108 kN-m (80.6 k-ft), which was closer to the experimental results (see Figure 4.15). The experimental ultimate curvature was $0.047 \text{ } \frac{1}{m}$ ($0.0012 \text{ } \frac{1}{in}$) and showed no ductility before failure. The experimental ultimate curvature based on ASTM test results was $0.05 \text{ } \frac{1}{m}$ ($1.3 \times 10^{-3} \text{ } \frac{1}{in}$) and $0.056 \text{ } \frac{1}{m}$ ($1.4 \times 10^{-3} \text{ } \frac{1}{in}$) based on manufacturer data.

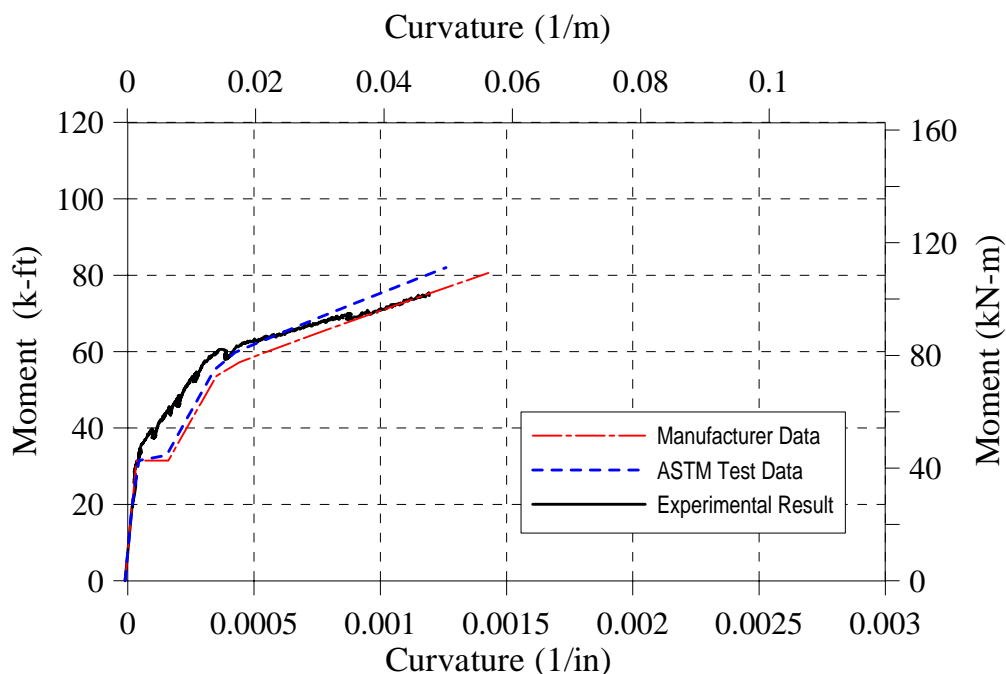


Figure 4.15: Moment vs. Curvature for Slab B

4.5.4. Slab C. Slab C reached the cracking moment at 34 kN-m (25.0 k-ft) and started to yield at 79 kN-m (58.3 k-ft). The experimental ultimate moment was 104 kN-m (76.7 k-ft). The analytical ultimate moment derived from the ASTM test results, 106 kN-m (78.5k-ft), was close to the experimental ultimate moment. Whereas the analytical ultimate moment derived from manufacturer data, 143 kN-m (105 k-ft), was 37% higher than experimental ultimate moment (see Figure 4.16). The slab ultimate curvature prior to failure was $0.054 \frac{1}{m}$ ($0.0014 \frac{1}{in}$) and showed no ductility. The analytical ultimate curvature based on the ASTM test results and the manufacturer data were $0.057 \frac{1}{m}$ ($1.4 \cdot 10^{-3} \frac{1}{in}$) and $0.083 \frac{1}{m}$ ($2.1 \cdot 10^{-3} \frac{1}{in}$), respectively.

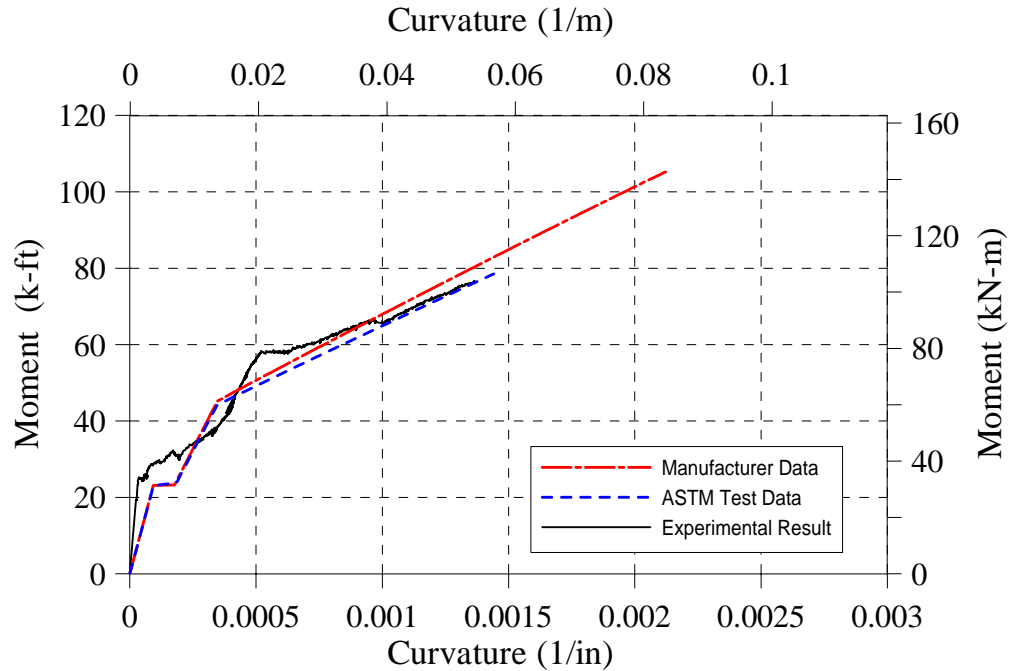


Figure 4.16: Moment vs. Curvature for Slab C

4.5.5. Slab D. The experimental and analytical moment curvature diagram plotted in Figure 4.17 resemble each other in behavior. Slab D reached the cracking moment at 35 kN-m (26.1k-ft) and started to yield at 75.5 kN-m (55.7 k-ft). The experimental moment increased gradually until they reached the ultimate moment at 115 kN-m (84.8 k-ft). The experimental ultimate curvature prior to failure was $0.083 \text{ } \frac{1}{m}$ ($2.1 \cdot 10^{-3} \text{ } \frac{1}{in}$) and showed considerable ductility. The predicted analytical ultimate moments, which were derived from the ASTM test results and the manufacturer data, were close to the slab ultimate moment. They were 105 kN-m (77.7 k-ft) and 115 kN-m (84.8 k-ft), respectively. The experimental ultimate curvatures were $0.073 \text{ } \frac{1}{m}$ ($1.8 \cdot 10^{-3} \text{ } \frac{1}{in}$) and $0.092 \text{ } \frac{1}{m}$ ($2.3 \cdot 10^{-3} \text{ } \frac{1}{in}$) as refer to the ASTM test results and manufacturer data.

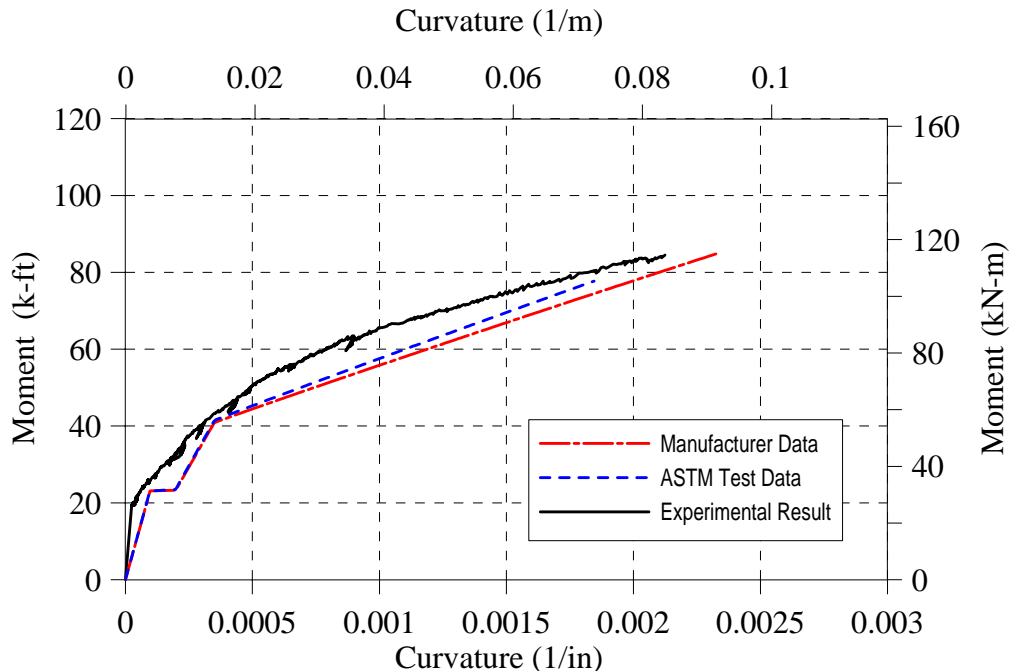


Figure 4.17: Moment vs. Curvature for Slab D

Table 4.2 shows the comparison between the experimental and analytical ultimate moment. It can be observed that the analytical ultimate moments, which were controlled by rupture of the CFRP system, are basically higher than experimental ultimate moment. The differences between the experimental and analytical ultimate moment for Slab B and D are less than 10%. This implied that prestressed CFRP plate with anchorage system and NSM reinforcement techniques are efficient and rupture of CFRP systems would more likely occurred. The experimental ultimate moment for Slab C is very close to the analytical ultimate moment based on ASTM test results. However, the experimental ultimate moment based on manufacturer data is 37.5% lower than the analytical ultimate moment. The ratio of experimental to analytical ultimate moment for Slab A was only about 0.7 due to bond failure.

Table 4.2: The Experimental and Analytical Ultimate Moments

<i>Ultimate Moment, kN-m (k-ft)</i>					
	<i>Experimental</i>	<i>ASTM</i>	<i>Manufacturer</i>		
<i>Slab</i>	M_{Exp}	M_{ASTM}	M_{Man}	M_{Exp}/M_{ASTM}	M_{Exp}/M_{Man}
<i>Control Slab</i>	47 (34.5)	N/A	N/A	N/A	N/A
<i>A</i>	77.5 (57.2)	112 (82.7)	110 (80.9)	0.69	0.71
<i>B</i>	103 (75.6)	111 (82.0)	108 (80.6)	0.93	0.95
<i>C</i>	104 (76.8)	106 (78.5)	143 (105)	0.98	0.73
<i>D</i>	115 (84.5)	105 (77.7)	115 (85.1)	1.09	0.99

5. ANALYTICAL STUDY

According to a survey done by Bonacci in 1996, debonding or peeling of FRP occurs in 64% of tests of beams strengthened for flexure. In only 22% of the tests surveyed, rupture of the FRP was achieved, with the rest of the beams failing in shear or compression. It is not unusual for a CFRP system to delaminate at a strain about half of its ultimate strain, oftentimes due to weakness in the concrete substrate rather than in the epoxy. Thus there poses an urgent need for rational evaluating or predicting the structure capacity due to this type of failure mode.

Many researchers have done significant work on the premature failure at the cut-off point of steel/FRP plates in steel/FRP strengthened beams and developed the corresponding failure criteria for predicting failure load. Niu and Wu (2001) found that debonding due to flexural cracks in the maximum moment region is more dominant than the debonding induced by the stress concentration at the curtailment zone of the FRP system [27]. Swamy et al. (1988) found that theoretical interface bond stresses, based on simple elastic behavior, have no consistent relationship to the measured peak values [28]. Taljsten (1997) and Malek et al. (1998) used the linear elastic theory to derive shear and peeling stresses at the externally reinforced plate [6, 22]. Roberts (1989) stated that the shear and normal stresses, in and adjacent to the adhesive layer, can be reduced significantly by using a more flexible adhesive, reducing the thickness of the plate, and for a simply supported system, by terminating the plate as close to the support as possible [29]. Arduini (1997) simulated and predicted the failure mode of FRP strengthened beams by taking into account the influence of concrete confinement in the compression zone due to the presence of the stirrups, and the tensile softening properties of concrete

[23, 24]. Until now, a nonlinear closed-form formula has not yet been derived for FRP strengthened flexural structures.

The analytical models developed by Roberts and Malek were studied and modified to calculate the shear and normal stresses along the externally bonded CFRP plate (Slab A) at a failure load obtained from the test. The analytical results presented herein were the maximum stresses at the cutoff point, which were calculated based on a simplified approach as discussed in Section 2. The detailed calculations for the stresses along the CFRP plate are showed in Appendix D.

5.1. ANALYTICAL APPROACH

At the cutoff point, the concrete slab undergoes biaxial stresses (see Figure 5.1). In this case, three components of stresses are present: σ_x , calculated from flexural analysis; σ_y and τ_{xy} , peeling and shear stresses calculated based on analytical models.

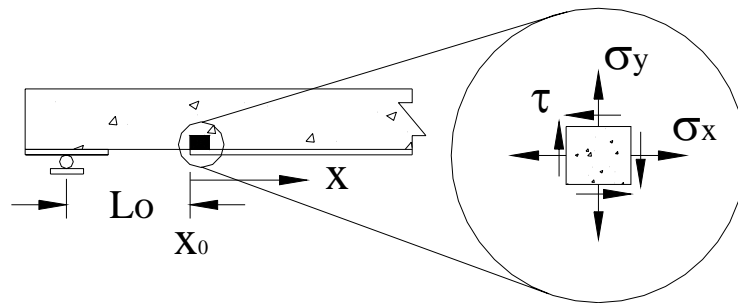


Figure 5.1: Stresses Acting at the Concrete-Adhesive Interface

The failure model for concrete under the biaxial state of stresses was used to check the local failure of the concrete slab (Kupfer and Gerstle 1973). According to this model, the strength of concrete under tension-tension of stresses is approximated by:

$$\sigma = f_{tu} = 0.295(f_{cu})^{2/3} \quad \text{Constant}(MPa) \quad (5.1a)$$

$$\sigma = f_{tu} = 0.155(f_{cu})^{2/3} \quad \text{Constant}(ksi) \quad (5.1b)$$

in which f_{tu} and f_{cu} = ultimate tensile and compressive strengths of concrete, respectively. The principal stress, σ_p , is calculated using stress transformation relation under plane stress condition.

$$\sigma_p = \frac{\sigma_x + \sigma_y}{2} + \sqrt{\frac{(\sigma_x - \sigma_y)^2}{4} + \tau^2} \quad (5.2)$$

The failure is assumed to begin when the principal stress, σ_p , equals the concrete strength under the biaxial state of stresses.

5.2. VALIDATION OF ROBERTS' ANALYTICAL APPROACH

The geometric and material properties, used to calculate the analytical shear and normal stresses along the CFRP plate of Slab A, are shown in Table 5.1 and Figures 5.2 and 5.3.

Table 5.1: Geometric and Material Properties

Material	Width, mm	Thick, mm	Height, mm	E Modulus, kN/mm^2	Area, cm^2
Concrete	b_c 1000	t_c 220	-- --	E_c 26	-- --
CFRP	b_f 50	t_f 1.2	h_f 223	E_f 164	-- --
Epoxy Gel*	b_a 50	t_a 1.5	-- --	E_a 1.7	-- --
Steel	-- --	-- --	h_s 190	E_s 200	A_s 6.45

* Shear modulus, G_a , of the epoxy gel is $0.59 kN/mm^2$

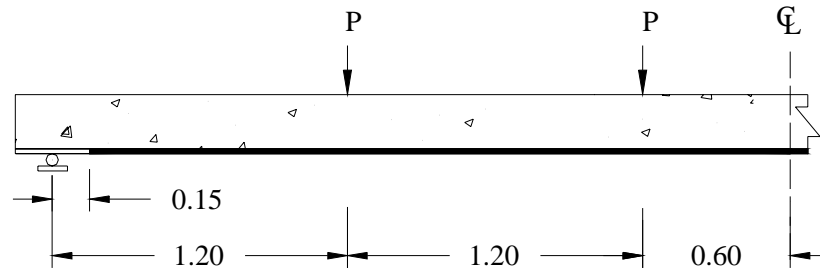


Figure 5.2: General View of the Test Setup

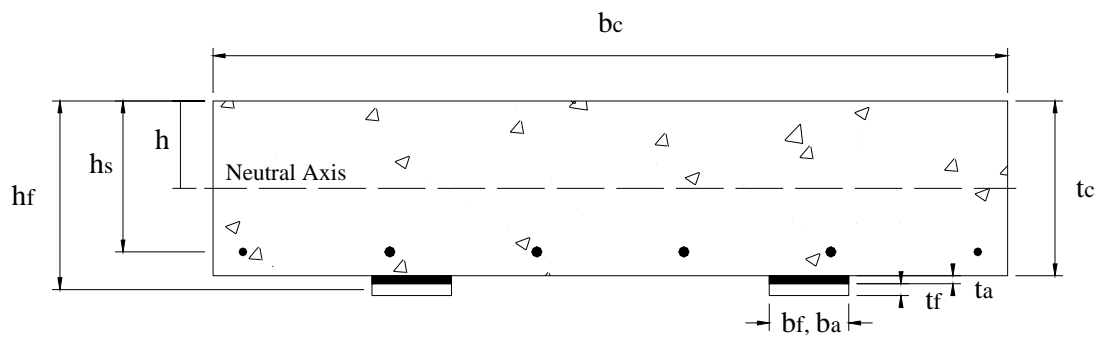


Figure 5.3: Cross Section of Slab A

Assuming linear material behavior and that the concrete cannot sustain tension, the depth of the neutral axis, h , is given by:

$$h = \frac{E_c b_c \frac{h_c^2}{2} + E_f b_f t_f \left(h_c + \frac{t_f}{2} \right)}{E_c b_c h_c + E_f b_f t_f} \quad (5.3)$$

$$h = 110\text{mm} \quad (4.30\text{in})$$

The second moment of area of the equivalent carbon fiber section, I_f , is given by:

$$I_{fr} = 1.46 * 10^8 \text{mm}^4 \quad (352\text{in}^4)$$

The section properties of the reinforcement concrete beam and CFRP laminate plate alone are given by:

$$E_c I_c = 2.31 * 10^{13} \text{N} \cdot \text{mm}^2 \quad (8.04 * 10^9 \text{Ib} \cdot \text{in}^2)$$

$$E_f I_f = 2.36 * 10^6 \text{N} \cdot \text{mm}^2 \quad (823 \text{Ib} \cdot \text{in}^2)$$

The shear and normal stresses at the cutoff point of the adhesive layer for an applied load of $P = 13.5 \text{ kN}$ (3.08 kips) can be summarized as follows:

$$\tau = 0.15 \text{ N/mm}^2 \quad (21.8 \text{ psi})$$

$$\sigma_y = 0.061 \text{ N/mm}^2 \quad (8.8 \text{ psi})$$

$$\sigma_x = 0.37 \text{ N/mm}^2 \quad (53.7 \text{ psi})$$

These values are in accordance with the results shown in Figure 5.4. The procedure to determine the distribution of the shear and normal stresses in the adhesive layer, along Slab A, is shown in Appendix D. The shear stress concentration at the cutoff point rapidly vanishes when moving toward the center of the beam. The normal reduces to zero over a very short distance from the cutoff point.

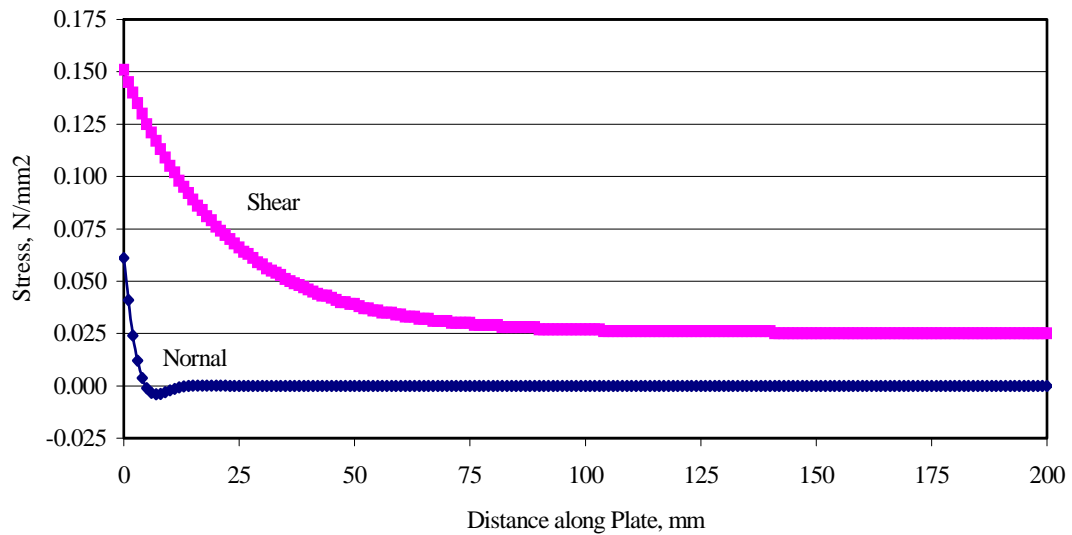


Figure 5.4: Interfacial Shear and Normal Stresses – Roberts' Analytical Model

Using conventional stress transformation relations, the maximum principal stress is calculated as (Equation 5.2):

$$\sigma_p = 0.44 \text{ N/mm}^2 \text{ (63.0 psi)}$$

Based on Equation 5.1, the ultimate tensile capacity of concrete under biaxial tensile stresses is:

$$\sigma = f_u = 0.295(f_{cu})^{2/3} = 3.09 \text{ N/mm}^2$$

The calculated stress of $\sigma_p = 0.44 \text{ N/mm}^2$ (63.0 psi) at the cutoff point is smaller than the tensile strength of $\sigma = 3.09 \text{ N/mm}^2$ (3.09 N/mm²), proving an adequate margin of safety. Therefore using the above plate with a cut off point 150 mm away from the support is acceptable.

5.3. VALIDATION OF MALEK'S ANALYTICAL APPROACH

The same geometrical and mechanical properties shown in Table 5.1 and Figures 5.2 and 5.3 are used in Malek's analytical model. The shear and normal stresses at the cutoff point of the adhesive layer at an applied load of $P = 13.5 \text{ kN}$ (3.08 kips) can be summarized as follows:

$$\tau = 0.146 \text{ N/mm}^2 \quad (21.2 \text{ psi})$$

$$\sigma_y = 0.059 \text{ N/mm}^2 \quad (8.5 \text{ psi})$$

$$\sigma_x = 0.538 \text{ N/mm}^2 \quad (78.0 \text{ psi})$$

$$\sigma_p = 0.62 \text{ N/mm}^2 \quad (90.0 \text{ psi})$$

These values are in accordance with the results shown in Figure 5.5. The procedure to determine the distribution of the shear and normal stresses in the adhesive layer, along Slab A, is shown in Appendix D.

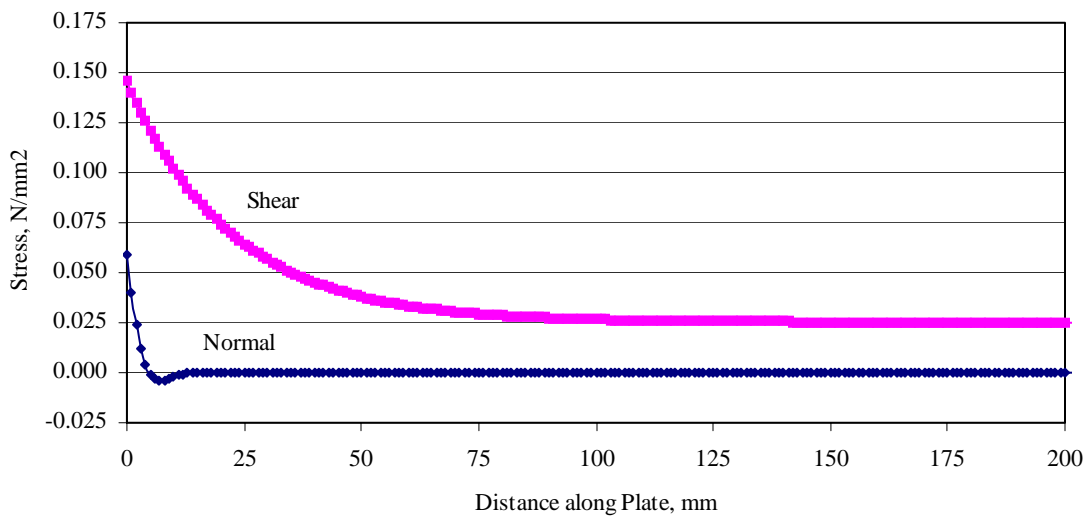


Figure 5.5: Interfacial Shear and Normal Stresses – Malek’s Analytical Model

The analytical models showed that the principal stress at the cutoff point at the failure load of $P = 13.5 \text{ kN}$ (3.08 kips) is smaller than the tensile strength of the concrete, proving an adequate margin of safety.

Both of the above analytical results show close agreement with the observation during the test. The failure mode of Slab A is caused by bond failure at the flexural cracks between the outermost crack and the maximum bending area. Shear stress concentration around flexural cracks may lead to local debonding of the plate. The debonding propagates towards the anchorage zones as the applied load increases and eventually causes the brittle failure. The shear stress concentration at the racks needs further studied to include design guidelines for externally bonded reinforcement.

6. DESIGN OF EXTERNALLY BONDED FRP SYSTEMS

This section presents the design guideline for flexural strengthening provided by ACI 440 and the Concrete Society Technical Report No.55. The geometry and material properties of Slab A are used to show the design procedures. The general concepts outline here can, however, be extended to other FRP EBR. In the case of prestressed FRP systems, the initial stress in the strip is included in the calculations, similar to the principles of conventional prestressing.

6.1. ACI-440

The following assumption are made in calculating the flexural resistance of a section strengthened with an externally applied FRP system:

- (a) The strains in the reinforcement and concrete are directly proportional to the distance from the neutral axis (that is, plane section before loading remains plane after loading);
- (b) The maximum useable compressive strain in the concrete is 0.003;
- (c) The tensile strength of concrete is neglected;
- (d) The FRP reinforcement has a linear elastic stress-strain relationship to failure;
- (e) Perfect bond exists between the concrete and FRP reinforcement.

The nominal capacity of an FRP strengthened member can be determined based on strain compatibility, internal force equilibrium, and the controlling mode of failure. Figure 6.1 illustrates an ultimate strength condition with the general distribution of strain used to compute the strain compatibility and the distribution of the internal force resultants used to check internal force equilibrium.

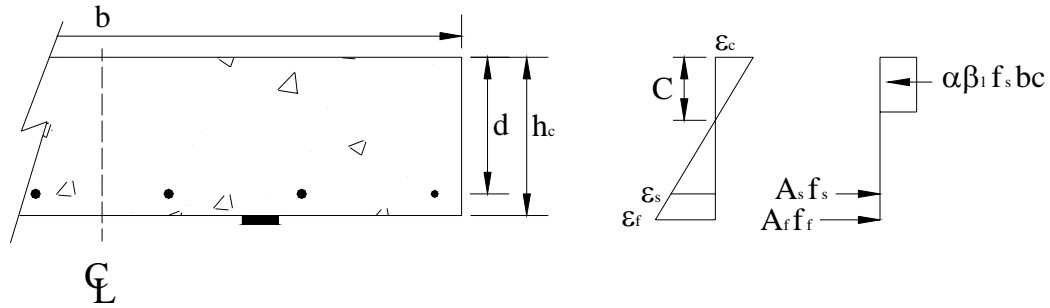


Figure 6.1: Stress and Strain Distribution in a Section at the Ultimate Limit State

The geometry and material properties shown in Table 5.1 and Figures 5.2 and 5.3 are used to compute the nominal flexural capacity of Slab A. The design procedures are following:

Step 1: Compute the FRP system design material properties. An environmental reduction factor for the appropriate fiber type and exposure condition is suggested by ACI-440-00. Assuming the strengthened Slab A is located in a relatively benign environment (i.e. indoor), an environmental reduction factor $C_e = 0.95$ is used.

$$f_{fu} = C_e f_{fu} = (0.95)(2500 \text{ N/mm}^2) = 2375 \text{ N/mm}^2$$

$$\varepsilon_{fu} = C_e \varepsilon_{fu} = (0.95)(1.6) = 1.52$$

Step 2: Determine the existing state of strain on the soffit. The existing state of strain is assumed to be zero during the installation of the FRP system.

$$\varepsilon_{bi} = 0$$

Step 3: Determine the bond-dependent coefficient of the FRP system. The dimensionless bond-dependent coefficient for flexural, “ κ_m ,” is calculated using:

$$\kappa_m = \begin{cases} 1 - \frac{nE_f t_f}{2,400,000} & \text{for } nE_f t_f \leq 1,200,000 \\ \frac{600,000}{nE_f t_f} & \text{for } nE_f t_f > 1,200,000 \end{cases} \quad (6.1a \text{ US})$$

$$\kappa_m = \begin{cases} 1 - \frac{nE_f t_f}{428,000} & \text{for } nE_f t_f \leq 214,000 \\ \frac{107,000}{nE_f t_f} & \text{for } nE_f t_f > 214,000 \end{cases} \quad (6.1b \text{ SI})$$

$$nE_f t_f = 196800 \text{ (SI)}$$

$$\kappa_m = 1 - \frac{nE_f t_f}{428,000} = 0.55 \text{ (SI)}$$

Step 4: Estimate “ c ,” the depth to the neutral axis. A reasonable initial estimate of “ c ” is $0.20 h_s$. The value of “ c ” is adjusted after checking equilibrium.

$$c = 0.2h_s = 38mm$$

Step 5: Determine the effective level of strain in the FRP reinforcement. The effective strain level in the FRP can be found from Equation 6.2.

$$\varepsilon_{fe} = 0.003 \left(\frac{h-c}{c} \right) + \varepsilon_{bi} \leq \kappa_m \varepsilon_{fu} \quad (6.2)$$

$$\varepsilon_{fe} = 0.015 > \kappa_m \varepsilon_{fu} = 0.0083$$

$$\varepsilon_{fe} = 0.0083$$

Step 6: Calculate the strain in the existing reinforcement steel. The strain in the reinforcing steel may be calculated using similar triangles according to Equation 6.3.

$$\varepsilon_s = (\varepsilon_{fe} + \varepsilon_{bi}) \left(\frac{d-c}{h-c} \right) \quad (6.3)$$

$$\varepsilon_s = 0.0069$$

Step 7: Calculate the stress level in the reinforcing steel and FRP. The stresses are calculated using Equation 6.4 and 6.5.

$$f_s = E_s \varepsilon_s \leq f_y \quad (6.4)$$

$$f_s = 414 \text{ N/mm}^2$$

$$f_{fe} = E_f \varepsilon_{fe} \quad (6.5)$$

$$f_{fe} = 1.33 \text{ kN/mm}^2$$

Step 8: Calculate the internal force resultants and check equilibrium. Force equilibrium is verified by checking the initial estimate of “ c ” with Equation 6.6. Since concrete crushing controls failure, γ may be taken as 0.85.

$$c = \frac{A_s f_s + A_f f_{fe}}{\gamma \beta_1 f_c' b} \quad (6.6)$$

$$c = 0.73 \neq 1.48$$

Step 9: Adjust “ c ” until force equilibrium is satisfied. Steps 5-8 are repeated several times with different value of “ c ” until equilibrium achieve. The results of the final iteration are summarized below:

$$c = 18.5 \text{ mm}$$

$$\varepsilon_s = 0.007 \rightarrow f_s = f_y = 414 \text{ N/mm}^2$$

$$\varepsilon_{fe} = 0.008 \rightarrow f_{fe} = 1330 \text{ N/mm}^2$$

Step 10: Calculate design flexural strength of the section. The nominal flexural capacity may be computed from Equation 6.7. An additional reduction factor, ψ_f , is applied to the flexural strength contribution of the FRP reinforcement. For flexural strengthening, an additional reduction factor of $\psi_f = 0.85$ is recommended. $\beta_1 = 0.8$ from ACI 318 10.2.7.3

$$M_n = A_s f_s \left(d - \frac{\beta_1 c}{2} \right) + \psi_f A_f f_{fe} \left(h - \frac{\beta_1 c}{2} \right) \quad (6.7)$$

$$M_n = 76.6 \text{ kN-m} \quad (56.5 \text{ k-ft})$$

Since $\varepsilon_s = 0.007 > 0.005$, a strength reduction factor of $\phi = 0.90$ is selected.

$$\phi = \begin{cases} 0.90 & \varepsilon_s \geq 0.005 \\ 0.70 + \frac{0.20(\varepsilon_s - \varepsilon_{sy})}{0.005 - \varepsilon_{sy}} & \text{for } \varepsilon_{sy} < \varepsilon_s < 0.005 \\ 0.70 & \varepsilon_s \leq \varepsilon_{sy} \end{cases} \quad (6.8)$$

$$\phi M_n = 68.9 \text{ kN-m} \quad (50.9 \text{ k-ft})$$

The experimental ultimate moment, 76.3 kN-m (56.3 k-ft), is very close to the nominal flexural capacity, 76.6 kN-m (56.5 k-ft). After multiplied with a reduction factor, ACI 440 design code gives a more conservative moment.

6.2. CONCRETE SOCIETY TECHNICAL REPORT NO. 55

The risks of debonding are exacerbated by the formation of wide flexural and shear cracks. The Concrete Society committee from the United Kingdom recommends that to avoid debonding failure, the strain in the FRP should not exceed 0.8% when the applied loading is uniformly distributed, and 0.6% if combined high shear forces and bending moment are present, such as when the load is concentrated at a point and at

hogging regions close to supports. The procedures for calculating the nominal strength of Slab A are summarized as follows:

Step 1: Determine the maximum allowable FRP strain and depth of neutral axis of strengthened section.

$$\varepsilon_f = 0.008$$

$$0.67 \frac{f'_c}{\gamma_{mc}} b(0.9c) = \frac{f_y}{\gamma_{ms}} + \varepsilon_f \frac{E_f}{\gamma_{mE}} A_f \quad (6.9)$$

$$c = 29mm$$

in which γ_{mc} = partial safety factor for concrete = 1.5 ; γ_{ms} = partial safety factor for steel = 1.05; γ_{mE} = partial safety factor for FRP system = 1.54.

Step 2: Calculate the strain in the concrete and the reinforcement steel. Equation 6.9 is valid only if the concrete do not crush and the steel yield when $\varepsilon_y = 0.008$.

$$\varepsilon_c = \frac{c}{h-c} \varepsilon_f = 0.0012 < 0.0035$$

$$\varepsilon_s = \varepsilon_f \frac{d-c}{h-c} = 0.0067 < \varepsilon_y$$

Step 3: Calculate the design flexural strength of the section. Taking moments about the bottom face, the moment of resistance for $\varepsilon_y = 0.008$, are given by:

$$z = d - 0.9 \frac{c}{2} \quad (6.10)$$

$$M = \left(0.67 \frac{f'_c}{\gamma_{mc}} \right) b (0.9c) (z + (h - d)) - \frac{f_y}{\gamma_{ms}} A_s (h - d) \quad (6.11)$$

$$M = 73.9 \text{ kN/mm}^2 \quad (54.5 \text{ k} - \text{ft})$$

The nominal moment is lower than the experimental ultimate moment. This verifies that the strain limit of 0.8% is reasonable for flexural strengthening. To avoid premature peeling failure, the Concrete Society committee also suggests that the longitudinal shear stress at the ultimate limit state should not exceed 0.8 N/mm^2 (116 psi) and anchoring the FRP by extending it beyond the point at which it is theoretically no longer required.

7. CONCLUSION

Significant increases in flexural capacity ranging from 63% to 145% were registered in all the strengthened slabs as compared to the control slab. During the test, it was observed that the CFRP EBR delayed the presence of the first visible cracks and reduced the deflection. The following conclusions can be drawn from this experimental, analytical and design phases carried out in this program.

7.1. EXPERIMENTAL PHASE

The slabs strengthened with cold cured adhesive bonded CFRP plates failed due to debonding initiated at the plate end. The formation of wide flexural cracks that occur as a result of the yielding of the embedded steel bars generate high stresses in the CFRP plate across the crack, which can only dissipate by debonding. This debonding can then propagate towards the plate end, leading to CFRP debonding failure.

The prestressed CFRP plates had a positive influence on the behavior of strengthened RC slab. The load capacity was substantially increased and the deflection and crack formations were substantially reduced. Even though the failure mode was caused by slippage at the fixed anchorage system, the CFRP plate almost reached the ultimate strength when the failure occurred.

The influence of high axial stiffness of the carbon fiber sheet on the strengthened slab, prior to yielding, was clearly observed. The slab strengthened with a ply of carbon fiber sheet failed due to fiber rupture at the highest moment region.

The test results showed that the slab strengthened with CFRP NSM reinforcement exhibited the highest ultimate moment and the CFRP bars were fully utilized prior to

failure. The test results clearly indicated the successful performance of CFRP NSM reinforcement.

7.2. ANALYTICAL PHASE

Roberts [19] stated that failure of epoxy-bonded plates was likely to occur at shear stresses between 3 - 5 N/mm² (0.43 - 0.73 ksi) combined with normal stresses between 1 - 2 N/mm² (0.145 - 0.29 ksi), although these limits are said to depend on the concrete and on the method of surface preparation.

Both the analytical approaches presented in Section 5 indicate that the shear and normal stresses at the cutoff point of CFRP plate were below the range of failure stresses state by Roberts. The principal stress at the cutoff point of CFRP plate was also less than the tensile strength of concrete, proving an adequate margin of safety.

7.3. DESIGN PHASE

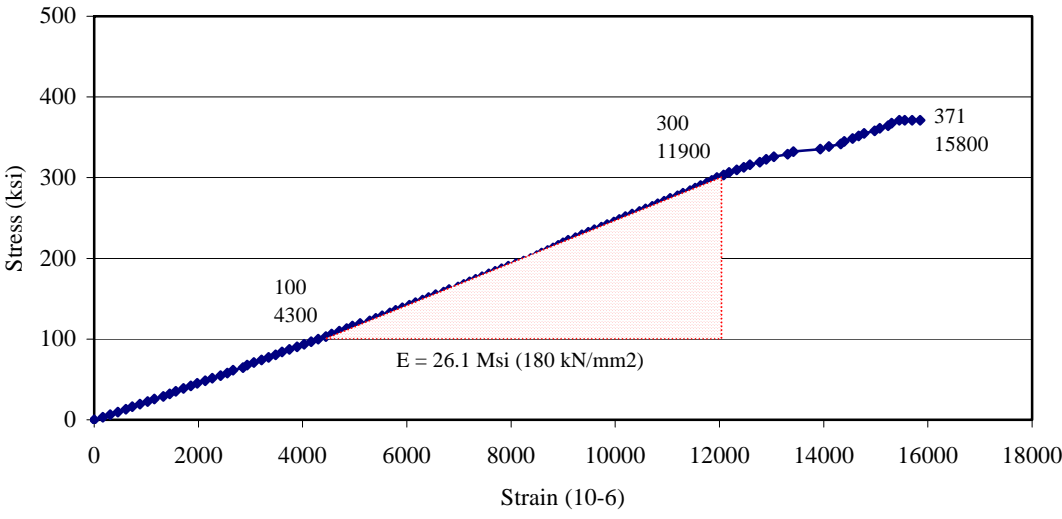
Both the ACI 440 and Concrete Society Technical Report No.55 apply strain limitation on the FRP to ensure that bond failure far from the anchorage will be prevented. The nominal moments obtain from both design codes were close to the experimental ultimate moment of Slab A. ACI 440 provides a more conservative moment after multiplying the nominal moment by a reduction factor.

Strain limitation is used mainly due to its simplicity for the practitioner. However, it represents a crude simplification of the real behavior, as the FRP strain corresponding to bond failure is not a fixed value but it depends on a series of parameter, including the moment shear relation, the train in the internal steel and the distribution of cracks.

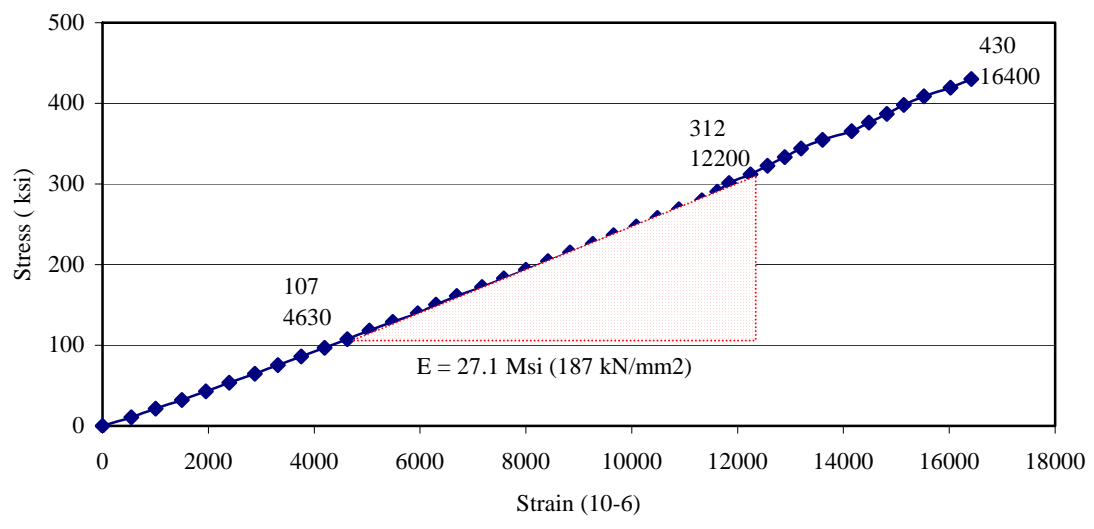
APPENDIX A.

TENSILE STRESS-STRAIN CURVES FOR CFRP SYSTEMS AND ADHESIVE

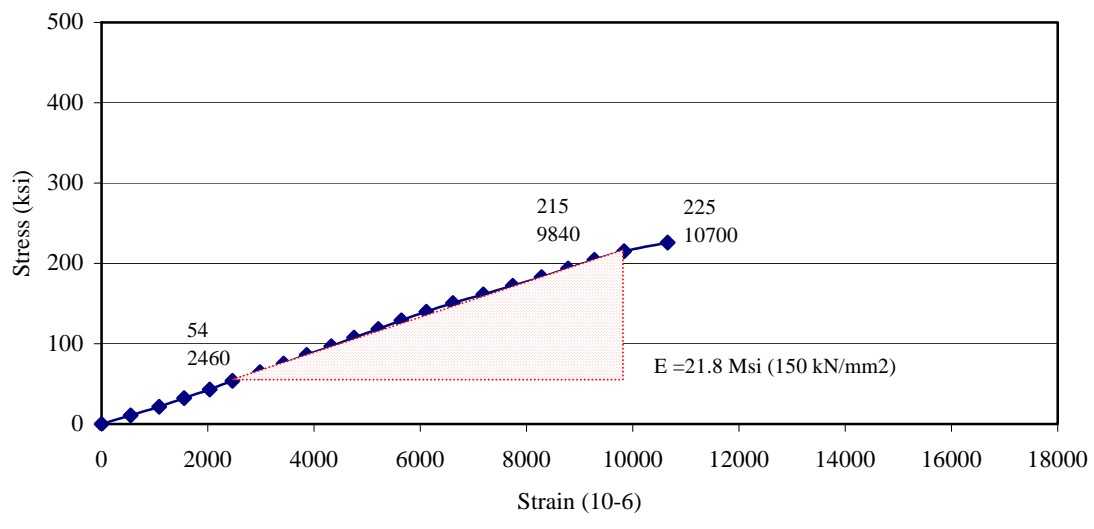
Tensile Stress-Strain Curves for CFRP Plate (1)



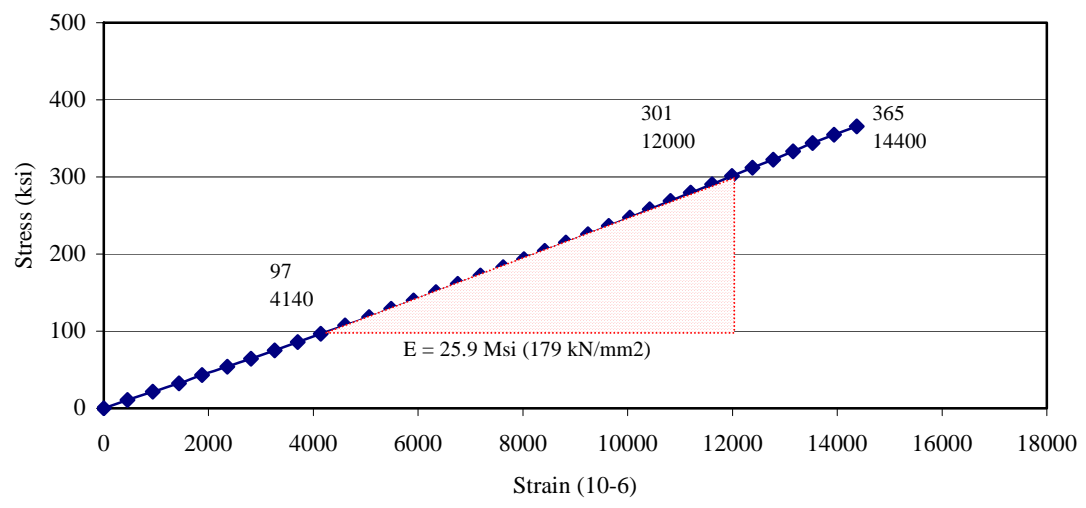
Tensile Stress-Strain Curves for CFRP Plate (2)

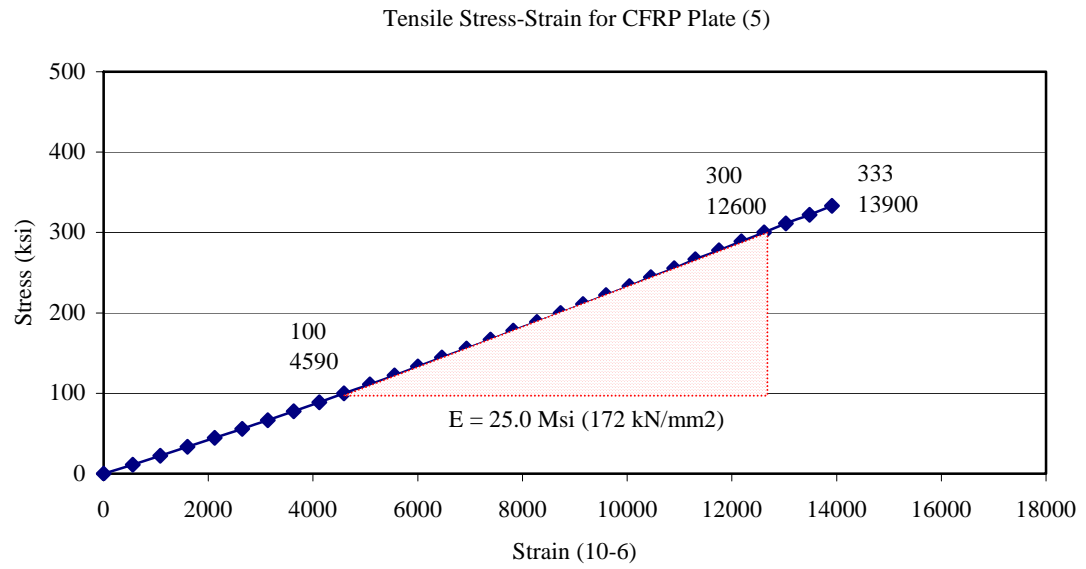


Tensile Stress-Strain Curves for CFRP Plate (3)

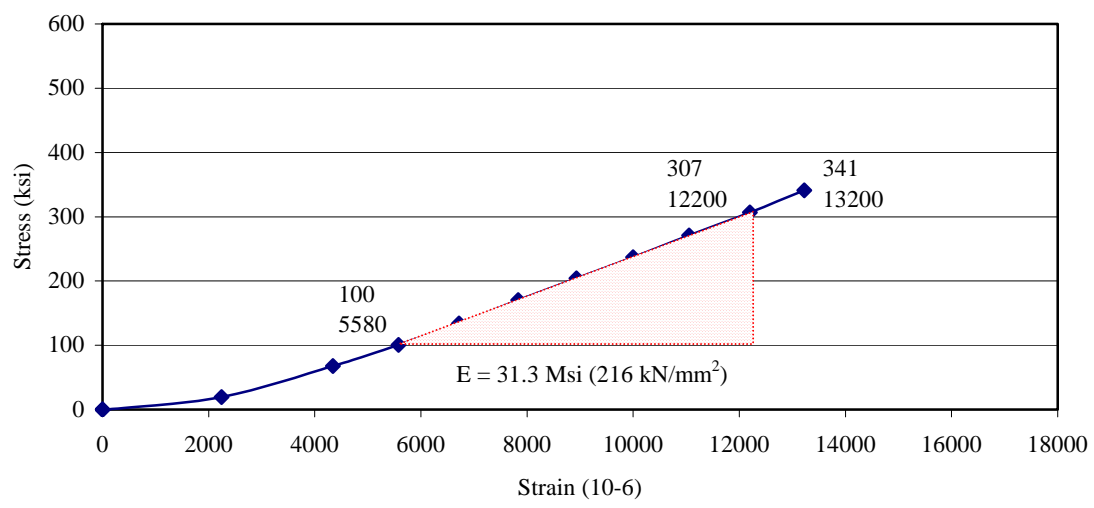


Tensile Stress-Strain Curves for CFRP Plate (4)

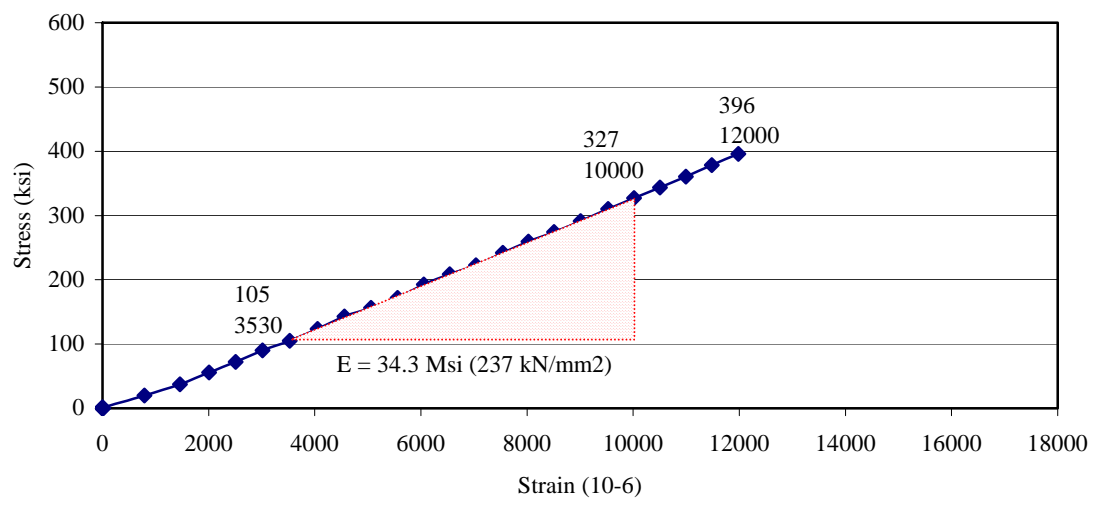




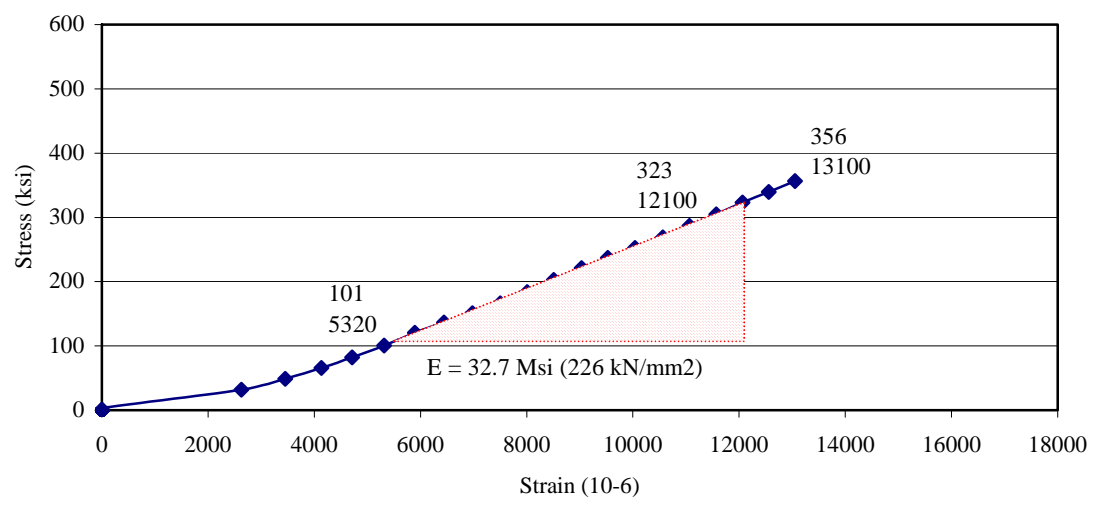
Tensile Stress-Strain for Carbon Fiber Sheet (1)



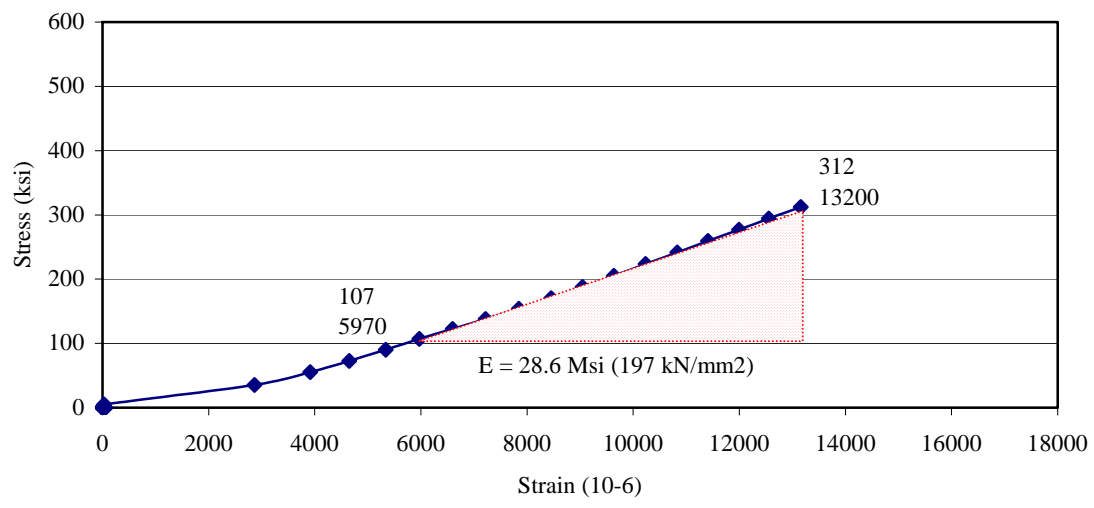
Tensile Stress-Strain for Carbon Fiber Sheet (2)



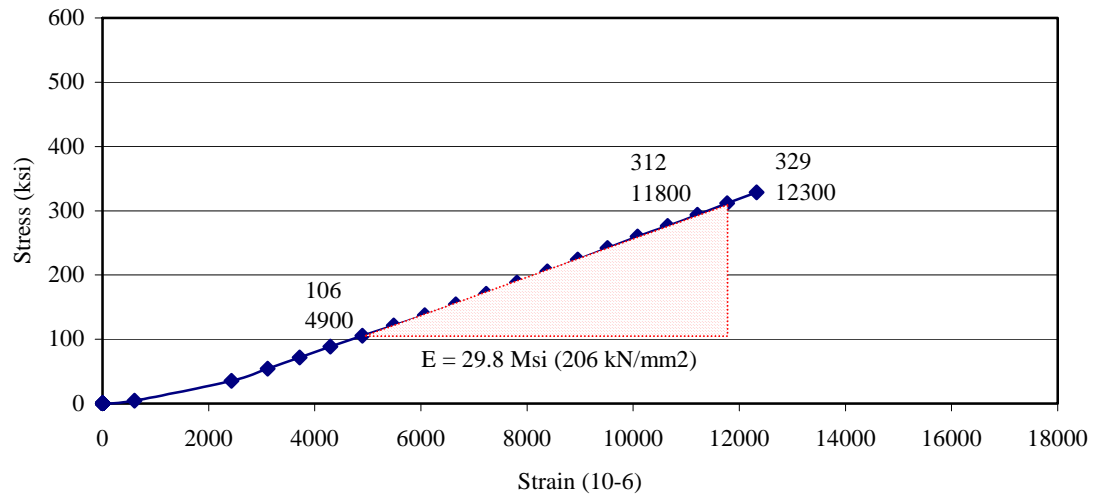
Tensile Stress-Strain Curves for Carbon Fiber Sheet (3)



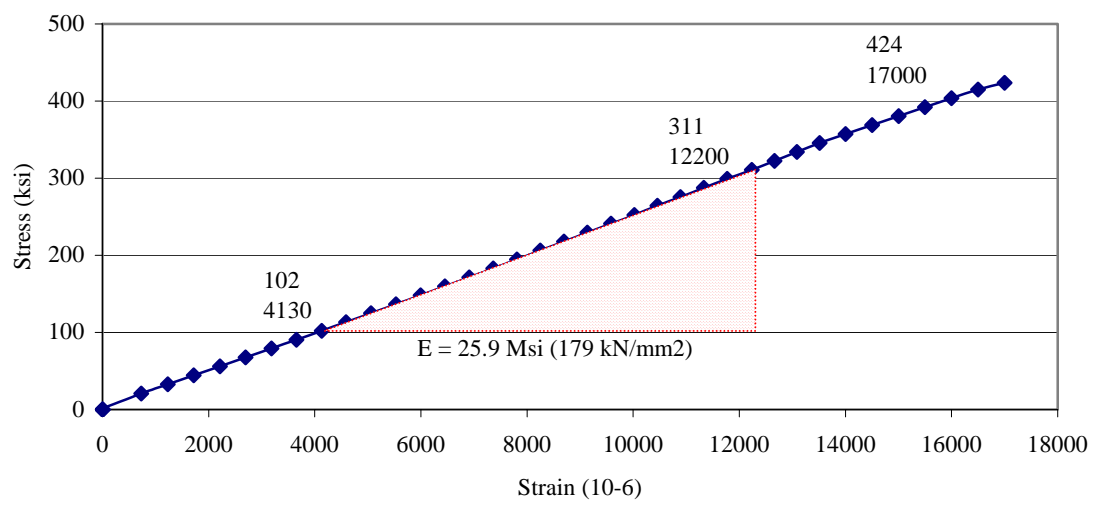
Tensile Stress-Strain Curves for Carbon Fiber Sheet (4)



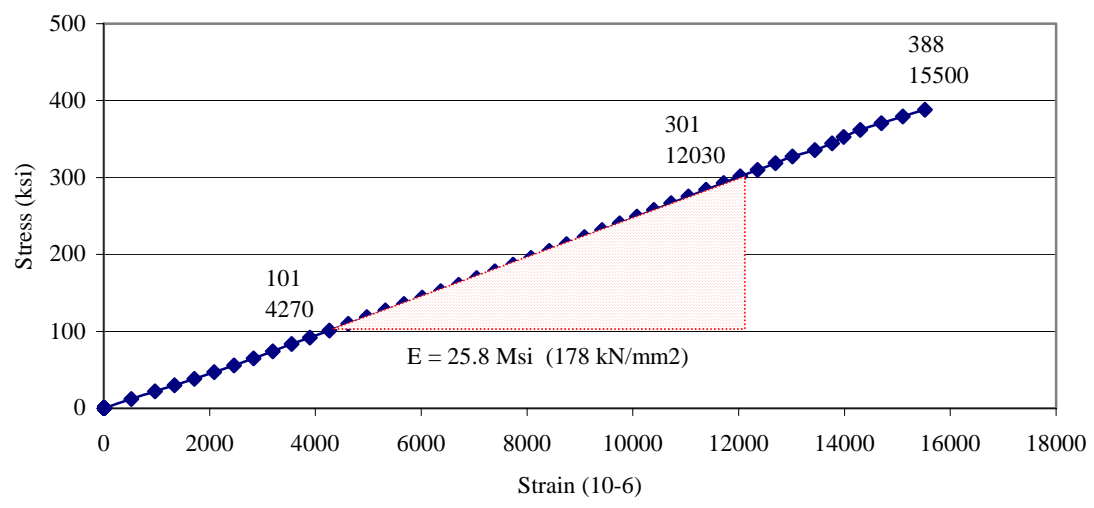
Tensile Stress-Strain Curves for Carbon Fiber Sheet (5)



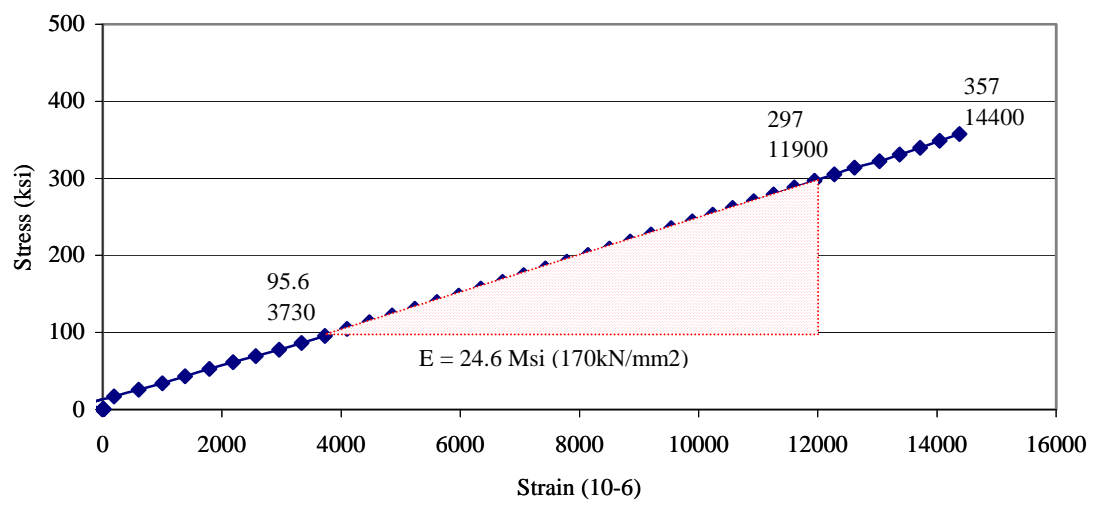
Tensile Stress-Strain Curves for CFRP Bar (1)



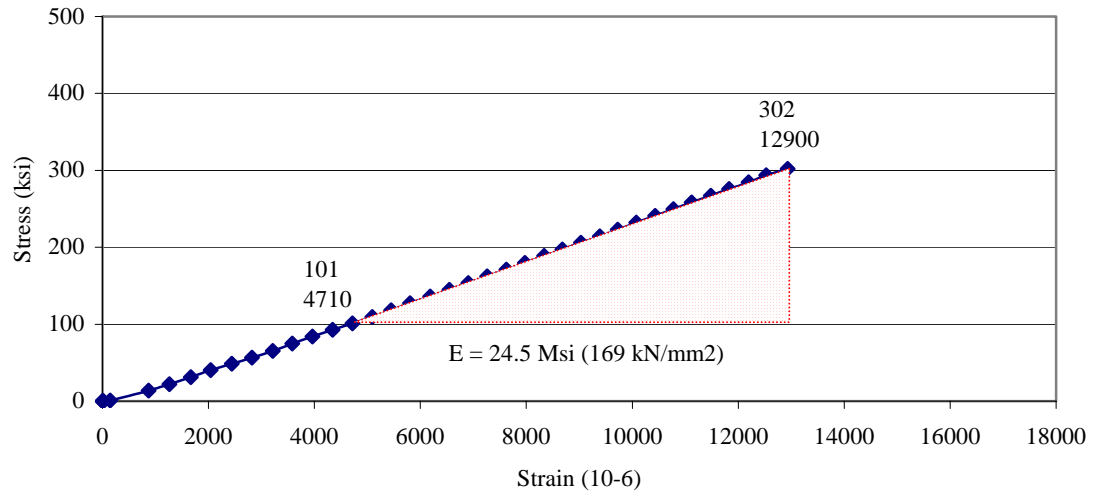
Tensile Stress-Strain Curves for CFRP Bar (2)



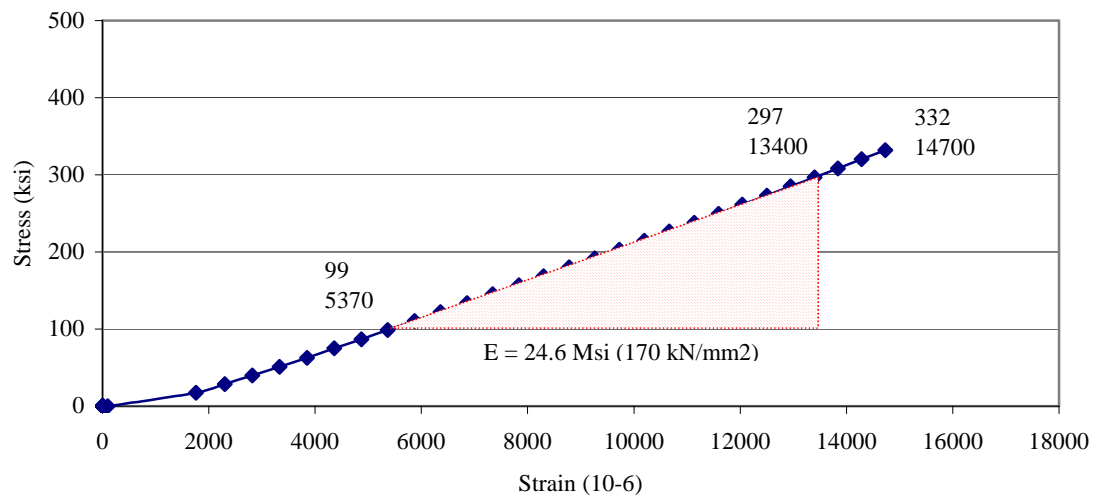
Tensile Stress vs. Strain Curves for CFRP Bar (3)



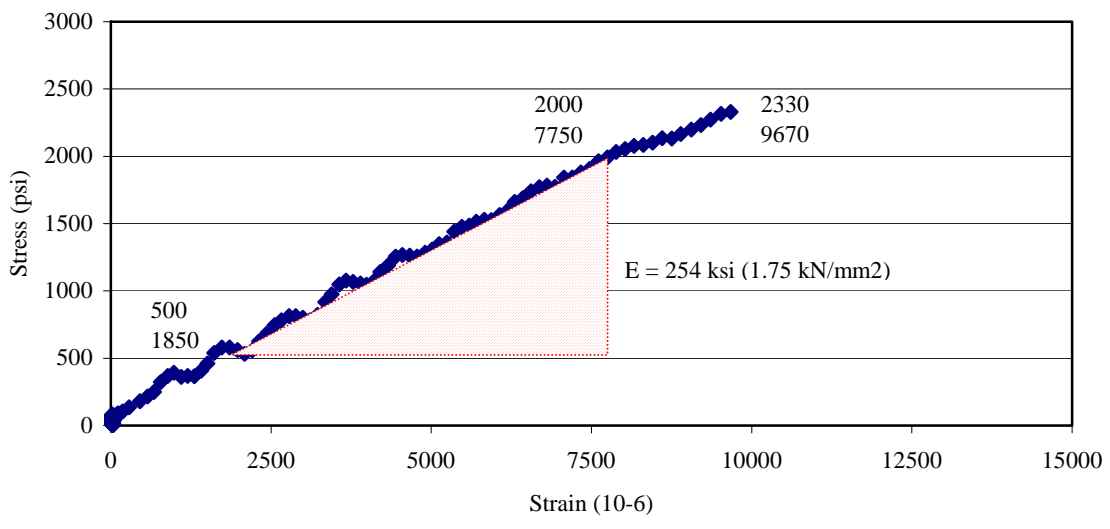
Tensile Stress-Strain Curves for CFRP Bar (4)



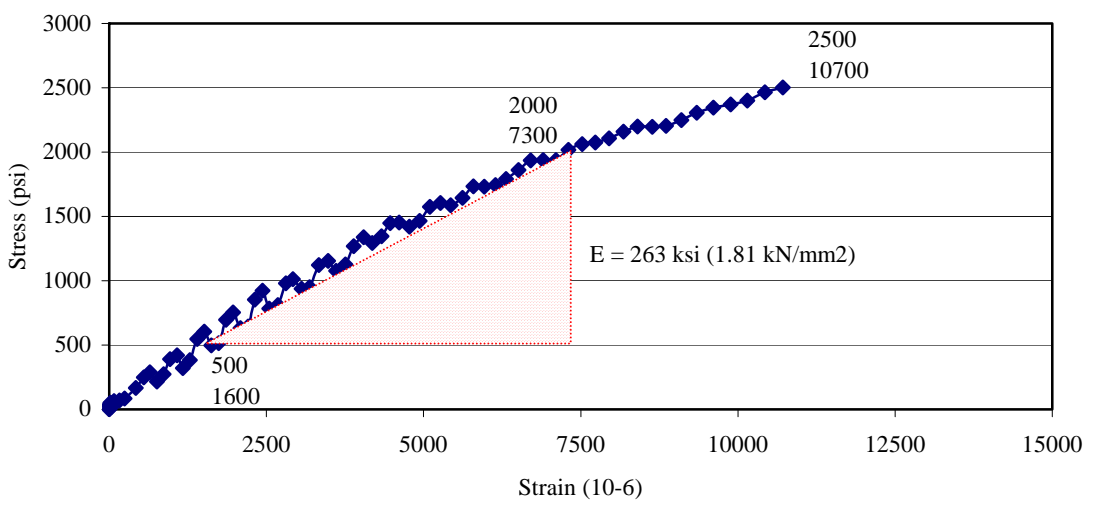
Tensile Stress-Strain Curves for CFRP Bar (5)



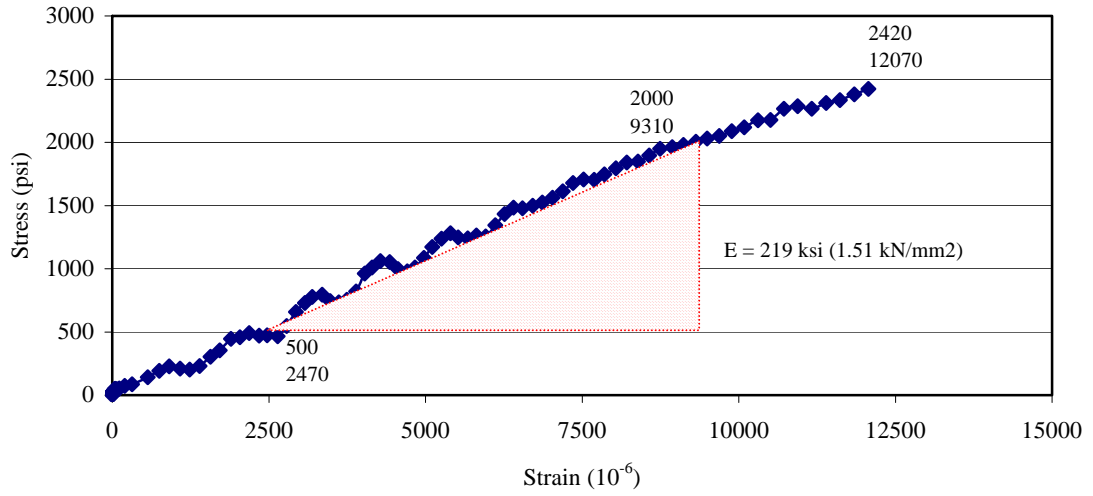
Tensile Stress-Strain Curves for Epoxy Gel (1)



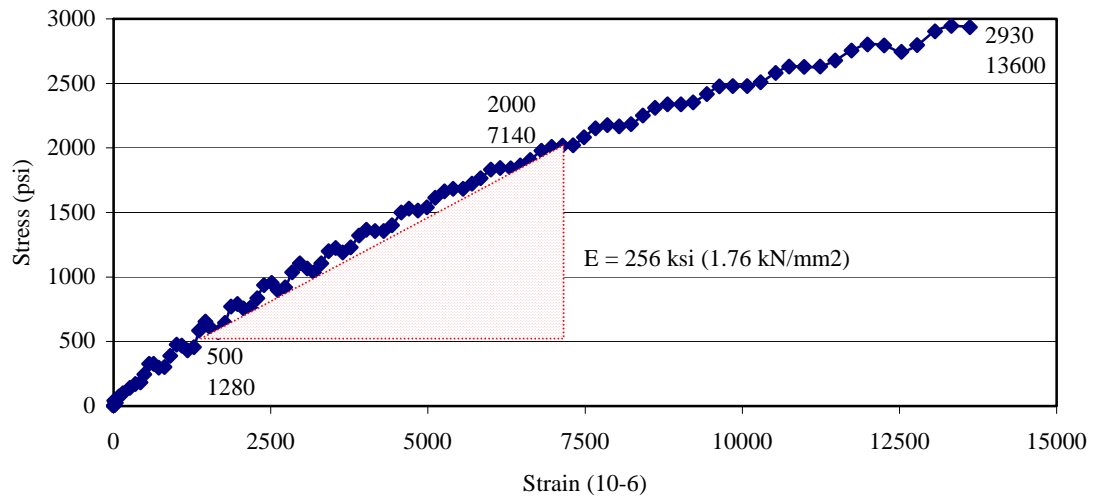
Tensile Stress-Strain Curves for Epoxy Gel (2)



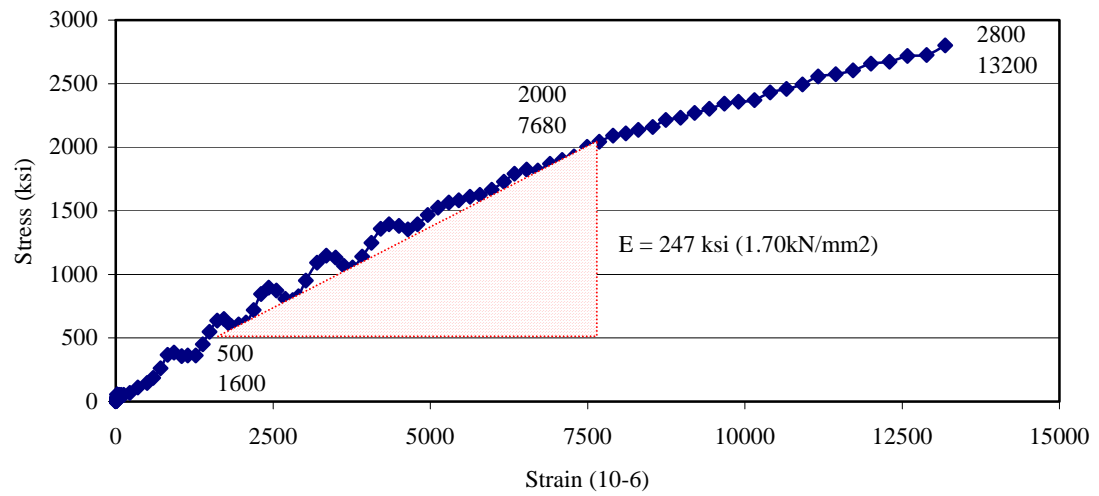
Tensile Stress- Strain Curves for Epoxy Gel (3)



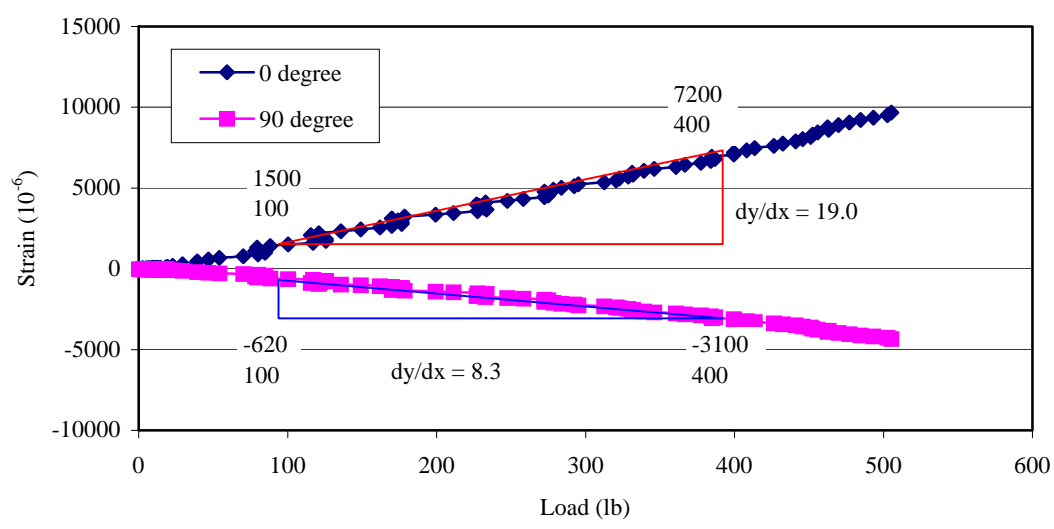
Tensile Stress-Strain Curves for Epoxy Gel (4)



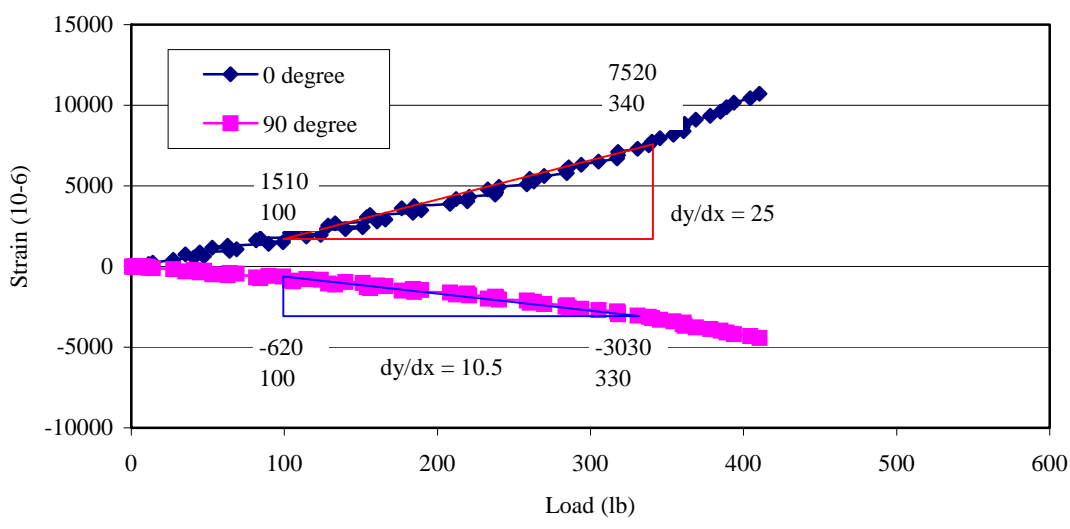
Tensile Stress-Strain Curves for Epoxy Gel (5)



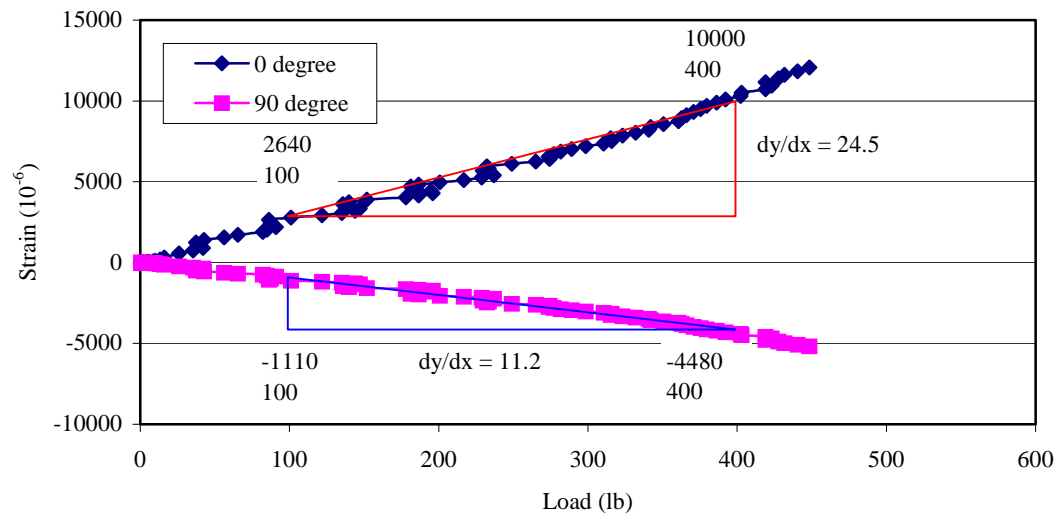
Strain vs. Load for Determination of Poisson's Ratio (1)



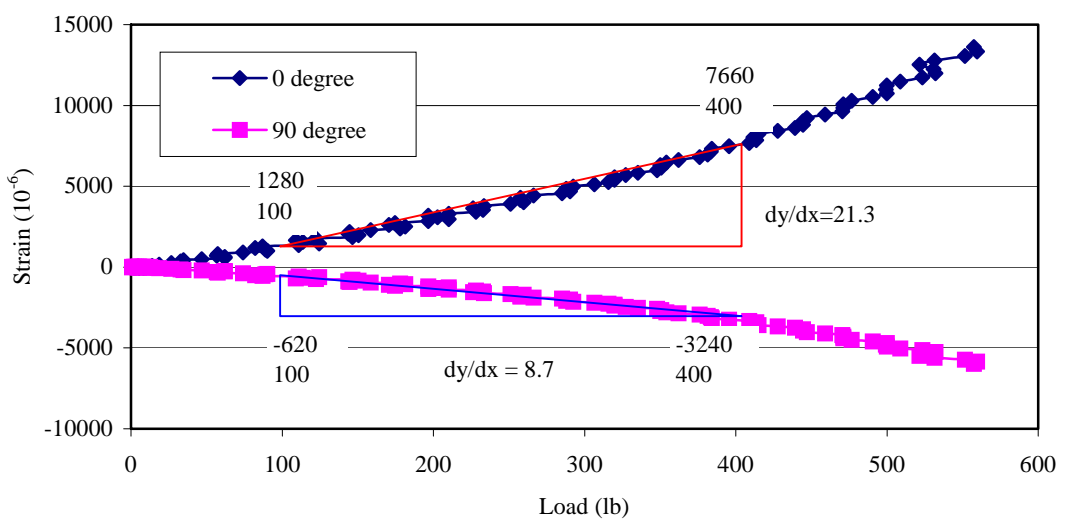
Strain vs. Load for Determination of Poisson's Ratio (2)



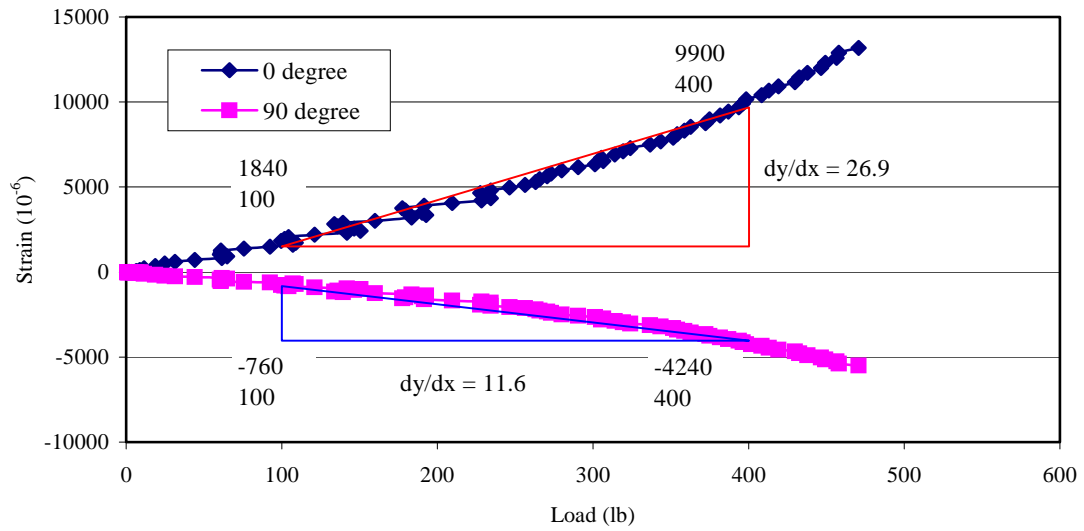
Strain versus Load for Determination of Poisson's Ratio (3)



Strain vs. Load for Determination of Poisson's Ratio (4)



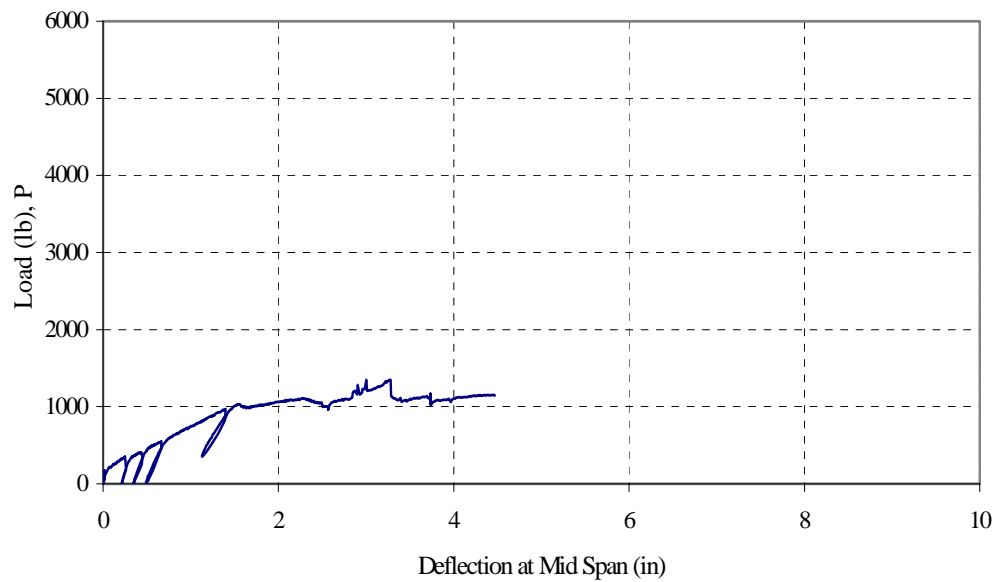
Strain vs. Load for Determination of Poisson's Ratio (5)



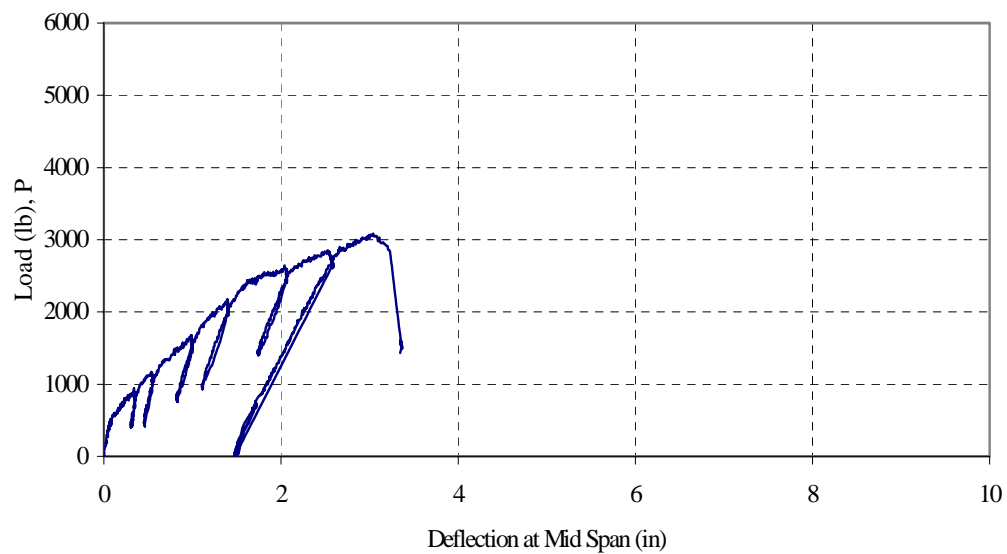
APPENDIX B.

EXPERIMENTAL LOAD-DEFLECTION AND LOAD-STRAIN CURVES

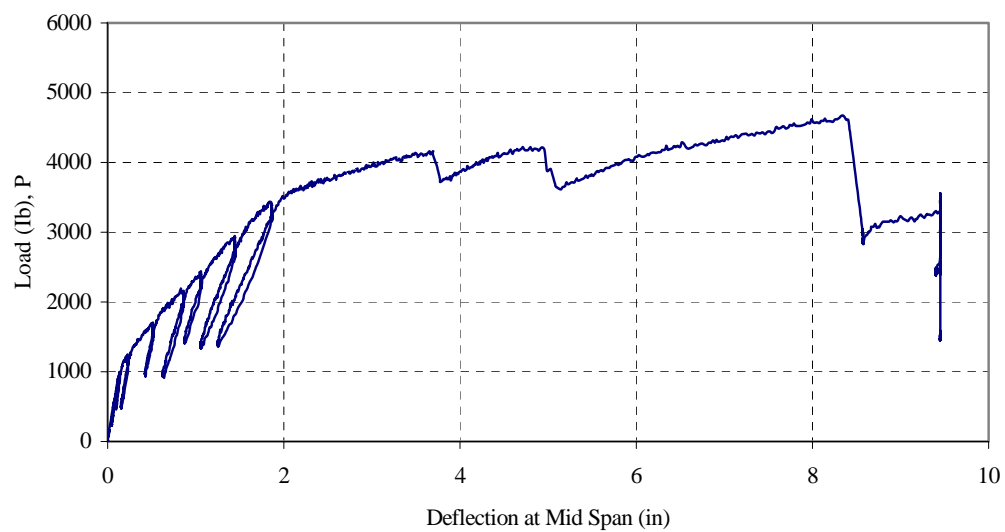
Load vs. Deflection Curves for Control Slab.



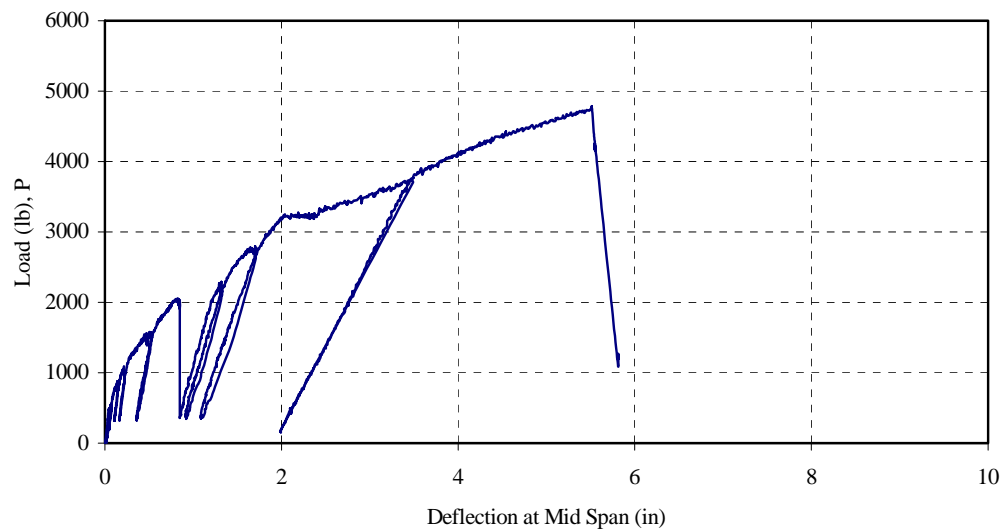
Load vs. Deflection Curves for Slab A.



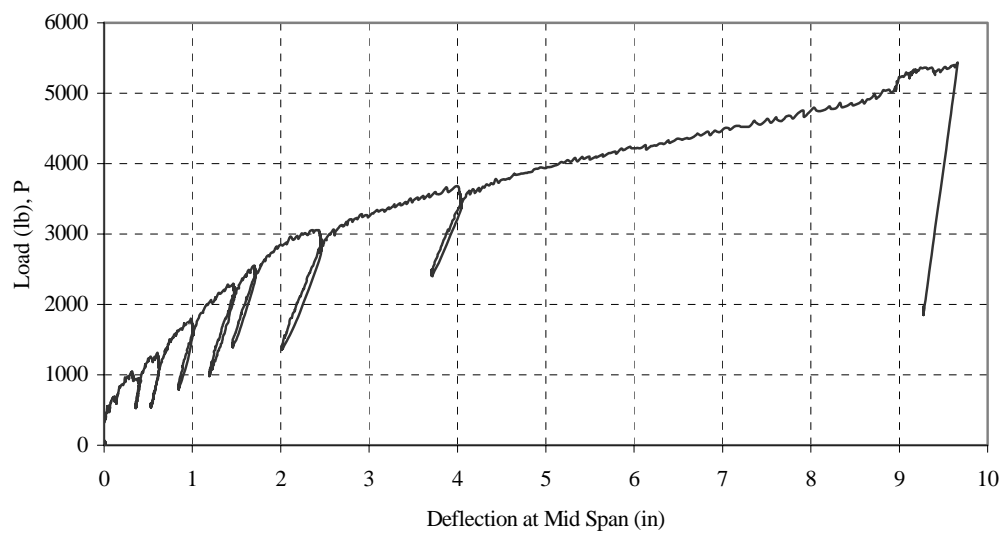
Load vs. Deflection Curves for Slab B



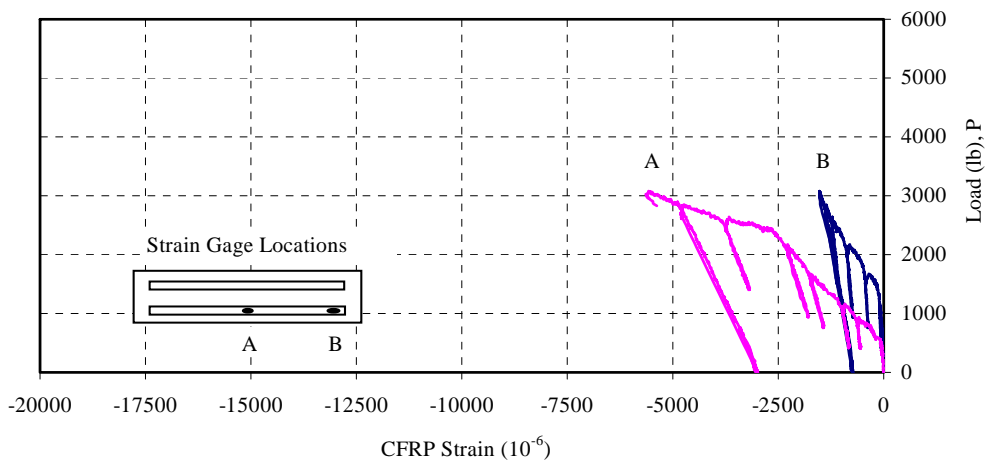
Load vs. Deflection Curves for Slab C



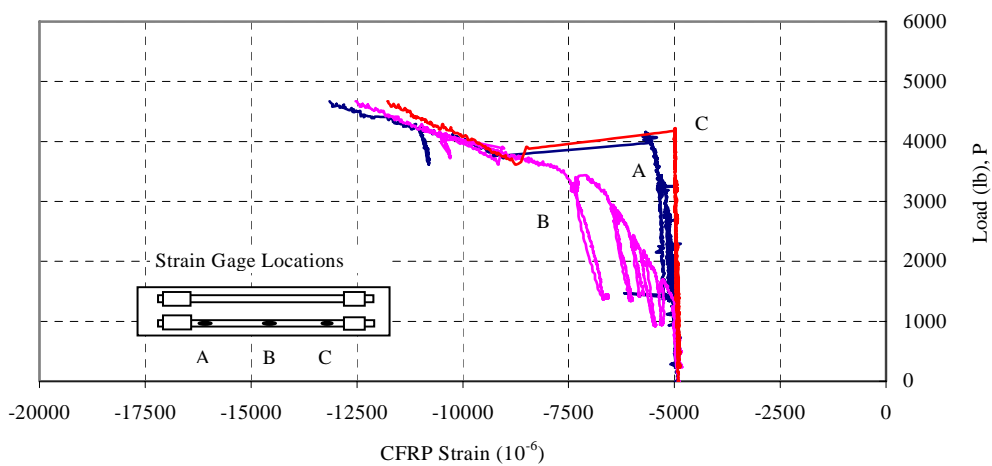
Load vs. Deflection Curves for Slab D



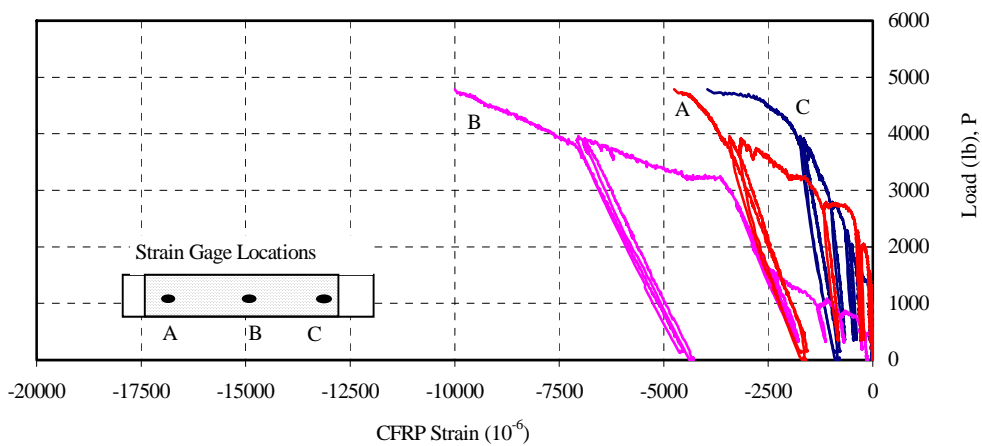
Load vs. CFRP Plate Strain Curves for Slab A



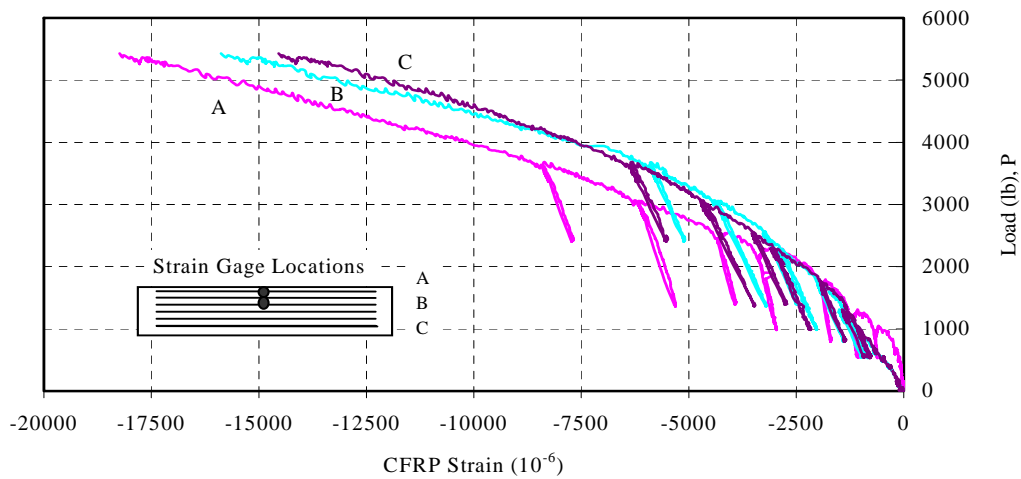
Load vs. CFRP Plate Strain Curves for Slab B



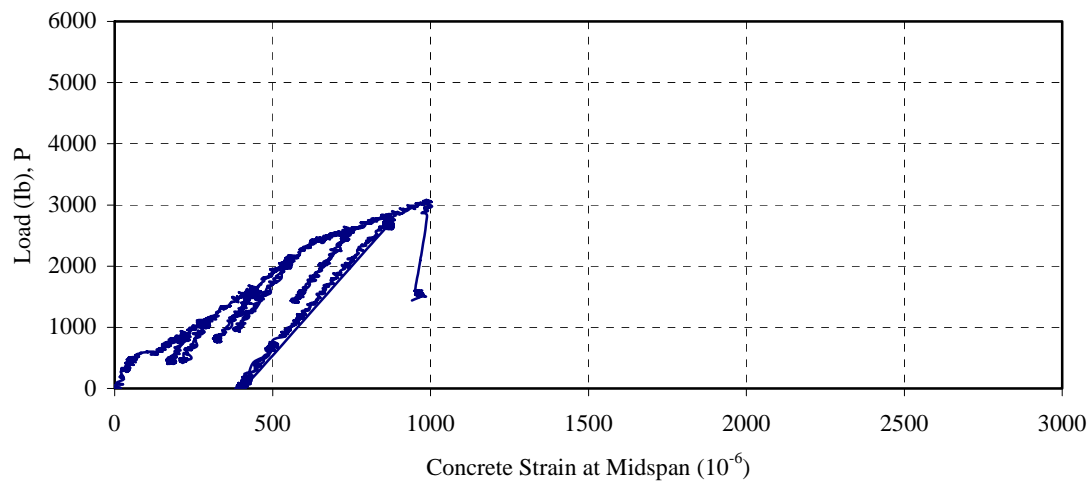
Load vs. Carbon Fiber Sheet Strain Curves for Slab C



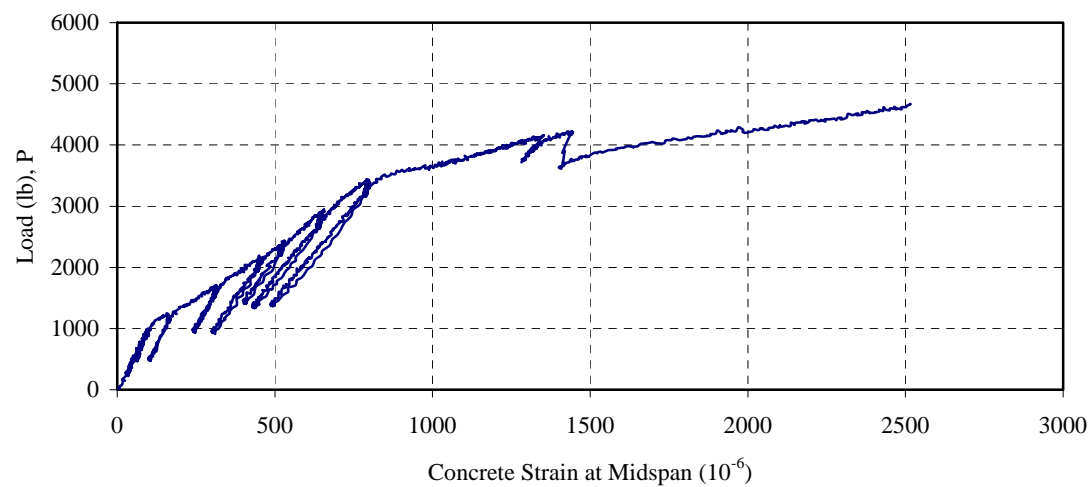
Load vs. CFRP Bars Strain Curves for Slab D



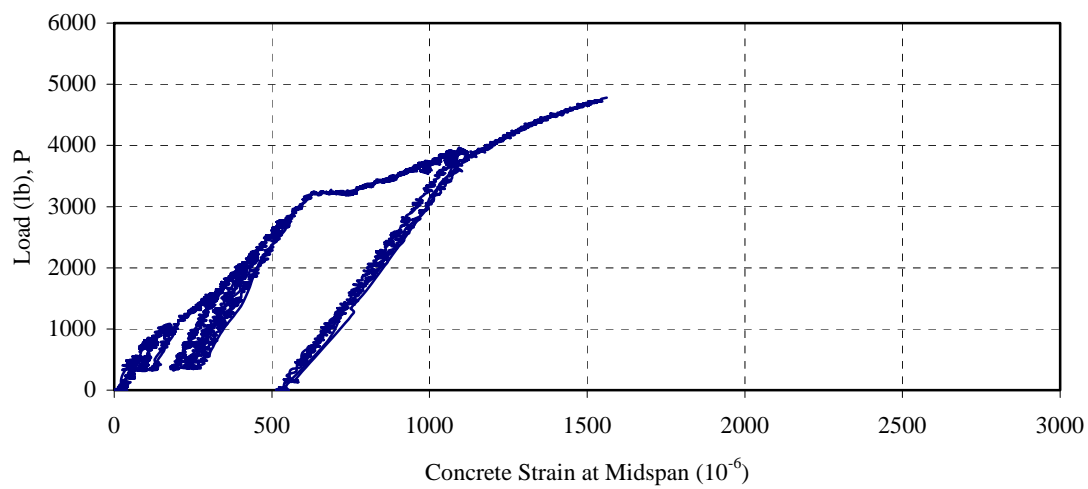
Load vs. Concrete Strain Curves for Slab A



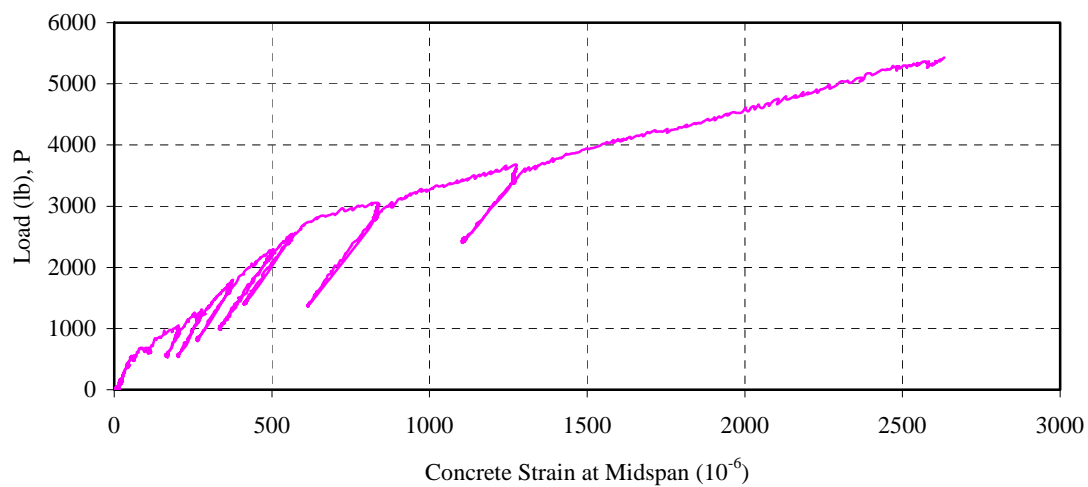
Load vs. Concrete Strain Curves for Slab B



Load vs. Concrete Strain Curves for Slab C



Load vs. Concrete Strain Curves for Slab D



APPENDIX C

MOMENT CURVATURE CALCULATION

Moment Curvature Calculation for Cold Cured Adhesive Bonded CFRP Plate

Geometry Property

$$h := 8.625 \text{ in} \quad d := 7.375 \text{ in} \quad b := 39.375 \text{ in} \quad L := 240 \text{ in} \quad y := 4.3 \text{ in}$$

Manufacturer's Material Property

$$f_c := 4900 \text{ psi} \quad f_y := 60000 \text{ psi} \quad f_{fu} := 3.6 \cdot 10^5 \text{ psi} \quad A_c = 2.358 \text{ ft}^2$$

$$E_c := 57000 \sqrt{f_c} \cdot \text{psi} \quad E_s := 29 \cdot 10^6 \cdot \text{psi} \quad E_f := 23 \cdot 10^6 \cdot \text{psi}$$

$$A_c = 339.609 \text{ in}^2 \quad A_s := 1.0 \text{ in}^2 \quad A_f = 0.186 \text{ in}^2$$

Moment of Inertia

$$I := \frac{(b \cdot h^3)}{12} \quad I = 2.105 \times 10^3 \text{ in}^4$$

Cracking strain and stress of concrete

$$\sigma := 7.5 \cdot \sqrt{f_c} \cdot \text{psi} \quad \sigma = 525 \text{ psi} \quad \epsilon_{cr} := \frac{\sigma}{E_c} \quad \epsilon_{cr} = 1.316 \times 10^{-4}$$

Moment causing flexural cracking at section due to externally applied loads, **M_{cr}**.

$$M_{cr} := \frac{\sigma \cdot I}{y} \quad M_{cr} = 2.142 \times 10^4 \text{ lbf} \cdot \text{ft}$$

Stress Block Factors

$$\epsilon := 0.002 \quad \epsilon_c := 0.000001, 0.00001, 0.003$$

$$\beta(\epsilon_c) := \frac{4 - \frac{\epsilon_c}{\epsilon}}{6 - \frac{2 \cdot \epsilon_c}{\epsilon}} \quad \alpha(\epsilon_c) := \frac{\frac{\epsilon_c}{\epsilon} - \frac{1}{3} \left(\frac{\epsilon_c}{\epsilon} \right)^2}{\beta(\epsilon_c)}$$

Balance Condition Without Consider ϵ_{bi}

$$\alpha \cdot \beta \cdot f_c \cdot b \cdot c(\epsilon_c) = A_s \cdot E_s \cdot \epsilon_c \cdot \left(\frac{d - c(\epsilon_c)}{c(\epsilon_c)} \right) + A_f \cdot E_f \cdot \left[\epsilon_c \cdot \left(\frac{h - c(\epsilon_c)}{c(\epsilon_c)} \right) \right]$$

$$B(\epsilon_c) := A_s \cdot E_s \cdot \epsilon_c + A_f \cdot E_f \cdot \epsilon_c$$

$$c(\epsilon_c) := \frac{-B(\epsilon_c) + \sqrt{(B(\epsilon_c))^2 + 4 \cdot \alpha(\epsilon_c) \cdot \beta(\epsilon_c) \cdot f_c \cdot b \cdot (A_s \cdot E_s \cdot \epsilon_c \cdot d + A_f \cdot E_f \cdot \epsilon_c \cdot h)}}{2 \cdot \alpha(\epsilon_c) \cdot \beta(\epsilon_c) \cdot f_c \cdot b}$$

Moment Curvature Calculation for Cold Cured Adhesive Bonded CFRP Plate

Balance Condition (without consider ϵ_{bi}) when steel yield

$$\alpha \cdot \beta \cdot f_c \cdot b \cdot c = A_s \cdot f_y + A_f \cdot E_f \cdot \left[\epsilon \cdot \left(\frac{h - c}{c} \right) \right]$$

Stress in steel

$$f_s(\epsilon) := E_s \cdot \epsilon \cdot \frac{d - c(\epsilon)}{c(\epsilon)}$$

$$f_s(\epsilon) := \begin{cases} f_s(\epsilon) & \text{if } f_s(\epsilon) < f_y \\ f_y & \text{otherwise} \end{cases}$$

$$c(\epsilon) := \begin{cases} c(\epsilon) & \text{if } f_s(\epsilon) < f_y \\ \frac{-(A_f \cdot E_f \cdot \epsilon - A_s \cdot f_y) + \sqrt{(A_f \cdot E_f \cdot \epsilon - A_s \cdot f_y)^2 + 4 \cdot \alpha(\epsilon) \cdot \beta(\epsilon) \cdot f_c \cdot b \cdot (A_f \cdot E_f \cdot \epsilon \cdot h)}}{2 \cdot \alpha(\epsilon) \cdot \beta(\epsilon) \cdot f_c \cdot b} & \text{otherwise} \end{cases}$$

Balance Condition (without consider ϵ_{bi}) when steel yield and laminate rupture

$$\alpha \cdot \beta \cdot f_c \cdot b \cdot c = A_s \cdot f_y$$

Stress in CFRP Plate

$$f_f(\epsilon) := E_f \cdot \epsilon \cdot \frac{h - c(\epsilon)}{c(\epsilon)}$$

$$c(\epsilon) := \begin{cases} c(\epsilon) & \text{if } f_f(\epsilon) < f_{fu} \\ \frac{A_s \cdot f_y}{\alpha(\epsilon) \cdot \beta(\epsilon) \cdot f_c \cdot b} & \text{otherwise} \end{cases}$$

$$f_f(\epsilon) := \begin{cases} f_f(\epsilon) & \text{if } f_f(\epsilon) < f_{fu} \\ 0 \cdot \text{psi} & \text{otherwise} \end{cases}$$

Moment and Curvature

$$M(\epsilon) := A_s \cdot f_s(\epsilon) \cdot (d - .5 \cdot \beta(\epsilon) \cdot c(\epsilon)) + A_f \cdot f_f(\epsilon) \cdot (h - .5 \cdot \beta(\epsilon) \cdot c(\epsilon))$$

$$\phi(\epsilon) := \frac{\epsilon}{c(\epsilon)} \qquad k := \frac{M_{cr}}{\epsilon_{cr}}$$

$$M(\epsilon) := \begin{cases} k \cdot \epsilon & \text{if } \epsilon < \epsilon_{cr} \\ M(\epsilon) & \text{otherwise} \end{cases}$$

Moment Curvature Calculation for Prestressed CFRP Plate

Geometry Property

$$\begin{array}{llll}
 h := 8.625 \text{ in} & b := 39.375 \text{ in} & I := \frac{b \cdot h^3}{12} & s := \frac{I}{0.5 \cdot h} \\
 d := 7.25 \text{ in} & L := 240 \text{ in} & I = 2.105 \times 10^3 \text{ in}^4 & s = 488.188 \text{ in}^3 \\
 e := 0.5 \cdot h & y := 4.3 \text{ in} & &
 \end{array}$$

Material Property

$$\begin{array}{llll}
 f_c := 4900 \text{ psi} & f_y := 60000 \text{ psi} & f_{fu} := 3.75 \cdot 10^5 \text{ psi} & \epsilon_{fu} := 0.016 \\
 E_c := 57000 \sqrt{f_c} \text{ psi} & E_s := 29 \cdot 10^6 \text{ psi} & E_f := 26 \cdot 10^6 \text{ psi} & \\
 A_c = 339.609 \text{ in}^2 & A_s := 1.0 \text{ in}^2 & A_f := 0.186 \text{ in}^2 &
 \end{array}$$

Prestressed force

$$\begin{array}{lll}
 F := 21000 \text{ lbf} & f_{se} := \frac{F}{A_f} & f_{se} = 1.129 \times 10^5 \text{ psi} \\
 \epsilon_{fe} := 0.0049 & &
 \end{array}$$

Initial State, M = 0 k-ft (No externally applied load)

$$\begin{array}{llll}
 f_{top} := \frac{-F}{A_c} + \frac{F \cdot e}{s} & f_{top} = 123.67 \text{ psi} & \epsilon_{top} := \frac{f_{top}}{E_c} & \epsilon_{top} = 3.1 \times 10^{-5} \\
 f_{bot} := \frac{-F}{A_c} - \frac{F \cdot e}{s} & f_{bot} = -247.343 \text{ psi} & \epsilon_{bot} := \frac{f_{bot}}{E_c} & \epsilon_{bot} = -6.199 \times 10^{-5} \\
 \phi := \frac{\epsilon_{top} - \epsilon_{bot}}{h} & \phi = 1.078 \times 10^{-5} \frac{1}{\text{in}} & \epsilon_{se} := \frac{f_{se}}{E_f} & \epsilon_{se} = 4.342 \times 10^{-3}
 \end{array}$$

Add f = 247.343 psi for $\epsilon = 0$

$$M_0 := \frac{-f_{bot} \cdot I}{0.5 \cdot h} \quad M_0 = 1.006 \times 10^4 \text{ lbf} \cdot \text{ft}$$

Now add M/s term to get ϵ and ϕ

$$\begin{array}{llll}
 f_{top} := f_{top} - \frac{M_0}{s} & f_{top} = -123.67 \text{ psi} & \epsilon_{top} := \frac{f_{top}}{E_c} & \epsilon_{top} = -3.1 \times 10^{-5} \\
 f_{bot} := f_{bot} + \frac{M_0}{s} & f_{bot} = 0 \text{ psi} & \epsilon_{bot} := \frac{f_{bot}}{E_c} & \epsilon_{bot} = 0 \\
 \phi_0 := \frac{-\epsilon_{top} + \epsilon_{bot}}{h} & \phi_0 = 3.594 \times 10^{-6} \frac{1}{\text{in}} & &
 \end{array}$$

Moment Curvature Calculation for Prestressed CFRP Plate**Moment = 19.35 k-ft (232200 lb-in)**

To reach Moment = 19.35 k-ft

$$\Delta M := 9290 \text{ lbf}\cdot\text{ft}$$

$$\Delta f := \frac{\Delta M \cdot y}{I} \quad \Delta f = 227.693 \text{ psi}$$

$$\Delta f_{ps} := \frac{E_f}{E_c} \cdot \frac{\Delta M \cdot y}{I} \quad \Delta f_{ps} = 1.484 \times 10^3 \text{ psi} \quad f_{se} = 1.129 \times 10^5 \text{ psi}$$

$$f_p := f_{se} + \Delta f_{ps} \quad f_p = 1.144 \times 10^5 \text{ psi} \quad F := A_f \cdot f_p \quad F = 2.128 \times 10^4 \text{ lbf}$$

$$\Delta \varepsilon := \frac{\Delta f}{E_c} \quad \Delta \varepsilon = 5.707 \times 10^{-5} \quad \Delta \phi := \frac{2 \cdot \Delta \varepsilon}{h} \quad \Delta \phi = 1.323 \times 10^{-5} \frac{1}{\text{in}}$$

$$\phi_{ini} := \phi_0 + \Delta \phi \quad \phi_{ini} = 1.683 \times 10^{-5} \frac{1}{\text{in}}$$

Moment at crackingTo reach cracking $f = f_{cr}$

$$f_{cr} := 7.5 \cdot \sqrt{f_c} \text{ psi} \quad \Delta f_{cr} := f_{cr}$$

$$\Delta M := \frac{\Delta f_{cr} \cdot I}{y} \quad \Delta M = 2.142 \times 10^4 \text{ lbf}\cdot\text{ft}$$

$$M_{cr} := M_0 + \Delta M \quad M_{cr} = 3.148 \times 10^4 \text{ lbf}\cdot\text{ft}$$

$$\Delta f_{ps} := \frac{E_f}{E_c} \cdot \frac{\Delta M \cdot y}{I} \quad \Delta f_{ps} = 3.421 \times 10^3 \text{ psi}$$

$$f_p := f_{se} + \Delta f_{ps} \quad f_p = 1.163 \times 10^5 \text{ psi} \quad F := A_f \cdot f_p \quad F = 2.164 \times 10^4 \text{ lbf}$$

$$\Delta \varepsilon_{cr} := \frac{\Delta f_{cr}}{E_c} \quad \Delta \varepsilon_{cr} = 1.316 \times 10^{-4} \quad \Delta \phi_{cr} := \frac{2 \cdot \Delta \varepsilon_{cr}}{h} \quad \Delta \phi_{cr} = 3.051 \times 10^{-5} \frac{1}{\text{in}}$$

$$\phi_0 = 3.594 \times 10^{-6} \frac{1}{\text{in}} \quad \Delta f := \frac{\Delta M \cdot y}{I}$$

$$\phi_{cr} := \phi_0 + \Delta \phi_{cr} \quad \phi_{cr} = 3.41 \times 10^{-5} \frac{1}{\text{in}} \quad \Delta f = 525 \text{ psi}$$

Checking

$$f_{top} := \frac{-F}{A_c} + \frac{F \cdot e}{s} - \frac{M_{cr}}{s} \quad f_{top} = -646.45 \text{ psi}$$

$$f_{bot} := \frac{-F}{A_c} - \frac{F \cdot e}{s} + \frac{M_{cr}}{s} \quad f_{bot} = 519.03 \text{ psi} \quad f_{cr} = 525 \text{ psi}$$

Moment Curvature Calculation for Prestressed CFRP Plate

Geometry Property

$$h := 8.625 \text{ in} \quad d := 7.375 \text{ in} \quad b := 39.375 \text{ in} \quad y := \frac{h}{2} \cdot \text{in}$$

Material Property

$$\begin{aligned} f_c &:= 4900 \text{ psi} & f_y &:= 60000 \text{ psi} & f_{fu} &:= 375000 \text{ psi} & \epsilon_{fu} &:= 0.016 \\ E_c &:= 57000 \sqrt{f_c} \text{ psi} & E_s &:= 29000000 \text{ psi} & E_f &:= 25900000 \text{ psi} & \epsilon_{ps0} &:= 5.0 \cdot 10^{-3} \\ A_c &:= 339.609 \text{ in}^2 & A_s &:= 1 \cdot \text{in}^2 & A_f &:= 0.186 \text{ in}^2 \end{aligned}$$

Stress Block Factors

$$\epsilon := 0.002 \quad \epsilon_c := 0.0003, 0.0004, 0.003$$

$$\beta(\epsilon_c) := \frac{4 - \frac{\epsilon_c}{\epsilon}}{6 - \frac{2 \cdot \epsilon_c}{\epsilon}} \quad \alpha(\epsilon_c) := \frac{\frac{\epsilon_c}{\epsilon} - \frac{1}{3} \cdot \left(\frac{\epsilon_c}{\epsilon}\right)^2}{\beta(\epsilon_c)}$$

Balance condition, the neutral axis, c , is given by

$$\alpha \cdot \beta \cdot f_c \cdot b \cdot c = A_s \cdot \left[E_s \cdot \epsilon_c \cdot \left(\frac{d - c}{c} \right) \right] + A_f \cdot E_f \cdot \left[\epsilon_c \cdot \left(\frac{h - c}{c} \right) + \epsilon_{ps0} \right]$$

$$B(\epsilon_c) := A_s \cdot E_s \cdot \epsilon_c - A_f \cdot E_f \cdot (\epsilon_{ps0} - \epsilon_c)$$

$$c(\epsilon_c) := \frac{-B(\epsilon_c) + \sqrt{B(\epsilon_c)^2 + 4 \cdot \alpha(\epsilon_c) \cdot \beta(\epsilon_c) \cdot f_c \cdot b \cdot (A_s \cdot E_s \cdot \epsilon_c \cdot d + A_f \cdot E_f \cdot \epsilon_c \cdot h)}}{2 \cdot \alpha(\epsilon_c) \cdot \beta(\epsilon_c) \cdot f_c \cdot b}$$

$$f_s(\epsilon_c) := E_s \cdot \epsilon_c \cdot \left(\frac{d - c(\epsilon_c)}{c(\epsilon_c)} \right)$$

$$f_s(\epsilon_c) := \begin{cases} f_s(\epsilon_c) & \text{if } f_s(\epsilon_c) < f_y \\ f_y & \text{otherwise} \end{cases}$$

Moment Curvature Calculation for Prestressed CFRP Plate

Balance condition when steel yield

$$\alpha \cdot \beta \cdot f_c \cdot b \cdot c = A_s \cdot f_y + A_f \cdot E_f \cdot \left[\varepsilon_c \cdot \left(\frac{h - c}{c} \right) + \varepsilon_{ps0} \right]$$

$$BB(\varepsilon_c) := A_f \cdot E_f \cdot (\varepsilon_c - \varepsilon_{ps0}) - A_s \cdot f_y$$

$$c(\varepsilon_c) := \begin{cases} c(\varepsilon_c) & \text{if } f_s(\varepsilon_c) < f_y \\ \frac{-BB(\varepsilon_c) + \sqrt{(BB(\varepsilon_c))^2 + 4 \cdot \alpha(\varepsilon_c) \cdot \beta(\varepsilon_c) \cdot f_c \cdot b \cdot (A_f \cdot E_f \cdot \varepsilon_c \cdot h)}}{2 \cdot \alpha(\varepsilon_c) \cdot \beta(\varepsilon_c) \cdot f_c \cdot b} & \text{otherwise} \end{cases}$$

$$ff(\varepsilon_c) := E_f \cdot \left(\varepsilon_c \cdot \frac{h - c(\varepsilon_c)}{c(\varepsilon_c)} + \varepsilon_{ps0} \right)$$

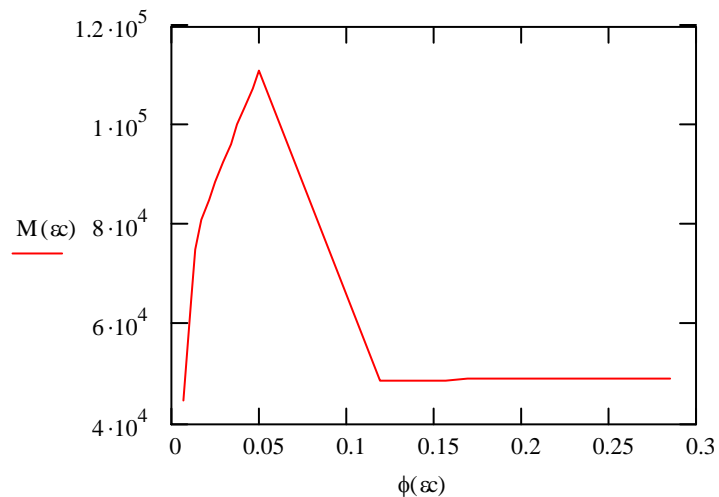
$$c(\varepsilon_c) := \begin{cases} c(\varepsilon_c) & \text{if } ff(\varepsilon_c) < ff_u \\ \frac{A_s \cdot f_y}{\alpha(\varepsilon_c) \cdot \beta(\varepsilon_c) \cdot f_c \cdot b} & \text{otherwise} \end{cases}$$

$$ff(\varepsilon_c) := \begin{cases} ff(\varepsilon_c) & \text{if } ff(\varepsilon_c) < ff_u \\ 0 \cdot \text{psi} & \text{otherwise} \end{cases}$$

Moment and curvature

$$M(\varepsilon_c) := A_s \cdot f_s(\varepsilon_c) \cdot (d - .5 \cdot \beta(\varepsilon_c) \cdot c(\varepsilon_c)) + A_f \cdot ff(\varepsilon_c) \cdot (h - .5 \cdot \beta(\varepsilon_c) \cdot c(\varepsilon_c))$$

$$\phi(\varepsilon_c) := \frac{\varepsilon_c}{c(\varepsilon_c)}$$



Moment Curvature Calculation for 1 Layer Of Carbon Fiber Sheet

Geometry Property

$$h := 8.625 \text{ in} \quad d := 7.375 \text{ in} \quad b := 39.375 \text{ in} \quad L := 240 \text{ in} \quad y := 4.3 \text{ in}$$

Manufacturer's Material Property

$$\begin{aligned} f_c &:= 6142 \text{ psi} & f_y &:= 60000 \text{ psi} & f_{fu} &:= 5.66 \cdot 10^5 \cdot \text{psi} & \epsilon_{fu} &:= 0.0155 \\ E_c &:= 57000 \sqrt{f_c} \cdot \text{psi} & E_s &:= 29 \cdot 10^6 \cdot \text{psi} & E_f &:= 34.8 \cdot 10^6 \cdot \text{psi} & t_f &:= 4.606 \times 10^{-3} \text{ in} \\ A_c &:= 339.609 \text{ in}^2 & A_s &:= 1.0 \text{ in}^2 & A_f &:= 0.181 \text{ in}^2 \end{aligned}$$

Moment of Inertial

$$I := \frac{(b \cdot h^3)}{12} \quad I = 2.105 \times 10^3 \text{ in}^4$$

Cracking stress and strain of concrete

$$\sigma := 7.5 \sqrt{f_c} \cdot \text{psi} \quad \sigma = 587.782 \text{ psi} \quad \epsilon_{cr} := \frac{\sigma}{E_c} \quad \epsilon_{cr} = 1.316 \times 10^{-4}$$

Moment causing flexural cracking at section due to externally applied loads, **M_{cr}**.

$$M_{cr} := \frac{\sigma \cdot I}{y} \quad M_{cr} = 2.398 \times 10^4 \text{ lbf} \cdot \text{ft}$$

Stress Block Factors

$$\epsilon := 0.002 \quad \epsilon_c := 0.000001, 0.00001, 0.003$$

$$\beta(\epsilon_c) := \frac{4 - \frac{\epsilon_c}{\epsilon}}{6 - \frac{2 \cdot \epsilon_c}{\epsilon}} \quad \alpha(\epsilon_c) := \frac{\frac{\epsilon_c}{\epsilon} - \frac{1}{3} \cdot \left(\frac{\epsilon_c}{\epsilon}\right)^2}{\beta(\epsilon_c)}$$

Balance Condition Without Consider ϵ_{bi}

$$\alpha \cdot \beta \cdot f_c \cdot b \cdot c = A_s \cdot E_s \cdot \epsilon_c \cdot \left(\frac{d-c}{c}\right) + A_f \cdot E_f \cdot \left[\epsilon_c \cdot \left(\frac{h-c}{c}\right)\right]$$

$$B(\epsilon_c) := A_s \cdot E_s \cdot \epsilon_c + A_f \cdot E_f \cdot \epsilon_c$$

$$c(\epsilon_c) := \frac{-B(\epsilon_c) + \sqrt{(B(\epsilon_c))^2 + 4 \cdot \alpha(\epsilon_c) \cdot \beta(\epsilon_c) \cdot f_c \cdot b \cdot (A_s \cdot E_s \cdot \epsilon_c \cdot d + A_f \cdot E_f \cdot \epsilon_c \cdot h)}}{2 \cdot \alpha(\epsilon_c) \cdot \beta(\epsilon_c) \cdot f_c \cdot b}$$

Moment Curvature Calculation for 1 Layer Of Carbon Fiber Sheet

Balance Condition (without consider ε_{bi}) when steel yield

$$\alpha \cdot \beta \cdot f_c \cdot b \cdot c = A_s \cdot f_y + A_f \cdot E_f \cdot \left[\varepsilon \cdot \left(\frac{h - c}{c} \right) \right]$$

Stress in steel

$$f_s(\varepsilon) := E_s \cdot \varepsilon \cdot \frac{d - c(\varepsilon)}{c(\varepsilon)}$$

$$f_s(\varepsilon) := \begin{cases} f_s(\varepsilon) & \text{if } f_s(\varepsilon) < f_y \\ f_y & \text{otherwise} \end{cases}$$

$$c(\varepsilon) := \begin{cases} c(\varepsilon) & \text{if } f_s(\varepsilon) < f_y \\ \frac{-(A_f \cdot E_f \cdot \varepsilon - A_s \cdot f_y) + \sqrt{(A_f \cdot E_f \cdot \varepsilon - A_s \cdot f_y)^2 + 4 \cdot \alpha(\varepsilon) \cdot \beta(\varepsilon) \cdot f_c \cdot b \cdot (A_f \cdot E_f \cdot \varepsilon \cdot h)}}{2 \cdot \alpha(\varepsilon) \cdot \beta(\varepsilon) \cdot f_c \cdot b} & \text{otherwise} \end{cases}$$

Balance Condition (without consider ε_{bi}) when steel yield and C-sheet rupture

$$\alpha \cdot \beta \cdot f_c \cdot b \cdot c = A_s \cdot f_y$$

Stress in C-sheet

$$f_f(\varepsilon) := E_f \cdot \varepsilon \cdot \frac{h - c(\varepsilon)}{c(\varepsilon)}$$

$$c(\varepsilon) := \begin{cases} c(\varepsilon) & \text{if } f_f(\varepsilon) < f_{fu} \\ \frac{A_s \cdot f_y}{\alpha(\varepsilon) \cdot \beta(\varepsilon) \cdot f_c \cdot b} & \text{otherwise} \end{cases}$$

$$f_f(\varepsilon) := \begin{cases} f_f(\varepsilon) & \text{if } f_f(\varepsilon) < f_{fu} \\ 0 \text{ psi} & \text{otherwise} \end{cases}$$

Moment and Curvature

$$M(\varepsilon) := A_s \cdot f_s(\varepsilon) \cdot (d - .5 \cdot \beta(\varepsilon) \cdot c(\varepsilon)) + A_f \cdot f_f(\varepsilon) \cdot (h - .5 \cdot \beta(\varepsilon) \cdot c(\varepsilon))$$

$$\phi(\varepsilon) := \frac{\varepsilon}{c(\varepsilon)} \qquad k := \frac{Mcr}{\varepsilon cr}$$

$$M(\varepsilon) := \begin{cases} k \cdot \varepsilon & \text{if } \varepsilon < \varepsilon cr \\ M(\varepsilon) & \text{otherwise} \end{cases}$$

Moment Curvature Calculation for 8 strips of NSM CFRP Bars

Geometry Property

$$h := 8.625 \text{ in} \quad d := 7.25 \text{ in} \quad b := 39.375 \text{ in} \quad L := 240 \text{ in} \quad y := 4.3 \text{ in}$$

Manufacturer's Material Property

$$f_c := 6133 \text{ psi} \quad f_y := 60000 \text{ psi} \quad f_{fu} := 4.2 \cdot 10^5 \cdot \text{psi} \quad \epsilon_{fu} := 0.018$$

$$E_c := 57000 \sqrt{f_c} \cdot \text{psi} \quad E_s := 29 \cdot 10^6 \cdot \text{psi} \quad E_f := 23 \cdot 10^6 \cdot \text{psi}$$

$$A_c = 339.609 \text{ in}^2 \quad A_s := 1.0 \text{ in}^2 \quad A_f = 0.174 \text{ in}^2$$

Moment of Inertial prior to cracking

$$I := \frac{(b \cdot h^3)}{12} \quad I = 2.105 \times 10^3 \text{ in}^4$$

Cracking Stress and strain of concrete

$$\sigma := 7.5 \cdot \sqrt{f_c} \cdot \text{psi} \quad \sigma = 587.351 \text{ psi} \quad \epsilon_{cr} := \frac{\sigma}{E_c} \quad \epsilon_{cr} = 1.316 \times 10^{-4}$$

Moment causing flexural cracking at section due to externally applied loads, **M_{cr}**.

$$M_{cr} := \frac{\sigma \cdot I}{y} \quad M_{cr} = 2.396 \times 10^4 \text{ lbf} \cdot \text{ft}$$

Stress Block Factors

$$\epsilon := 0.002 \quad \epsilon_c := 0.000001, 0.00001, 0.003$$

$$\beta(\epsilon_c) := \frac{4 - \frac{\epsilon_c}{\epsilon}}{6 - \frac{2 \cdot \epsilon_c}{\epsilon}} \quad \alpha(\epsilon_c) := \frac{\frac{\epsilon_c}{\epsilon} - \frac{1}{3} \cdot \left(\frac{\epsilon_c}{\epsilon}\right)^2}{\beta(\epsilon_c)}$$

Balance condition without consider **ε_{bi}**

$$\alpha \cdot \beta \cdot f_c \cdot b \cdot c = A_s \cdot E_s \cdot \epsilon_{cc} \cdot \left(\frac{d - c}{c}\right) + A_f \cdot E_f \cdot \left(\epsilon_{cc} \cdot \frac{h - c}{c}\right)$$

$$B(\epsilon_c) := A_s \cdot E_s \cdot \epsilon_c + A_f \cdot E_f \cdot \epsilon_c$$

$$c(\epsilon_c) := \frac{-B(\epsilon_c) + \sqrt{(B(\epsilon_c))^2 + 4 \cdot \alpha(\epsilon_c) \cdot \beta(\epsilon_c) \cdot f_c \cdot b \cdot (A_s \cdot E_s \cdot \epsilon_c \cdot d + A_f \cdot E_f \cdot \epsilon_c \cdot h)}}{2 \cdot \alpha(\epsilon_c) \cdot \beta(\epsilon_c) \cdot f_c \cdot b}$$

Moment Curvature Calculation for 8 strips of NSM CFRP Bars

Balance Condition (without consider ϵ_{bi}) when steel yield

$$\alpha \cdot \beta \cdot f_c \cdot b \cdot c = A_s \cdot f_y + A_f \cdot E_f \cdot \left[\epsilon \cdot \left(\frac{h - c}{c} \right) \right]$$

Stress in Steel

$$f_s(\epsilon) := E_s \cdot \epsilon \cdot \frac{d - c(\epsilon)}{c(\epsilon)}$$

$$f_s(\epsilon) := \begin{cases} f_s(\epsilon) & \text{if } f_s(\epsilon) < f_y \\ f_y & \text{otherwise} \end{cases}$$

$$c(\epsilon) := \begin{cases} c(\epsilon) & \text{if } f_s(\epsilon) < f_y \\ \frac{-(A_f \cdot E_f \cdot \epsilon - A_s \cdot f_y) + \sqrt{(A_f \cdot E_f \cdot \epsilon - A_s \cdot f_y)^2 + 4 \cdot \alpha(\epsilon) \cdot \beta(\epsilon) \cdot f_c \cdot b \cdot (A_f \cdot E_f \cdot \epsilon \cdot h)}}{2 \cdot \alpha(\epsilon) \cdot \beta(\epsilon) \cdot f_c \cdot b} & \text{otherwise} \end{cases}$$

Balance Condition (without consider ϵ_{bi}) when steel yield and laminate strips rupture

$$\alpha \cdot \beta \cdot f_c \cdot b \cdot c = A_s \cdot f_y$$

Stress in CFRP bar

$$f_p(\epsilon) := E_f \cdot \epsilon \cdot \frac{h - c(\epsilon)}{c(\epsilon)}$$

$$c(\epsilon) := \begin{cases} c(\epsilon) & \text{if } f_p(\epsilon) < f_{fu} \\ \frac{A_s \cdot f_y}{\alpha(\epsilon) \cdot \beta(\epsilon) \cdot f_c \cdot b} & \text{otherwise} \end{cases}$$

$$f_p(\epsilon) := \begin{cases} f_p(\epsilon) & \text{if } f_p(\epsilon) < f_{fu} \\ 0 \cdot \text{psi} & \text{otherwise} \end{cases}$$

Moment and Curvature

$$M(\epsilon) := A_s \cdot f_s(\epsilon) \cdot (d - 0.5 \cdot \beta(\epsilon) \cdot c(\epsilon)) + A_f \cdot f_p(\epsilon) \cdot (h - 0.5 \cdot \beta(\epsilon) \cdot c(\epsilon))$$

$$\phi(\epsilon) := \frac{\epsilon}{c(\epsilon)} \quad k := \frac{M_{cr}}{\epsilon_{cr}}$$

$$M(\epsilon) := \begin{cases} k \cdot \epsilon & \text{if } \epsilon < \epsilon_{cr} \\ M(\epsilon) & \text{otherwise} \end{cases}$$

APPENDIX D

ANALYTICAL SHEAR AND NORMAL STRESSES AT THE PLATE END

Roberts' Analytical Model: Approximate Analysis of Shear and Normal Stress Concentrations in the Adhesive Layer of Plated RC Slab

Dimensions and material properties

$$\begin{array}{llll}
 bc := 1000\text{ mm} & hc := 220\text{ mm} & hf := 223\text{ mm} & Ec := 26 \cdot 10^9 \cdot \text{Pa} \\
 bf := 100\text{ mm} & tf := 1.2\text{ mm} & hs := 190\text{ mm} & Ef := 164 \cdot 10^9 \cdot \text{Pa} \\
 ba := 100\text{ mm} & ta := 1.5\text{ mm} & Ga := 5.94 \cdot 10^8 \cdot \text{Pa} & Ea := 1.7 \cdot 10^9 \cdot \text{Pa} \\
 As := 645\text{ mm}^2 & Af := 120\text{ mm}^2 & Ac := 2.2 \cdot 10^5 \cdot \text{mm}^2 & Es := 200 \cdot 10^9 \cdot \text{Pa}
 \end{array}$$

Assume linear material behaviour and that the concrete cannot sustain tension, the depth of the neutral axis, h , is given by:

The modular ratio is

$$ns := \frac{Es}{Ec} \quad ns = 7.692 \quad nf := \frac{Ef}{Ec} \quad nf = 6.308$$

The transformed area of the steel and CFRP laminate plate are:

$$Asc := (ns - 1) \cdot As \quad Asc = 4.317 \times 10^{-3} \text{ m}^2$$

$$Afc := nf \cdot Af \quad Afc = 7.569 \times 10^{-4} \text{ m}^2$$

$$h := \frac{Ec \cdot bc \cdot \frac{hc^2}{2} + Ef \cdot bf \cdot tf \cdot \left(hc + \frac{tf}{2} \right)}{Ec \cdot bc \cdot hc + Ef \cdot bf \cdot tf} \quad h = 110.379\text{ mm}$$

The second moment of area of the equivalent fiber section is given by

$$I := \frac{Ec}{Ef} \cdot \left[\frac{bc \cdot hc^3}{12} + Ac \cdot (h - 0.5 \cdot hc)^2 + Asc \cdot (h - hs)^2 + Afc \cdot (h - hf)^2 \right] \quad I = 1.465 \times 10^8 \text{ mm}^4$$

The section moment of inertia of the concrete beam and fiber plate alone given by

$$Ic := \frac{bc \cdot hc^3}{12} \quad Ic = 8.873 \times 10^8 \text{ mm}^4 \quad Ec \cdot Ic = 2.307 \times 10^{13} \text{ N} \cdot \text{mm}^2$$

$$If := \frac{bf \cdot tf^3}{12} \quad If = 14.4\text{ mm}^4 \quad Ef \cdot If = 2.362 \times 10^6 \text{ N} \cdot \text{mm}^2$$

The solution presented herein for determining the maximum shear and normal stresses in the adhesive layer, based on the failure load of Slab A :

Stage 1: Stresses are determined assuming fully composite action between reinforced concrete beam and externally bonded laminate plate. Owing to applied loading, an element of the laminate plate, length δx , is subjected to resultant axial forces, t_1 and shear force/unit length τ_1 in the adhesive layer.

$$L_o := 150 \text{ mm}$$

$$x := 0 \text{ mm}, 1 \text{ mm}, \dots, 1200 \text{ mm}$$

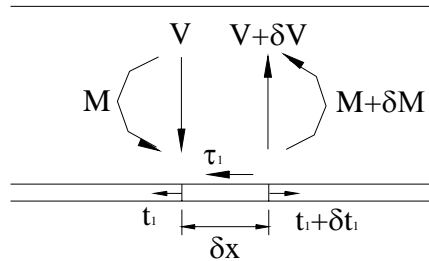
$$P := 13700 \text{ N}$$

$$V := 27400 \text{ N}$$

$$m(x) := V \cdot x$$

$$\tau_1 := \frac{V \cdot b_f \cdot t_f}{I \cdot b_a} \cdot (h_f - h)$$

$$t_1(x) := \frac{m(x) \cdot b_f \cdot t_f}{I} \cdot (h_f - h)$$



Values of the τ_1 and t_1 evaluated at the ends of the laminate plate ($x = 0$; $M = M_o$; $F = F_o$) are denoted by τ_{10} , and t_{10} , respectively.

$$M_o := V \cdot \left[\frac{(h_c + t_f)}{2} \right]$$

$$M_o = 3.03 \times 10^6 \text{ N} \cdot \text{mm}$$

$$\tau_{10} := \frac{V \cdot b_f \cdot t_f}{I \cdot b_a} \cdot (h_f - h)$$

$$\tau_{10} = 0.025 \frac{\text{N}}{\text{mm}^2}$$

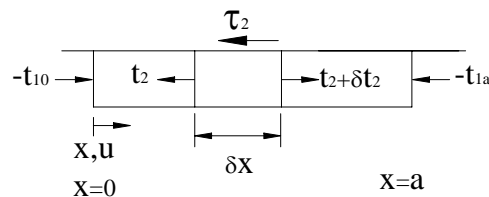
$$t_{10} := \frac{M_o \cdot b_f \cdot t_f}{I} \cdot (h_f - h)$$

$$t_{10} = 279.479 \text{ N}$$

State 2: The actual boundary conditions at the end of the laminate plate are considered. Since the axial forces t_1 do not exist in practice, the next stage of the solution is to applied opposite forces $-t_1$ to the end of the laminate plate as shown below. An approximation of this problem can be obtained by assuming the laminate plate to be bonded to an assumed rigid concrete beam by an adhesive layer having a shear stiffness/unit length k_s given by

$$k_s := G_a \cdot \frac{b_a}{t_a}$$

$$k_s = 3.96 \times 10^4 \frac{\text{N}}{\text{mm}^2}$$



Considering the equilibrium of an element of the steel plate, length δx , gives:

$$\tau_2 = k_s \cdot u$$

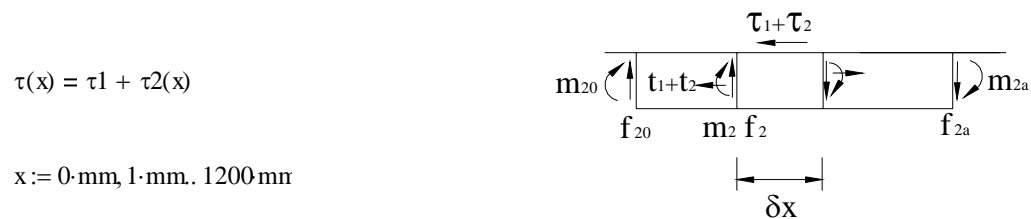
where u is the displacement of the laminate plate in the x -direction leading to the differential equation .

$$\frac{d^2 u}{dx^2} - \alpha^2 = 0 \quad \alpha := \sqrt{\frac{k_s}{E_f \cdot b_f \cdot t_f}} \quad \alpha = 0.045 \frac{1}{\text{mm}}$$

$$\tau_2(x) := \frac{1}{b_a} \cdot \left(\frac{k_s}{E_f \cdot b_f \cdot t_f} \right)^{0.5} \cdot (t_{10} \cdot \cosh(\alpha \cdot x) - t_{10} \cdot \sin(\alpha \cdot x))$$

$$\tau_{20} := \frac{1}{b_a} \cdot \left(\frac{k_s}{E_f \cdot b_f \cdot t_f} \right)^{0.5} \cdot (-t_{10} \cdot \sinh(\alpha \cdot 0 \cdot \text{mm}) + t_{10} \cdot \cosh(\alpha \cdot 0 \cdot \text{mm})) \quad \tau_{20} = 0.125 \frac{\text{N}}{\text{mm}^2}$$

The resultant forces in the fiber plate at the end of stage 2 are as shown in figure below in which m denotes moment and f denotes shear force.



$$\tau(x) := \frac{V \cdot b_f \cdot t_f}{I \cdot b_a} \cdot (h_f - h) + \frac{1}{b_a} \cdot \left(\frac{k_s}{E_f \cdot b_f \cdot t_f} \right)^{0.5} \cdot (t_{10} \cdot \cosh(\alpha \cdot x) - t_{10} \cdot \sinh(\alpha \cdot x))$$

$$\tau(x) = 0.025 + 0.125 \cosh(0.045x) - 0.125 \sinh(0.045x)$$

The maximum normal stress at the cutoff point is

$$x := 0 \cdot \text{mm}$$

$$\tau(x) = 0.151 \frac{\text{N}}{\text{mm}^2}$$

At the end of the laminate plate, the curvature of the concrete slab and laminate plate are approximately equal and hence m_{20} related to the global bending moment M_0 by the following equation:

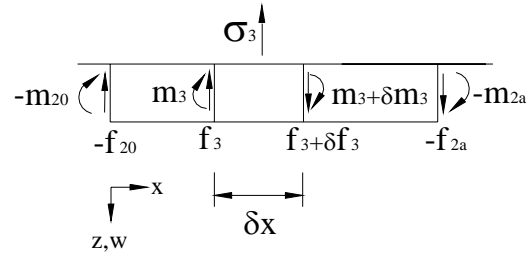
$$m_{20} := M_0 \cdot \left(\frac{E_f \cdot I_f}{E_f \cdot I_f + E_c \cdot I_c} \right) \quad m_{20} = 0.31 \text{ N} \cdot \text{mm}$$

$$f_{20} := \left(\frac{E_f \cdot I_f}{E_f \cdot I_f + E_c \cdot I_c} \right) \cdot V + b_a \cdot (\tau_{10} + \tau_{20}) \cdot \frac{t_f}{2} \quad f_{20} = 9.041 \text{ N}$$

Stage 3: Since the moment m_{20} and M_{2a} and shear forces f_{20} and f_{2a} do not exist in practice, the next stage of solution is to apply opposite moments and shear at $x=0$ and $x=a$, as show in figure below. An approximate solution of this problem can be obtained by assuming the steel plate to be bonded to an assumed rigid concrete beam by an adhesive layer having a normal stiffness/unit length k_n given by

$$k_n := E_a \cdot \frac{b a}{t a}$$

$$k_n = 1.133 \times 10^5 \frac{\text{N}}{\text{mm}^2}$$



Noting that the normal force in the adhesive σ_3 is given by

$$\sigma_3 = \frac{k_n \cdot w}{b a}$$

where w is the relative displacement of the laminate plate in the z direction, the governing differential equation can be obtained as

$$\frac{d^4 w}{dx^4} + 4\gamma^4 w = 0 \quad \gamma := \sqrt[4]{\frac{k_n}{4 \cdot E_f \cdot I_f}} \quad \gamma = 0.331 \frac{1}{\text{mm}}$$

Assuming that w tends to zero with increasing x ,

$$x := 0 \text{ mm}, 1 \text{ mm}, 1200 \text{ mm}$$

$$\sigma(x) := \frac{2}{b a} \cdot e^{-\gamma \cdot x} \cdot \left[(f_{20} \gamma + m_{20} \gamma^2) \cdot \cos(\gamma \cdot x) - m_{20} \gamma^2 \cdot \sin(\gamma \cdot x) \right]$$

$$\sigma(x) = e^{-0.331 \cdot x} \cdot (0.061 \cos(0.331 \cdot x) - 0.00068 \sin(0.331 \cdot x))$$

The maximum shear stress at the cutoff point is

$$x := 0 \text{ mm}$$

$$\sigma(x) = 0.061 \frac{\text{N}}{\text{mm}^2}$$

The concrete cover delamination is assume to begin if the maximum principal stress σ_p at the cutoff point is larger than the strength of the concrete, σ_2 (Kupfer and Gerstle, 1973)

$$f_{cu} := 33.8 \text{ MPa}$$

$$\sigma_2 := 0.295(f_{cu})^{0.667} \cdot \frac{\text{N}}{\text{mm}^2}$$

$$\sigma_2 = 3.088 \frac{\text{N}}{\text{mm}^2}$$

$$\sigma_y := \sigma(x)$$

$$\sigma_y = 0.061 \frac{\text{N}}{\text{mm}^2}$$

$$\sigma_x := \frac{M_o \cdot (hc - h)}{I_c}$$

$$\sigma_x = 0.374 \frac{\text{N}}{\text{mm}^2}$$

$$\tau := \tau(x)$$

$$\tau = 0.151 \frac{\text{N}}{\text{mm}^2}$$

$$\sigma_p := \frac{\sigma_x + \sigma_y}{2} + \sqrt{\left(\frac{\sigma_x - \sigma_y}{2}\right)^2 + \tau^2}$$

$$\sigma_p = 0.435 \frac{\text{N}}{\text{mm}^2}$$

Since $\sigma_2 > \sigma_p$, no concrete cover delamination failure

Malek's Analytical Model: Evaluation of delamination using Malek's approximation solution

Dimensions and material properties

$$\begin{array}{llll}
 bc := 1000\text{mm} & hc := 220\text{mm} & hf := 223\text{mm} & Ec := 26 \cdot 10^9 \cdot \text{Pa} \\
 bf := 100\text{mm} & tf := 1.2\text{mm} & hs := 190\text{mm} & Ef := 164 \cdot 10^9 \cdot \text{Pa} \\
 ba := 100\text{mm} & ta := 1.5\text{mm} & Ga := 5.94 \cdot 10^8 \cdot \text{Pa} & Ea := 1.7 \cdot 10^9 \cdot \text{Pa} \\
 As := 645 \cdot \text{mm}^2 & Af := 120 \cdot \text{mm}^2 & Ac := 2.2 \cdot 10^5 \cdot \text{mm}^2 & Es := 200 \cdot 10^9 \cdot \text{Pa}
 \end{array}$$

Section properties

Assume linear material behaviour and that the concrete cannot sustain tension, the depth of the neutral axis, h , is given by:

The modular ratio is

$$ns := \frac{Es}{Ec} \quad ns = 7.692 \quad nf := \frac{Ef}{Ec} \quad nf = 6.308$$

The transformed area of the steel and CFRP laminate plate are:

$$Asc := (ns - 1) \cdot As \quad Asc = 4.317 \times 10^{-3} \text{m}^2$$

$$Afc := nf \cdot Af \quad Afc = 7.569 \times 10^{-4} \text{m}^2$$

$$h := \frac{0.5 \cdot hc \cdot Ac + As \cdot hs + Af \cdot hf}{Ac + As + Af} \quad h = 110.295\text{mm}$$

The moment of initial of transform section based on concrete, I_{tr}

$$I_{tr} := \frac{bc \cdot hc^3}{12} + Ac \cdot (h - 0.5 \cdot hc)^2 + Asc \cdot (h - hs)^2 + Afc \cdot (h - hf)^2 \quad I_{tr} = 9.244 \times 10^8 \text{mm}^4$$

The cross-section properties of concrete and laminate plate alone are as follow:

$$yc := 110\text{mm} \quad Ic := \frac{bc \cdot hc^3}{12} \quad Ic = 8.873 \times 10^8 \text{mm}^4$$

$$yf := \frac{tf}{2} \quad If := \frac{bf \cdot tf^3}{12} \quad If = 14.4\text{mm}^4$$

The solution presented herein for determinating the maximum shear and normal stresses in the adhesive layer, based on the failure load of Slab A.

The expression for the bending moment at the ultimate load of 13.7kN (3.08kip) is given by:

$$L_o := 150 \text{ mm} \quad P := 13700 \text{ N}$$

$$M(x_o) = a_1 \cdot x_o^2 + a_2 \cdot x_o + a_3$$

$$M(x_o) := 27400 x_o$$

where x_o is at the edge of laminate plate. Therefore, the coefficients of the polynomial are:

$$a_1 := 0 \cdot \frac{\text{N}}{\text{m}} \quad a_2 := 27400 \text{ N} \quad a_3 := 0 \cdot \text{N} \cdot \text{m}$$

The interface shear stress between laminate plate and epoxy can be calculated by considering the equilibrium of an infinitesimal part of the laminate plate. The shear stress can be define by:

$$\tau(x) = t_f \cdot (b_3 \cdot \sqrt{A} \cosh(\sqrt{A} x) - b_3 \sqrt{A} \cdot \sinh(\sqrt{A} x) + 2b_1 \cdot x + b_2)$$

where

$$b_1 := \frac{(h_f - h) \cdot a_1 \cdot E_f}{I_{tr} \cdot E_c}$$

$$b_1 = 0 \frac{\text{N}}{\text{mm}^4}$$

$$b_2 := \frac{(h_f - h) \cdot E_f}{I_{tr} \cdot E_c} \cdot (2 \cdot a_1 \cdot L_o + a_2)$$

$$b_2 = 0.021 \frac{\text{N}}{\text{mm}^3}$$

$$b_3 := E_f \cdot \left[\frac{(h_s - h)}{I_{tr} \cdot E_c} (a_1 \cdot L_o^2 + a_2 \cdot L_o + a_3) + 2 \cdot b_1 \cdot \frac{t_a \cdot t_f}{G_a} \right]$$

$$b_3 = 2.235 \frac{\text{N}}{\text{mm}^2}$$

$$A := \frac{G_a}{t_a \cdot t_f \cdot E_f}$$

$$A = 2.012 \times 10^{-3} \frac{1}{\text{mm}^2}$$

The equation of shear stress distribution along the interface can now be expressed by:

$$x := 0 \text{ mm}, 1 \text{ mm}, 1200 \text{ mm}$$

$$\tau(x) := t_f \cdot (b_3 \cdot \sqrt{A} \cosh(\sqrt{A} x) - b_3 \sqrt{A} \cdot \sinh(\sqrt{A} x) + 2b_1 \cdot x + b_2)$$

$$\tau(x) = 0.12 \cdot \cosh(0.045x) - 0.12 \cdot \sinh(0.045x) + 0.021$$

and the tensile stress in the CFRP laminate plate can be written as

$$f_p(x) := b_3 \cdot \sinh(\sqrt{A} x) - b_3 \cdot \cosh(\sqrt{A} x) + b_1 \cdot x^2 + b_2 \cdot x + b_3$$

$$f_p(x) = 2.235 \sinh(0.045x) - 2.235 \cosh(0.045x) + 0.021 \cdot x + 2.235$$

The maximum shear stress at the cutoff point is calculated at $x=0$:

$$x := 0 \text{ mm}$$

$$\tau(x) = 0.146 \frac{\text{N}}{\text{mm}^2}$$

$$f_p(x) = 0 \text{ Pa}$$

The normal stress in the epoxy layer can be expressed as:

$$\sigma(x) = e^{-\beta \cdot x} \cdot (D1 \cdot \cos(\beta \cdot x) + D2 \cdot \sin(\beta \cdot x)) + \frac{q \cdot E_f \cdot I_f}{b_f \cdot E_c \cdot I_c}$$

where

$$K_n := \frac{E_a}{t_a} \qquad K_n = 1.133 \times 10^3 \frac{\text{N}}{\text{mm}^3}$$

$$\beta := \left(\frac{K_n \cdot b_f}{4 \cdot E_f \cdot I_f} \right)^{0.25} \qquad \beta = 0.331 \frac{1}{\text{mm}}$$

$$D1 = \frac{K_n}{E_f \cdot I_f} \cdot \frac{V_p}{2 \cdot \beta^3} - \frac{K_n}{E_c \cdot I_c} \cdot \frac{V_c + \beta \cdot M_o}{2 \cdot \beta^3} \qquad D2 = \frac{K_n}{E_c \cdot I_c} \cdot \frac{M_o}{2 \cdot \beta^2}$$

which V_c and V_p are shear forces at the plate end, in the concrete and laminate plate due to interfacial shear stresses, respectively.

$$V_o := 27400 \text{ N}$$

$$M_o := V_o \cdot L_o + L_o \cdot t_f \cdot b_f \cdot \gamma_c \cdot (b_3 \cdot \sqrt{A} + b_2) \qquad M_o = 4.35 \times 10^6 \text{ N} \cdot \text{mm}$$

$$V_c := V_o - b_f \cdot \gamma_c \cdot t_f \cdot (b_3 \cdot \sqrt{A} + b_2) \qquad V_c = 2.58 \times 10^4 \text{ N}$$

$$V_p := -0.5 \cdot b_f \cdot t_f^2 \cdot (b_3 \cdot \sqrt{A} + b_2) \qquad V_p = -8.737 \text{ N}$$

$$D1 := \frac{K_n}{E_f \cdot I_f} \cdot \frac{V_p}{2 \cdot \beta^3} - \frac{K_n}{E_c \cdot I_c} \cdot \frac{V_c + \beta \cdot M_o}{2 \cdot \beta^3} \qquad D1 = -0.059 \frac{\text{N}}{\text{mm}^2}$$

$$D2 := \frac{K_n}{E_c \cdot I_c} \cdot \frac{M_o}{2 \cdot \beta^2} \qquad D2 = 9.755 \times 10^{-4} \frac{\text{N}}{\text{mm}^2}$$

The equation for the normal stress is obtained as:

$$x := 0\text{-mm}, 1\text{-mm}, 1200\text{ mm} \quad q := 0 \cdot \frac{\text{N}}{\text{m}}$$

$$\sigma(x) := -e^{-\beta \cdot x} \cdot (D1 \cdot \cos(\beta \cdot x) + D2 \cdot \sin(\beta \cdot x)) + \frac{q \cdot E_f \cdot I_f}{b_f \cdot E_c \cdot I_c}$$

$$\sigma(x) = e^{-0.331 \cdot x} \cdot (-0.059 \cos(0.331 \cdot x) + 0.00098 \sin(0.331 \cdot x))$$

At the cutoff point ($x=0$) the maximum value of normal stress is obtained as:

$$x := 0\text{-mm}$$

$$\sigma(x) = 0.059 \frac{\text{N}}{\text{mm}^2}$$

The concrete cover delamination is assume to begin if the maximum principal stress σ_p at the cutoff point is larger than the strength of the concrete, σ_2 (Kupfer and Gerstle, 1973)

$$f_{cu} := 33.8 \text{ MPa}$$

$$\sigma_2 := 0.295(f_{cu})^{0.667}$$

$$\sigma_2 = 3.088 \frac{\text{N}}{\text{mm}^2}$$

$$\sigma_y := \sigma(x)$$

$$\sigma_y = 0.059 \frac{\text{N}}{\text{mm}^2}$$

$$\sigma_x := \frac{M_o \cdot (h_c - h)}{I_c}$$

$$\sigma_x = 0.538 \frac{\text{N}}{\text{mm}^2}$$

$$\tau := \tau(x)$$

$$\tau = 0.146 \frac{\text{N}}{\text{mm}^2}$$

$$\sigma_p := \frac{\sigma_x + \sigma_y}{2} + \sqrt{\left(\frac{\sigma_x - \sigma_y}{2}\right)^2 + \tau^2}$$

$$\sigma_p = 0.579 \frac{\text{N}}{\text{mm}^2}$$

Since $\sigma_2 > \sigma_p$, no concrete cover delamination failure

APPENDIX E

**FLEXURAL STRENGTHENING OF SLAB A BASED ON ACI 440 AND
TECHNICAL REPORT NO.55**

Flexural strengthening of Slab A based on ACI 440

Geometry Property

$$h := 8.625\text{-in} \quad d := 7.375\text{-in} \quad b := 39.37\text{-in} \quad L := 240\text{-in}$$

Manufacturer's Material Property

$$\begin{aligned} f_c &:= 4900\text{psi} & f_y &:= 60000\text{psi} & f_{fu} &:= 3.6 \cdot 10^5 \cdot \text{psi} & \beta_1 &:= 0.8 \\ E_c &:= 57000 \sqrt{f_c} \cdot \text{psi} & E_s &:= 29 \cdot 10^6 \cdot \text{psi} & E_f &:= 23 \cdot 10^6 \cdot \text{psi} & \gamma &:= 0.85 \\ A_c &:= h \cdot b & A_s &:= 1.0 \text{in}^2 & \epsilon_{fu} &:= 0.016 & \psi &:= 0.85 \\ A_c &= 339.566 \text{in}^2 & & & A_f &= 0.186 \text{in}^2 & t_f &:= 0.047\text{-in} \end{aligned}$$

Step 1: Compute the FRP system design material properties.

Assume that the slab is located in a interior space and CFRP material will be used. Therefore, an environmental reduction factor of 0.95 is suggested.

$$C_e := 0.95$$

$$f_{fu} := C_e \cdot f_{fu} \quad f_{fu} = 3.42 \times 10^5 \text{psi}$$

$$\epsilon_{fu} := C_e \cdot \epsilon_{fu} \quad \epsilon_{fu} = 0.015$$

Step 2: Preliminary Calculation

Properties of the existing reinforcement steel

$$\rho_s := \frac{A_s}{b \cdot d} \quad \rho_s = 3.444 \times 10^{-3}$$

$$n_s := \frac{E_s}{E_c} \quad n_s = 7.268$$

Properties of the externally bonded FRP reinforcement

$$\rho_f := \frac{A_f}{b \cdot d} \quad \rho_f = 6.406 \times 10^{-4}$$

$$n_f := \frac{E_f}{E_c} \quad n_f = 5.764$$

Step 3: Determine the existing state of strain on the soffit

Assume no initial strain during the FRP installation.

$$\epsilon_{bi} := 0$$

Step 4: Determine the bond-dependent coefficient of the FRP system

The dimensionless bond-dependent coefficient for flexural, κ_m , is calculated as follows:

$n = 1$ single layer of FRP system

$$n \cdot E_f \cdot t_f = 1.081 \times 10^6 \frac{\text{lbf}}{\text{in}}$$

$$\kappa_m := \begin{cases} 1 - \left(\frac{n \cdot E_f \cdot t_f}{2400000 \frac{\text{lbf}}{\text{in}}} \right) & \text{if } n \cdot E_f \cdot t_f \leq 1200000 \frac{\text{lbf}}{\text{in}} \\ \frac{600000 \frac{\text{lbf}}{\text{in}}}{n \cdot E_f \cdot t_f} & \text{otherwise} \end{cases}$$

$$\kappa_m := \begin{cases} \kappa_m & \text{if } \kappa_m \leq 0.9 \\ 0.9 & \text{otherwise} \end{cases}$$

$$\kappa_m = 0.55$$

Step 5: Estimate "c", the depth to the neutral axis

Estimate the value of "c". The value of "c" is adjusted after checking equilibrium.

$$c := 0.099d \quad c = 0.73 \text{ in}$$

Step 6: Determine the effective level of strain in the FRP reinforcement

The effective strain level in the FRP may be found as follows:

$$\kappa_m \cdot \varepsilon_{fu} = 8.354 \times 10^{-3}$$

$$\varepsilon_{fe} := 0.003 \left(\frac{h - c}{c} \right) - \varepsilon_{bi} \quad \varepsilon_{fe} = 0.032$$

$$\varepsilon_{fe} := \begin{cases} \varepsilon_{fe} & \text{if } \varepsilon_{fe} \leq \kappa_m \cdot \varepsilon_{fu} \\ \kappa_m \cdot \varepsilon_{fu} & \text{otherwise} \end{cases}$$

$$\varepsilon_{fe} = 8.354 \times 10^{-3}$$

Step 7: Calculate the strain in the existing reinforcement steel

The strain in the reinforcing steel may be calculated using similar triangles as follows:

$$\varepsilon_s := (\varepsilon_{fe} + \varepsilon_{bi}) \cdot \left(\frac{d - c}{h - c} \right) \quad \varepsilon_s = 7.031 \times 10^{-3}$$

Step 8: Calculate the stress level in the reinforcing steel and FRP

$$f_s := E_s \cdot \varepsilon_s$$

$$f_s := \begin{cases} f_s & \text{if } f_s \leq f_y \\ f_y & \text{otherwise} \end{cases} \quad f_s = 6 \times 10^4 \text{ psi}$$

$$f_{fe} := E_f \cdot \varepsilon_{fe} \quad f_{fe} = 1.921 \times 10^5 \text{ psi}$$

Step 9: Calculate the internal force resultants and check equilibrium.

Force equilibrium is verified by checking the initial estimate of "c" with the following equation:

$$c := \frac{A_s \cdot f_s + A_f \cdot f_{fe}}{\gamma \cdot \beta_1 \cdot f_c \cdot b} \quad c = 0.73 \text{ in}$$

Step 10: Adjust "c" until force equilibrium is satisfied

Step 6-9 were repeated several times with different values of "c" until equilibrium was achieved. The results of the final iteration are summarized below:

$$c = 0.73 \text{ in}$$

$$\varepsilon_s = 7.031 \times 10^{-3} \quad f_s = 6 \times 10^4 \text{ psi}$$

$$\varepsilon_{fe} = 8.354 \times 10^{-3} \quad f_{fe} = 1.921 \times 10^5 \text{ psi}$$

Step 11: calculate design flexural strength of the section

The design flexural strength is calculated using the equation as show below. An additional reduction factor, $\psi_f = 0.85$, is applied to the contribution of the FRP system. Since $\varepsilon_s = 0.007 > 0.005$, a strength reduction factor of $\phi = 0.90$ is appropriate.

$$\varepsilon_y := \frac{f_y}{E_s} \quad \varepsilon_y = 2.069 \times 10^{-3}$$

$$\phi := \begin{cases} 0.9 & \text{if } \varepsilon_s \geq 0.005 \\ \left[0.7 + \frac{0.2 \cdot (\varepsilon_s - \varepsilon_y)}{0.005 - \varepsilon_y} \right] & \text{if } \varepsilon_y < \varepsilon_s < 0.005 \\ 0.7 & \text{otherwise} \end{cases}$$

$$\phi = 0.9$$

$$M_n := A_s \cdot f_s \cdot \left(d - \frac{\beta_1 \cdot c}{2} \right) + \psi \cdot A_f \cdot f_{fe} \cdot \left(h - \frac{\beta_1 \cdot c}{2} \right)$$

$$M_n = 5.651 \times 10^4 \text{ lbf} \cdot \text{ft} \quad \phi \cdot M_n = 5.086 \times 10^4 \text{ lbf} \cdot \text{ft}$$

Flexural strengthening of Slab A based on Concrete Society Technical Report No.55

Geometry Property

$$h := 220\text{ mm} \quad d := 190\text{ mm} \quad b := 1000\text{ mm} \quad L := 6\text{ m}$$

Manufacturer's Material Property

$$\begin{aligned} f_{cu} &:= 33.8 \frac{\text{N}}{\text{mm}^2} & f_y &:= 413.7 \frac{\text{N}}{\text{mm}^2} & f_{fu} &:= 2500 \frac{\text{N}}{\text{mm}^2} & \gamma_{mc} &:= 1.5 \\ E_c &:= 4730 \sqrt{f_{cu}} \frac{\text{N}}{\text{mm}^2} & E_s &:= 2 \cdot 10^5 \frac{\text{N}}{\text{mm}^2} & E_f &:= 164 \cdot 10^3 \frac{\text{N}}{\text{mm}^2} & \gamma_{ms} &:= 1.05 \\ A_c &:= 2.2 \times 10^5 \text{ mm}^2 & A_s &:= 645 \text{ mm}^2 & A_f &:= 120 \text{ mm}^2 & b_f &:= 50\text{ mm} \\ \epsilon_{cu} &:= 0.0035 & \epsilon_y &:= \frac{f_y}{E_s} & \epsilon_{fu} &:= 0.016 & t_f &:= 1.2\text{ mm} \end{aligned}$$

Partial safety factors for fiber strength, γ_{mF} , and modulus of elasticity, γ_{mE} , at the ultimate limit state

$$\gamma_{mF} := 1.54 \quad \gamma_{mE} := 1.1$$

Debonding

The Concrete Society committee recommended that to avoid debonding failure, the strain in the FRP should not exceed 0.8% when the applied loading is uniformly distributed.

$$\epsilon_f := 0.008 \quad x := 0.003\text{ m}$$

Given

$$0.67 \frac{f_{cu}}{\gamma_{mc}} \cdot 0.9 \cdot x \cdot b = \frac{f_y}{\gamma_{ms}} \cdot A_s + \epsilon_f \cdot \frac{E_f}{\gamma_{mE}} \cdot A_f$$

$$\text{Find}(x) = 0.029\text{ m} \quad x := 0.029\text{ m}$$

$$\epsilon_c := \frac{x}{h - x} \cdot \epsilon_f \quad \epsilon_c = 1.215 \times 10^{-3} \quad \text{Since } \epsilon_c < 0.0035, \text{ no concrete crushing}$$

$$f_s := E_s \cdot \left(\epsilon_f \cdot \frac{d - x}{h - x} \right) \quad f_s = 1.349 \times 10^3 \frac{\text{N}}{\text{mm}^2} \quad \text{Since } f_s > f_y, \text{ steel yield}$$

$$z := d - 0.9 \cdot \frac{x}{2}$$

Taking moment about the bottom face, the moment is given by:

$$M := \left(0.67 \frac{f_{cu}}{\gamma_{mc}} \right) \cdot b \cdot 0.9 \cdot x \cdot [z + (h - d)] - \left(\frac{f_y}{\gamma_{ms}} \right) \cdot A_s \cdot (h - d)$$

$$M = 7.392 \times 10^4 \text{ N}\cdot\text{m} \quad M = 5.452 \times 10^4 \text{ lbf}\cdot\text{ft}$$

Longitudinal shear stress, τ

$$\tau = \frac{V \cdot \alpha_f \cdot A_f \cdot (h - x)}{I_{cr} \cdot b a}$$

$$P := 9430 \text{ N}$$

$V =$ ultimate sheat force

$$V := 2 \cdot P$$

Short term modulud ratio of FRP to concrete

$$\alpha_f := \frac{E_f}{\gamma_m E_c}$$

Depth of the neutral axis, x , of strengthened section

Sum the moments of area about the neutral axis of concrete, x

Given

$$b \cdot \frac{x^2}{2} + \frac{E_f}{E_c} \cdot A_f \cdot (x - h) = 0$$

$$\text{Find}(x) = 0.017 \text{ m} \quad x := 17 \text{ mm}$$

Second moment of area of strengthened concrete equivalent cracked section, I_{ce} (Ignore the presence of steel reinforcement).

$$I_{ce} := \frac{b \cdot x^3}{12} + b \cdot x \left(\frac{x}{2} \right)^2 + \frac{E_f}{E_c} \cdot A_f \cdot (h - x)^2 \quad b a := 100 \text{ mm}$$

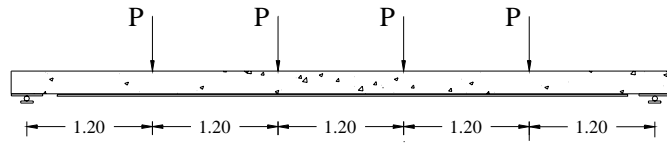
$$\tau := \frac{V \cdot \alpha_f \cdot A_f \cdot (h - x)}{I_{ce} \cdot b a}$$

$$\tau = 0.8 \frac{\text{N}}{\text{mm}^2}$$

$$M := 3.6 \cdot m \cdot P$$

$$M = 3.395 \times 10^4 \text{ N} \cdot \text{m}$$

$$M = 2.504 \times 10^4 \text{ lbf} \cdot \text{ft}$$



APPENDIX F

RESEARCH PROGRAM VIDEOS ON CD-ROM

1. INTRODUCTION

Included with this thesis is a CD_ROM. Which contains four video clips that show the failure modes of Slab A, Slab B, Slab C, and Slab D. The video clips are in AVI Video format and can be viewed using Real One Player.

2. CONTEXT

Test for Slab A.avi

Test for Slab B.avi

Test for Slab C.avi

Test for Slab D.avi

BIBLIOGRAPHY

1. Alfarabi Sharif, Al-Sulaiman, G. J., Basunbul, I. A., Baluch, M. H., and Ghaleb, B. N. (1994). "Strengthening of initially loaded reinforced concrete beams using FRP plates". *ACI Structural Journal*, Vol. 91, No. 2, pp. 160-168.
2. Burgoyne, C. J. (1999). "Advanced composites in civil engineering in Europe." *Journal of The International Association of Bridge and Structural Engineering: www.iabse.ethz.ch/sei/backissues/abstracts.sei9904/burgoyne.pdf*. Vol. 9, No. 4/1999.
3. Taerwe, L., Matthys, S., Pilakoutas, K., and Guadagnini, M. (2001). "European activities on the use of FRP reinforcement, fib Task Group 9.3 and the ConFibreCrete network." *5th International Conference on FRP Reinforcement Concrete Structures (FRPRCS-5)*, Cambridge, UK, July 16-18, 2001, Vol. 1, pp. 3-15.
4. Swamy, R. N. and P. Mukhopadhyaya. (1995). "Role and effectiveness of non-metallic plates in strengthening and upgrading concrete structures." *Non-metallic (FRP) Reinforcement for Concrete Structure*, E&FN, London, 1995, pp. 473-482.
5. Jones, R., Swamy, R. N., and Charif, A. (1988). "Plate separation and anchorage of reinforced concrete beams strengthened by epoxy –bonded steel plates." *The Structural Engineer*, Vol. 66, No. 5, pp. 85-94.
6. Taljsten, B. (1997). "Strengthening of beams by plate bonding." *Journal of Materials in Civil Engineering*, Vol. 9, No. 4, Nov. 1997, pp. 206-212.
7. Blaschko, M., Niedermeier, R. and Zilch, K. (1998). "Bond failure modes of flexural members strengthened with FRP." *2nd International Conference on Composites in Infrastructure*, Tucson, Arizona, 1998.
8. Stocklin and Meier, U. (2001). "Strengthening of concrete structures with prestressed and gradually anchored CFRP strips." *5th International Conference on FRP Reinforcement Concrete Structures (FRPRCS-5)*, Cambridge, UK, July 16-18, 2001, Vol. 1, pp. 291-296.

9. Ferrier, E., Ennaceur, C., Bigaud, D. and Hamelin, P. (2001) “ Prestressed externally bonded FRP reinforcement for RC beams.” *5th International Conference on FRP Reinforcement Concrete Structures (FRPRCS-5)*, Cambridge, UK, July 16-18, 2001, Vol. 1, pp. 271-280.
10. S&P Clever Reinforcement Company. (2000). “Design guide line for S&P FRP systems.” WWW.reinforcement.ch, Brunnen, Switzerland.
11. Thomas, J., Kline, T., Emmons, P. and Kliger, H. (1996). “Externally bonded carbon fiber for strengthening concrete.” *Material for the new millennium: Proc. of the 4th Materials Engineering Conference*, Washington, D.C., Vol.2, pp.924-930.
12. Yoshizawa, H., Myojo, T., Okoshi, M., Mizukoshi, M. and Kliger, H. S. (1996). “Effect of sheet bonding condition on concrete members having externally bonded carbon fiber sheet.” *Material for the new millennium: Proc. of the 4th Materials Engineering Conference*, Washington, D.C., Vol.2, pp.1608-1616.
13. Tumialan, J. G. (1998). Concrete cover delamination in reinforced concrete beam strengthened with CFRP sheets.” *MS thesis*, Department of Civil Engineering, University of Missouri-Rolla.
14. Alkhrdaji, T., Nanni, A., Chen, G. and Barker, M. (1999). “Upgrading the transportation infrastructure: solid RC decks strengthened with FRP.” *Concrete International: Design and Construction*, Vol. 21, No. 10, pp. 37-41.
15. Nanni, Antonio. (2000). “FRP reinforcement for bridge structures.” *Proc., Structural Engineering Conference*, The University of Kansas, Lawrence, KS, March 16, 2000, 5 pp.
16. Bjorn Taljsten and Anders Carolin. (2001). “Concrete beams strengthened with near surface mounted CFRP laminates.” *5th International Conference on FRP Reinforcement Concrete Structures (FRPRCS-5)*, Cambridge, UK, July 16-18, 2001, Vol. 1, pp.107-116.
17. De Lorenzis, L., Nanni, A. and La Tegola, A. (2000). “Flexural and shear strengthening of reinforced concrete structures with near surface mounted FRP rods.”

- Proc., 3rd Inter. Conf. On Advantage Composite Materials in Bridges and Structures, Ottawa, Canada, August 15-18, 2000, pp.521-528.*
18. Smith, S. T. and Teng, J.G. (2001). "Strength Models for plate end debonding in FRP Strengthened RC beams." *5th International Conference on FRP Reinforcement Concrete Structures (FRPRCS-5)*, Cambridge, UK, July 16-18, 2001, Vol. 1, pp. 419-428.

 19. Roberts, T.M. (1989). "Approximate analysis of shear and normal stress concentration in the adhesive layer of plated RC beams." *The Structural Engineer*, Vol. 67, No. 12/20, pp. 229-233.

 20. Quantrill, R. J., Hollaway, L. C. and Thorne, A.M. (1996). "Prediction of the maximum plate end stresses of FRP strengthened beam: Part II." *Magazine of Concrete Research*, Vol. 48, No. 177, pp. 343-351.

 21. Saadatmanesh, H. and Malek A. M. (1998). "Design guidelines for flexural strengthening of RC beams with FRP plates." *Journal of Composites for Construction*, Vol.2, No.4, pp. 158-164.

 22. Malek, A. M., Saadatmanesh, H. and Ehsani, M. R. (1998). "Prediction of failure load of RC beams strengthened with FRP plate due to stress concentration at the plate end." *ACI Structural Journal*, Vol. 95, No. 1, pp. 142-152.

 23. Adduini, M. and Nanni, A. (1997). "Parametric study of beams with externally bonded FRP reinforcement." *ACI Structural Journal*, Vol. 94, No. 5, pp. 1-10.

 24. Adduini, M., Di Tommaso, A. and Nanni, A. "Brittle failure in FRP plate and sheet bonded beams." Thesis, University of Bologna, Bologna, Italy.

 25. Collins, M. P. and Mitchell, D. (1997). "Reinforced Concrete Structures." Response Publications, Canada.

 26. MacGregor, J. G. (1997). "Reinforced Concrete Mechanics and Design." Third Edition, Prentice Hall, Upper Saddle River, New Jersey.

 27. Niu, HeDong and Wu, ZhiShen. (2001). "Prediction of debonding failure load due to flexural cracks of concrete for FRP strengthened structures." *5th International*

- Conference on FRP Reinforcement Concrete Structures (FRPRCS-5)*, Cambridge, UK, July 16-18, 2001, Vol. 1, pp. 361-370.
28. Jones, R., Swamy, R. N. and Charif, A. (1988) "Plate separation and anchorage of reinforced concrete beams strengthened by epoxy-bonded steel plates." *The Structural Engineer*, Vol.66, No. 5, pp. 85-94.
29. Roberts, T. M. and Haji-Kazami, H. (1989). "Theoretical study of the behaviour of reinforced concrete beams strengthened by externally bonded steel plates." *Proceedings of the Institution of Civil Engineers: Structural Engineering Group*, Part 2, 87, pp. 39-55.
30. Roberts, T.M. (1989). "Shear and normal stresses in adhesive joints." *Journal of Engineering Mechanics*, Vol. 55 No. 11, pp. 2460-2479.
31. Dat Duthinh and Monica Starnes (2001). "Strength and ductility of concrete beams reinforced with carbon FRP and steel." U.S. Department of Commerce, Gaithersburg, Maryland.
32. The Concrete Society (2000). "Design guidance for strengthening concrete structures using fibre composite materials." *Concrete Society Technical Report No. 55*. Center House, Telford Avenue, Crowthorne, Berkshire, UK.
33. American Concrete Institute International (2002). "Guide for the design and construction of externally bonded FRP systems for strengthening concrete structures." *ACI-440.2R-02*, Farmington Hill, Michigan.

VITA

Kah Yong Tan was born in Triang, Pahang, Malaysia, on June 19, 1976. He received his primary and secondary education in Chinese and Malay media schools in Triang and graduated in December 1995. He proceeded to pursue his Bachelor's Degree in Civil Engineering at the University of Technology Malaysia (UTM). During the course of his undergraduate studies, Kah Yong was an active member of UTM Equestrian Club and president of the Civil Engineer Club for an academic year. He graduated from that university in 1999, receiving his degree after presenting his undergraduate thesis titled "Evaluation of Reinforced Shear Wall for Tall Building with Opening in the Central."

After receiving his Bachelor's Degree, Kah Yong worked as a junior engineer in a project management consultant firm in Petaling Jaya, Malaysia for one year. With high ambition and passion to study abroad, Kah Yong enrolled in the Civil Engineering Graduate Degree Program at University of Missouri- Rolla (UMR) in 2000. During the course of his studies in UMR, he was a research assistant at the Center for Infrastructure Engineering Studies. His major assignment was to conduct flexural tests on 5 full-scale RC slabs strengthened with three different carbon fiber reinforced polymer (CFRP) systems. In January 2003, Kah Yong was assigned to conduct flexural tests for 10 RC slabs strengthened with steel reinforced polymer (SRP) systems in University of Naples, Italy. He received the Master of Science Degree in Civil Engineering in May 2003.